LOW VELOCITY GAS FLOW MEASUREMENT

by

R. L. Bass, III

T. E. Owen

C. R. Gerlach

S A. Suhler

FINAL TECHNICAL REPORT
Contract No. NAS8-26117
Control No. DCN-1-0-40-01580 (IF)
SwRI Project No. 02-2851

Prepared for
National Aeronautics and Space Administration
George C. Marshall Space Flight Center
Marshall Space Flight Center, Alabama 35812

February 1971

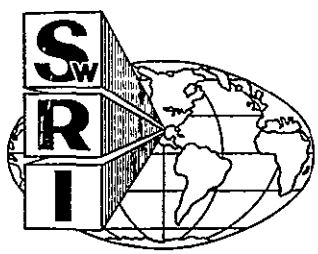

SOUTHWEST RESEARCH INSTITUTE
SAN ANTONIO HOUSTON

SOUTHWEST RESEARCH INSTITUTE
Post Office Drawer 28510, 8500 Culebra Road
San Antonio, Texas 78228

LOW VELOCITY GAS FLOW MEASUREMENT

by
R. L. Bass, III
T. E Owen
C. R. Gerlach
S. A. Suhler

FINAL TECHNICAL REPORT
Contract No. NAS8-26117
Control No. DCN-1-0-40-01580 (IF)
SwRI Project No. 02-2851

Prepared for
National Aeronautics and Space Administration
George C. Marshall Space Flight Center
Marshall Space Flight Center, Alabama 35812

February 1971

Approved:

C. Richard Gerlach

C. Richard Gerlach, Manager
Hydro-Mechanical Systems

TABLE OF CONTENTS

TABLE OF CONTENTS (Cont'd)

I. INTRODUCTION

This report summarizes all work performed by Southwest Research Institute during the past ten-month period on studies of low velocity gas flow measurement techniques The work was conducted under Contract NAS8-26117 "Low Velocity Gas Flow Measurement" for the George C. Marshall Space Flight Center of the National Aeronautics and Space Administration with Mr. Tom Marshall of the Measurement Instruments Branch of the Instruments and Communications Division serving as Technical Manager.

Objective and Scope of Work

The objective of this investigation is to perform a study and experimental program to find and evaluate new methods and techniques for low velocity measurements, with emphasis placed on instrumentation other than hot wire anemometers. As a result of this effort, a recommendation of the best measurement principle for an instrument development program is to be made, along with specifications and scope of work for such a program.

The desired features and specifications for the low velocity gas flowmeter are:

(1) Range: 0-100 fpm

(2) Accuracy: $\pm$ 1 fpm or better

(3) Output: 0-5 VDC or digital and linear

(4) Environmental Pressure: 3-15 psia

(5) Environmental Temperature: 60-80^{o}F

(6) Response: about 1 Hz

(7) Omni-directional capabilities with negligible effect of the airflow direction

(8) Rugged but handy design with no flow profile distortion because of its presence, and being of one of two configurations:

(a) A portable instrument with self contained power supply

(b) A Telephone Version with the control box on the wall and a long coiled cord.

In order to meet the objectives, this program was conducted in two phases. The first phase consisted of (1) screening the literature to find applicable low velocity measurement methods, (2) a preliminary evaluation to determine the feasibility of a given method in meeting the required low velocity instrument specifications, and (3) choosing, for additional study, those methods which appeared to have the most promise in meeting the instrument requirements. As a result of the first phase study, acoustic and ion-tracer techniques were chosen for additional evaluation.

The second project phase consisted of an experimental program where laboratory bread-board models of the acoustic and ion-discharge anemometers were constructed and tested in a low velocity flow facility to ascertain the relative merits and drawbacks of each method. The program results were evaluated, and the ion-tracer method was chosen as the best for development into a package meeting the instrument requirements of this program. Finally, as a result of this evaluation, specifications and the scope of work for a low velocity measurement instrument development program are outlined.

II. PRELIMINARY CANDIDATE SURVEY

II. 1 Introduction

Maintaining adequate ventilation and circulation of air in living and working quarters is something we take for granted in our daily lives. For the astronaut in a space vehicle, however, low gravity conditions can cause critical gas stagnation problems if adequate circulation is not maintained. To assure that the ventilation in a given vehicle is adequate requires some means for monitoring air flow patterns, and this creates problems from the standpoint of presently available techniques for gas velocity measurement. One problem is that existing techniques are not sensitive enough or accurate enough in low velocity gas streams. In addition, environmental changes such as gas density, gas constituents and gravity place special requirements on developing an instrument for ground testing as well as in-flight recording.

In gas dynamics work, measurement of velocities for subsonic flows has traditionally been accomplished by use of a simple Pitot device where only steady state measurements were required, or with the supplemental use of a hot-wire or hot-film system where dynamic measurements were needed. In the past, however, the predominance of work has been for flow velocities considerably above the range required for the proposed study (0-100 fpm). Very little work has been done to develop instrumentation for accurate low velocity gas measurements. The purpose of the initial study effort was to review the various techniques which might be used for low gas velocity measurements, and to point out potential advantages, disadvantages and probable required development effort.

A thorough review of the literature revealed a multitude of possible methods for measuring flow velocities. The methods which have potential for this application can be categorized as follows:

1) Total or Impact Pressure Methods
2) Convective Cooling Methods
3) Fluidic Methods
4) Acoustic Methods
5) Optical Methods
6) Tracer Methods

Each category represents a velocity measuring method based on a particular principle which may be implemented in one or more ways. In studying these methods, the implementation which appeared the most promising for meeting the specifications in this program was evaluated in enough detail to either reject or accept the method for additional study. The important points uncovered in this study, for each method, are presented below.

II. 2 Impact/Pressure Type Velocity Meters

Impact/Pressure type devices for measuring flow velocities can be listed into the following categories:

1. Pitot method - Measures the difference between total stream pressure ($P_s + 1/2\ \rho\ V^2$) and the local static pressure (P_s).

2. Impact force method - The force exerted on an object as the result of the dynamic stream pressure ($1/2\ \rho\ V^2$) is monitored by

    a) recording strains produced by the impact force

    b) recording deflections produced by the impact force.

The resulting differential pressures, deflections or strains are proportional to the flow velocity. Utilizing these methods to measure velocities from 0-100 fpm requires the measurement of extremely small differential pressures with a pitot tube, or minute deflections or strains with the impact force technique. A more detailed analysis follows.

Pitot Method

In low subsonic flows the pitot probe yields a differential pressure which is the difference between the total pressure ($P_s + 1/2\ \rho\ V^2$) and the static pressure (P_s). The resulting ΔP, the dynamic head ($1/2\ \rho\ V^2$), is shown in Figure 1 for the required range of velocities (0 to 100 fpm) and pressures (3-15 psia) at the mean environmental temperature of 70°F in air. The dynamic pressures range from 0 to 10^{-5} psi at 100 fpm and 15 psia. Commercially available instruments such as the MKS Baratron and Lion Research Corporation Model PM 100 pressure meter can accurately detect ΔP as low as 2×10^{-7} psi. No other instrument is currently known

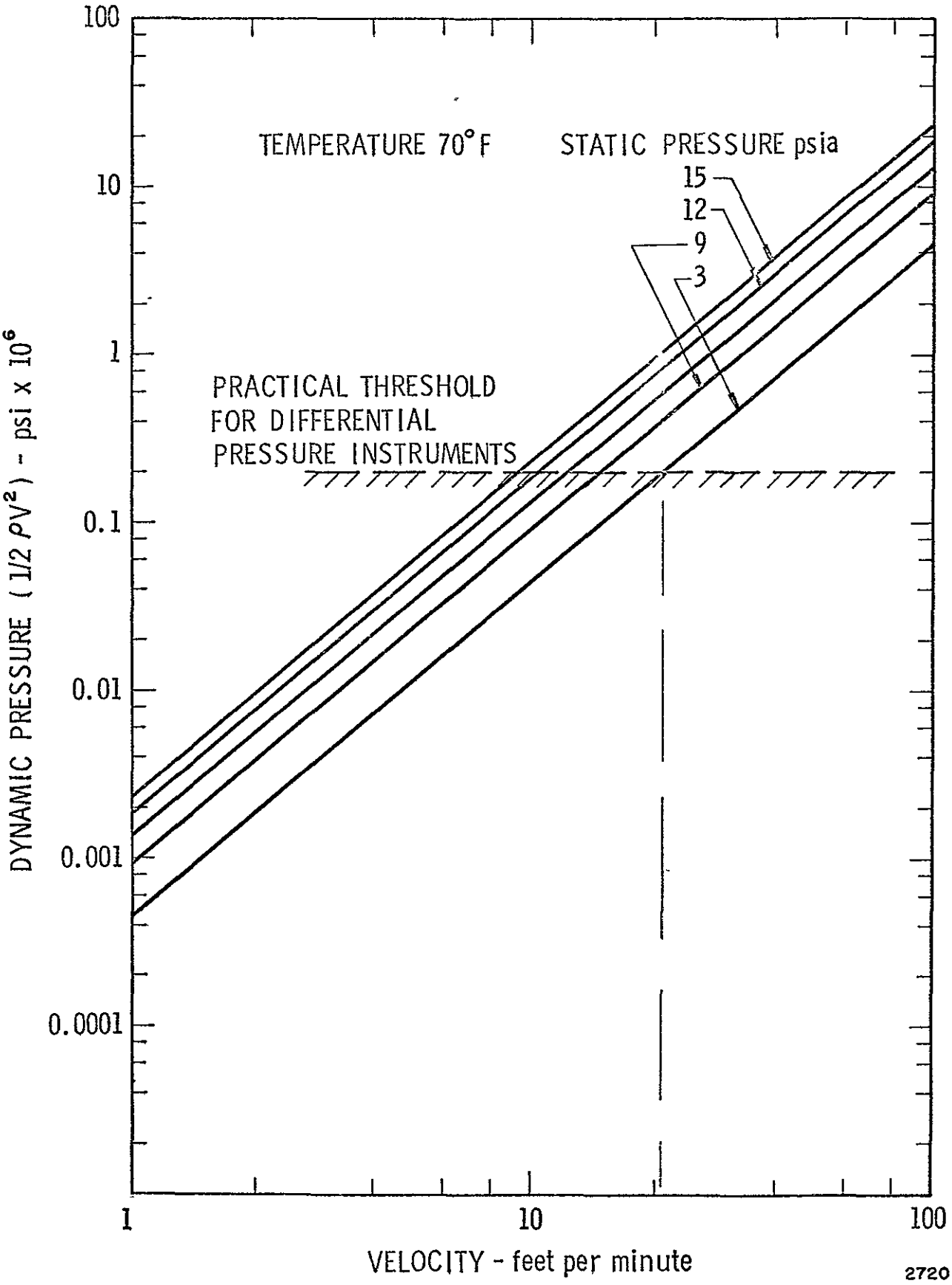

Figure 1. Dynamic Differential Pressure Range As A Function Of Velocity And Ambient Pressure

which will sense differential pressures below 10^{-7} psi, therefore a lower limit of 20 fpm at 3 psia is placed on velocity measured by the pitot technique.

The output voltage of the pressure transducers* will be proportional to the product of the environmental density and the air velocity squared. Consider a pitot probe of the following configuration:

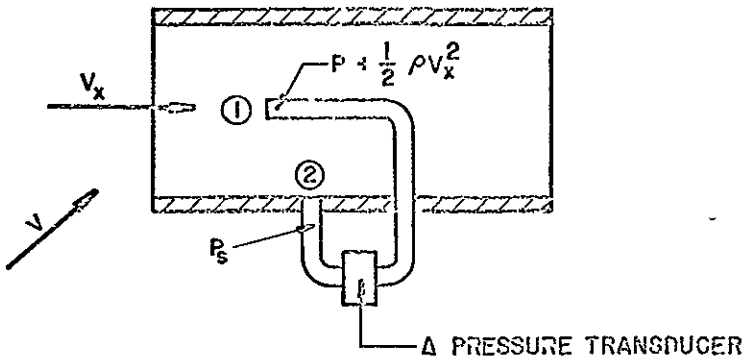

Pitot Probe Configuration

The differential pressure transducer output will be $EMF = C\ \rho\ V_x^2$ where C is an instrument constant, ρ is the environmental density and V_x the desired velocity component. The environmental density can be accurately determined from the ideal gas law utilizing cabin measurements of temperature and pressure. Therefore

$$EMF = \left(\frac{C\ P_s}{RT}\right) V_x^2 \qquad (1)$$

Linearization of the output signal to component velocity after compensation for density changes can be easily accomplished. If accurate ΔP's representing the true dynamic pressure can be recorded (down to 2×10^{-7} psi) velocities from 20 to 100 fpm are readily obtained.

* These instruments employ a diaphragm type transducer in which the diaphragm displacement resulting from the sensed ΔP is detected by a variable capacitance or reluctance electronic technique.

With respect to obtaining a true measure of the dynamic head, consider the actual reading of the differential transducer. The total pressure will be picked up at point (1) and the static pressure at (2) in the previous sketch.

The actual velocity V_x at (1) will be determined by

$$1/2\ \rho_1\ V_x^2 = P_{T_1} - P_{s_1}$$

while the apparent velocity V_{ax} will be determined by

$$1/2\ \rho_a\ V_{ax}^2 = P_{T_1} - P_{s_2}$$

Some inaccuracy will exist from not measuring both the static (P_s), and total pressure (P_T) at location (1). Therefore

$$\rho_1\ V_x^2 - \rho_a\ V_{ax}^2 = P_{s_2} - P_{s_1}$$

Assuming that only the temperature changes between (1) and (2) yields

$$\frac{V_{ax}}{V_x} = \sqrt{1 + \frac{2\,g\,R\,\Delta T_{1-2}}{V_x^2}} \qquad (2)$$

and for only density changes between (1) and (2)

$$\frac{V_{ax}}{V_x} = \sqrt{\frac{\rho_1}{\rho_a} + \frac{R\,T\,\Delta\rho_{1-2}}{\rho_a\ V_x^2}} \qquad (3)$$

The effects of small temperature changes between (1) and (2) on instrument accuracy are shown in Figure 2. It is obvious that very small changes in the environmental characteristics between the static and total ports can grossly affect the accuracy of the velocity measurement at velocities lower than 90 fpm. This inaccuracy will be magnified in an omni-directional device where the 3 components are measured at slight separation distances from the desired measurement point. Additional problems encountered with this method could result from the total pressure at (1), as sensed by the probe, being different from the actual total pressure in the flow with the probe removed. This could result from entrance or interference problems caused

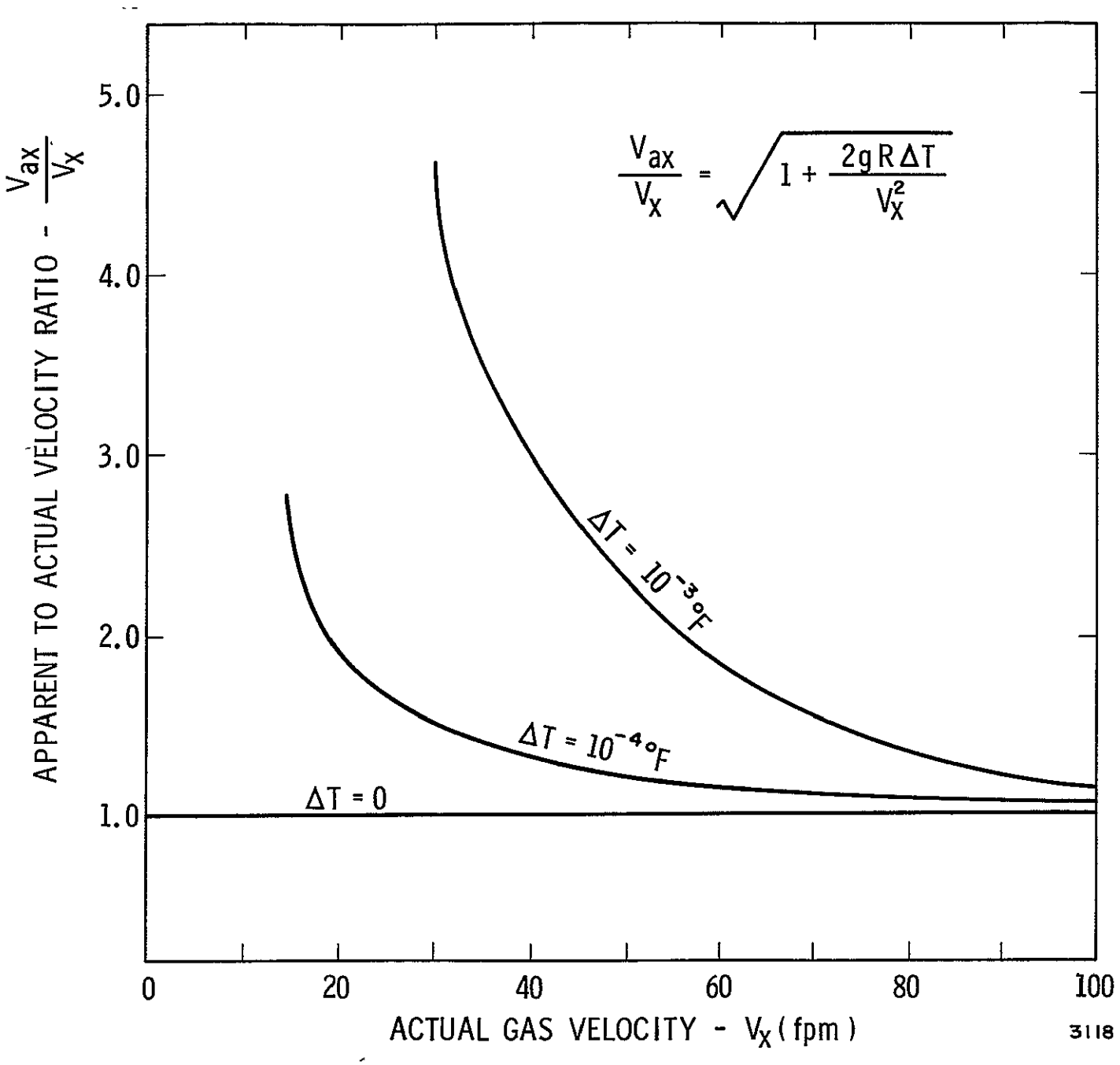

Figure 2. Apparent vs Actual Velocity with Temperature Change Between Total and Static Pitot Pressure Ports

by the guide tube which directs the flow across the probe. These types of errors would have to be calibrated out of the instrument by experimental tests, and success of such a calibration is judged as not likely.

Impact Force Methods

Impact force methods utilize the forces created by the flow dynamic pressure. In general this force is given by

$$F = C_D (1/2\ \rho\ V^2\ A) \tag{4}$$

where C_D and A are the drag coefficient and area respectively of the impact object. The drag coefficient is usually a function of the Reynolds number and may vary considerably over the velocity range of interest. The forces measured for velocities of 0 to 100 fpm will be quite small for a compact instrument. That is,

$$C_D \cong 1$$

$$1/2\ \rho\ V^2 \cong 10^{-5} \quad @\ 100\ \text{fpm}$$

$$A \cong 1 \text{ to } 10\ \text{in}^2 \text{ for small instruments}$$

so

$$F \cong 10^{-4}\ \text{lbs maximum.}$$

Three types of velocity measuring devices which operate on the impact force principle have been investigated. One method uses a microammeter to measure target vane deflections, another method uses optical techniques to measure a fiber deflection and the third method measures the strains produced in the cantilever support of an impact sphere.

Microammeter

This method, described in References 1 and 2 , nulls out the air current force exerted on a target vane by adjusting current to the ammeter coil. The device was reported to have good sensitivity down to 12 fpm. A subsequent evaluation of this technique, Reference 3, indicates good sensitivity at low velocities but indicates other problem areas which would make this instrument undesirable for the present application. Among these is the fact that the anemometer current is a function of the

vane angle (β) with respect to the flow as well as the flow velocity, therefore

$$I = I\ (V, \beta\ )$$

Thus a change in flow velocity will change the vane orientation from the original condition. The ammeter current will therefore be a function of velocity and vane angle, which will change with each flow condition, and calibrations for both deflection angle and velocity will be required. Also, changes in environmental conditions will cause the density ρ and possibly the drag coefficient C_D in Equation (4) to vary resulting in additional calibrations to ensure accurate readings over the 3-15 psia cabin pressure range.

In addition, a three component system would be bulky and the microammeters sensitive to vibration.

Fiber Deflection

This technique, described in References 4 and 5, uses a small diameter fiber ($\sim$ .00125") which deflects under the impact force of the flow field. This deflection can be measured optically with a photo cell and light source. The load on the fiber is given by Equation (4). The drag coefficient for cylinders at low Reynolds numbers is approximately

$$C_D = 1.97 + \frac{8.28}{(R_e)_d} - \frac{0.247}{(R_e)_d^2}$$

and the fiber deflection from simple bending moment theory is

$$S = \frac{\rho}{E}\left(\frac{D}{d}\right)^4 (1.215\ V^2\ d + 6.57\ V\nu\ - .314\ \nu^2/d) \qquad (5)$$

where d and D are fiber and flow tube diameters respectively; ρ and ν are flow density and kinematic viscosity respectively, and E is Young's modulus of the fiber. Velocities down to 18 fpm were accurately measured, and experimental values agreed fairly well with those determined from Equation (5). However, in this application large density variations will exist and the fiber deflection as given in Equation (5) will be a function of density as well as velocity. The instrument would have to include compensation for density changes.

An omnidirectional device could employ three heads with vector addition. The smallness of the fiber indicates that this type of instrument would probably not be rugged and would require periodic examination and re-calibration.

Strain Gage Anemometer

The strain gage anemometer measures three-component strains on an impact sphere and is described in Reference 6. The impact forces for the three component directions are

$$F_1 = C_D \; 1/2 \; \rho \; V^2 \; \cos \alpha$$

$$F_2 = C_D \; 1/2 \; \rho \; V^2 \; \cos \beta$$

$$F_3 = C_D \; 1/2 \; \rho \; V^2 \; \cos \gamma$$

and

$$\cos^2 \alpha \; + \; \cos^2 \beta \; + \; \cos^2 \gamma = 1$$

The three force components are measured by semi-conductor strain gages, and the three component velocities are determined from the previous equations. This instrument was found to give adequate results down to 40 fpm. Below this range electrical noise created errors equivalent to the magnitude of the flow velocity. Other problems were encountered with vibration isolation and temperature compensation for the strain gages. This instrument is complex both mechanically and electrically.

Summary - Impact Force/Pitot Methods

In general, the small impact forces and dynamic pressures encountered for low velocity measurement make these techniques difficult to utilize. Impact force instruments must employ elements which have small resistances to the minute impact forces in order that a deflection or strain can be measured. The instruments based on this method that are described in the literature are delicate, requiring vibration isolation. Also, an accurate estimate of the drag coefficient, the impact vane orientation and shape and flow Reynolds number is required to implement this method. As a result of this study both the pitot and impact force methods are considered undesirable for the present application.

II. 3 Convective Cooling Methods

Flow measurement with hot wires or films are based on the principle that if a gas stream is passed over an electrically heated surface the heating current, I , flowing through the surface is related to the stream velocity V . Although hot wires were specifically eliminated as possible candidates for this application, a brief evaluation is given as a basis of comparison. For low velocity flow measurement with variable environmental properties the instrument output will be affected by fluid property changes as well as natural convection effects. The theoretical velocity (Reference 7) for this situation is

$$V = \frac{\left(\frac{I^2R_w}{\Delta t}\right)^2 - 0.76k_f\left(\frac{I^2R_w}{\Delta t}\right)[N_{Pr}]_f^{0.2}K_1}{[\rho_f(C_p)_f^{2/3}k_f^{1/3}/\mu_f^{1/3}]K_2}$$

$$+ \frac{k_f^2(\{0.38[N_{Pr}]_f^{0.2}\}^2 - \{0.25([N_{Gr}]_f[N_{Pr}]_f)^{1/8} + 0.45([N_{Gr}]_f[N_{Pr}]_f)^{1/4}\}^2)K_1^2}{[\rho_f(C_p)_f^{2/3}k_f^{1/3}/\mu_f^{1/3}]K_2}$$

The velocity is observed to be a complicated function of the fluid and surface properties, and therefore this technique is considered undesirable for this application. Our own experience with hot wire systems also verifies this conclusion.

II. 4 Fluidic Method

A fluidic velocity sensor utilizes a free jet which is directly deflected by the measured flow. A fluid jet is directed from a nozzle toward two impact (total head) probes, and perpendicular to the measured flow. Thus, the flow deflects the jet, producing a pressure difference between the two impact probes. Sensor operation depends on the jet entraining and mixing with the surrounding fluid. Entrainment by the jet of a cross flow causes a deflection proportional to the cross flow velocity.

Basic design principles are founded on the experimentally verified assumptions that (1) the jet pressure profile has a linear slope over a certain span (see sketch), and (2) the jet deflection is linear with cross-flow velocity, and that this cross flow does not distort the jet dynamic pressure profile (References 8, 9).

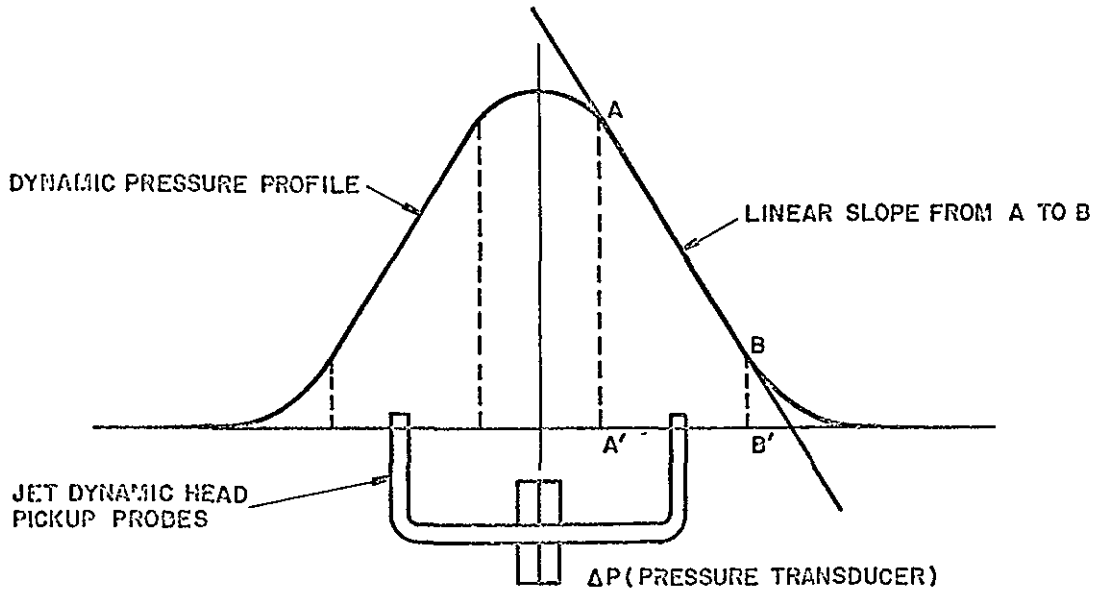

Fluidic Velocity Sensor

The two pick-up probes are centered on the jet center line, and a change in cross flow velocity will produce a force on the jet such that its deflection at any point along the jet center line is expressed by

$$y = \left(\frac{1}{2} \quad \frac{V}{T} \quad \frac{dQ}{dx}\right) \quad x^2 \tag{6}$$

where

y = jet deflection

x = distance from nozzle exit

$\frac{dQ}{dx}$ = rate of entrainment due to the jet and

T = jet thrust

This is derived from Reference 10, which assumes that since the jet thrust and the entrainment are uniform along its length, the jet can be considered as a line sink of uniform strength in the cross flow velocity field. Equation (6) holds only for low cross flow velocities, large values cause more mixing of the jet and cross flow, and hence decrease the pressure profile slope, reducing sensitivity also.

Letting L represent the pick-up probe distance from the power nozzle, Equation (6) becomes

$$y = \left(\frac{1}{2} \quad \frac{V}{T} \frac{d\Omega}{dx}\right) \quad L^2 \tag{7}$$

For a fixed nozzle thrust (T) and distance between nozzle and the pick-up probes, the deflection is linear with free stream velocity for very low values of V . Reference 10 verifies that Equation (7) is linear over the lower velocity range for certain (distance to pick-up probes/nozzle diameter) ratios L/d, and a specified (supply pressure/$P_{ambient}$) ratio.

Optimum sensitivity can be obtained by proper variation of $P_{supply}/P_{ambient}$ and L/d. A very large pressure ratio will increase the sensitivity but will cause the jet profile to be nonlinear at the pick-up probes which causes a nonlinear variation of output with cross flow velocity. Too small a value of L/d produces the same result since the jet has not had sufficient time to spread before it reaches the probes.

This instrument requires compensation for environmental pressure changes, and present designs have a lower velocity limit of 10 fpm. It would be difficult to provide omnidirectional capabilities with a single-head device, and the free jet can disturb the environment. Since this technique would be difficult to implement for the present application, it is considered undesirable.

II. 5 Optical Methods

The most promising optical method uncovered for measuring low velocities is the Laser Doppler velocimeter. Laser Doppler velocimeters have been used extensively in the study of flowing fluids. This device, first conceived by Foreman et al, (Reference 11) has since been improved and applied to such diverse measurement problems as mapping the three-dimensional fluid flow profile at the base of a Saturn rocket, (Reference 12) and the detection of clear air turbulence (Reference 13).

The operation of the laser Doppler velocimeter can be described by reference to the following diagram:

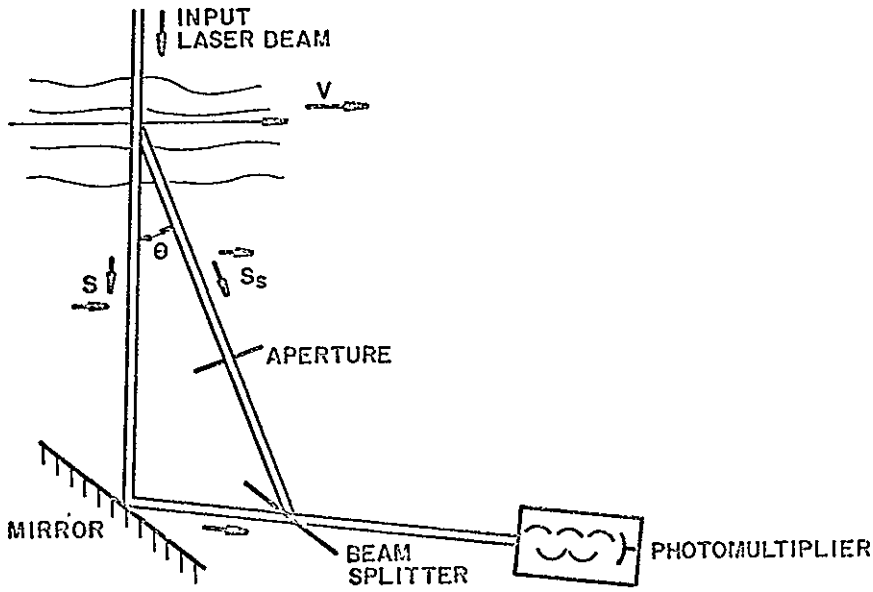

Laser Doppler Velocimeter

The incident laser beam passes through the fluid flowing with velocity V. The major portion of the beam continues through without being scattered. The remainder is scattered and this radiation is intercepted at an angle θ by a sampling aperture which helps to limit the size of the sampled volume. This scattered light which has been frequency shifted by the moving scatterers is superimposed upon the transmitted beam which has no frequency shift When the two beams are superimposed upon a square-law detector they produce a difference frequency f which is a direct measure of the velocity V of the flowing gas The velocity in any given direction is

$$V = \frac{f \lambda}{2 \sin \frac{\theta}{2} \sin \left(\phi + \frac{\theta}{2} \right)} \tag{8}$$

where ϕ is the angle between s and V.

The high accuracy, signal-to-noise ratio, and sensitivity of the laser Doppler velocimeter indicated that a study of its potential for measurement of the flow velocities in a space cabin environment might be warranted. However, instrument operation depends on the presence of contaminant particles in the measured flow field. As the concentration

of contaminant particles decreases, the probability of having sufficient numbers of scatterers within the coherent scattering volume to produce a readable velocity decreases rapidly. Calculations made for some possible extreme cases of particulate concentration indicated that it will not be possible to use a laser Doppler velocimeter for routine determination of low velocity flow patterns. In addition, this type of device would be rather bulky compared to other methods and is therefore considered unsuitable for the present application.

II. 6 Acoustic Method

Acoustic techniques have been employed to measure mass transport effects in a wide range of applications which include accurate measurement of the wind components (anemometry), and the measurement of fluid flow velocities. When employed in flowmeter applications, threshold sensitivities of 2 fpm have been reported by Kalmus (Reference 14). The accuracy of his method is dependent upon an accurate knowledge of the speed of sound. In this gas flow application, where a range of gas compositions and temperatures are likely to be encountered, it is doubtful that simple electronic techniques can be found to compensate Kalmus' method for changes in sound speed. An alternate acoustic technique, similar to that reported by Brown, (Reference 15) that does not require knowledge of the speed of sound, and uses electronic leverage and averaging for additional accuracy and resolution. This acoustic technique is inherently independent of pressure and density, and the fact that the speed of sound is not required further implies that it is independent of temperature and gas composition. Therefore, this method appears especially suited to the present application.

In practical applications of this technique, two oppositely directed source-receiver combinations are separated at a distance X, and each pair operates at a distinct transmitter frequency. The flow velocity is determined by

$$V = \frac{X}{2} \quad (f_1 - f_2) \tag{9}$$

where f_1 and f_2 are frequencies associated with the transit periods required for the wave front to travel with and against the flow respectively. Initial paper studies of this method concentrated on evaluating the two expected major sources of errors, (1) the effects of the velocity defects in the wakes produced by the transducer and receiver supports and (2) uncertainties in the transducer separation distances, and subsequent time delays

in the electronic frequency counters. The results showed that the accuracy of the acoustic method decreases as the separation distance decreases, indicating a minimum sensor head size to meet the required accuracy. However, it appeared that this method could meet the specifications in this application, and this technique was chosen for additional studies.

Additional information on the theory and application of this technique is given in the acoustic evaluation section of this report.

II. 7 Tracer Methods

Tracer methods present a direct measure of flow velocity by measuring the time required for a tracer to travel a known distance. Two tracer techniques applicable to measuring low velocities utilize either a heated gas (Hot Spot Anemometer) or ion cloud (Ion Discharge Anemometer) as tracers

Evaluation of the Hot Spot Anemometer

The state-of-the-art for the hot spot anemometer (HSA) is apparently represented by the work of Kung and Binder (Reference 3). Therefore, the following is based on an evaluation of this work, plus additional comments based on our own laboratory work to answer additional questions about this technique.

The HSA is a gas tracer device which employs a heated "spot" of gas to define a "point" in the moving flow, and measurement of the transient time of this spot between two sensors gives a direct indication of velocity. Ideally this method gives an absolute velocity indication, meaning no calibration should be required. In actual practice, however, the method is subject to two sources of error which cause difficulties when measurements below about 10 fps are attempted. These errors are (a) dispersion of the heated gas, and (b) buoyancy of the heated gas

Judging from the results of Reference 3, the relative importance of these errors depends on how the device is implemented. In Reference 3 the method of measuring transient time inherently produced a large error from dispersion, while the effect of buoyancy in their experiments was not so severe. Roughly speaking, their results showed an error of about 20 to 30 fpm because of dispersion and about 5 fpm because of buoyancy.

Had transient time been measured differently by these authors, the error attributable to dispersion could likely have been reduced by an

order of magnitude. Their circuit employed a time measurement system which triggered initially from the pulse to the heating wire and was stopped by the initial rise of the sensor output pulse. The resultant measured time, t_1, was actually smaller than the true hot spot transient time (shown as t_2 in Figure 3) by some amount Δt. Thus, their system gave uncorrected output velocity readings which were too high by roughly a constant amount. In fact, their system gave an uncorrected output of about 20 to 30 fpm when the velocity was actually zero.

Had Kung and Binder used a trigger circuit which sought the peak of the sensor output (giving approximately time t_2), their results would have been much better, and errors from dispersion would have been of second order rather than of first order. Using such an improved triggering system, the error from dispersion would have been reduced to the order of 3 fpm, and the system could have read zero velocity.

However, the major problem with this method will be correcting for buoyancy when making vertical velocity measurements. Estimates of the criticality of the buoyancy problem were determined in our laboratory. Measurements of the buoyant velocity were made by placing a 0.7 mil platinum detector wire directly above a heated 10 mil tungsten wire and recording the rise time of the heated cloud at various vertical distances above the heat source. Current to the heated wire was adjusted to a level such that the detector wire would record a clear signal when the heated cloud passed. Results indicate that the vertical buoyant velocity was of the order of 30 fpm at distances up to 1/2" above the heat source. Results in Figure 4 show that with a buoyant velocity vector, V_b, of 30 fpm, even at separation distances, x, of 1/16", appreciable deflection of the hot cloud from the horizontal flow direction can occur, especially at flow velocities below (20-30 fpm). Reducing the current to the heat source will reduce the buoyant velocity vector but will result in a weaker detected signal. Correcting for buoyancy in a unidirectional instrument would be difficult, and contending with buoyancy problems in developing an omnidirectional instrument based on the hot spot method, makes this approach highly undesirable. Therefore, this method is considered undesirable for the present application. It may have merit, however, for applications near zero gravity and might be considered in the future for this purpose.

Ion-discharge Methods

Three different techniques utilizing ionized gas are available to measure gas velocity with only one being truly a tracer method One method (Reference 16) measures the change in discharge current across

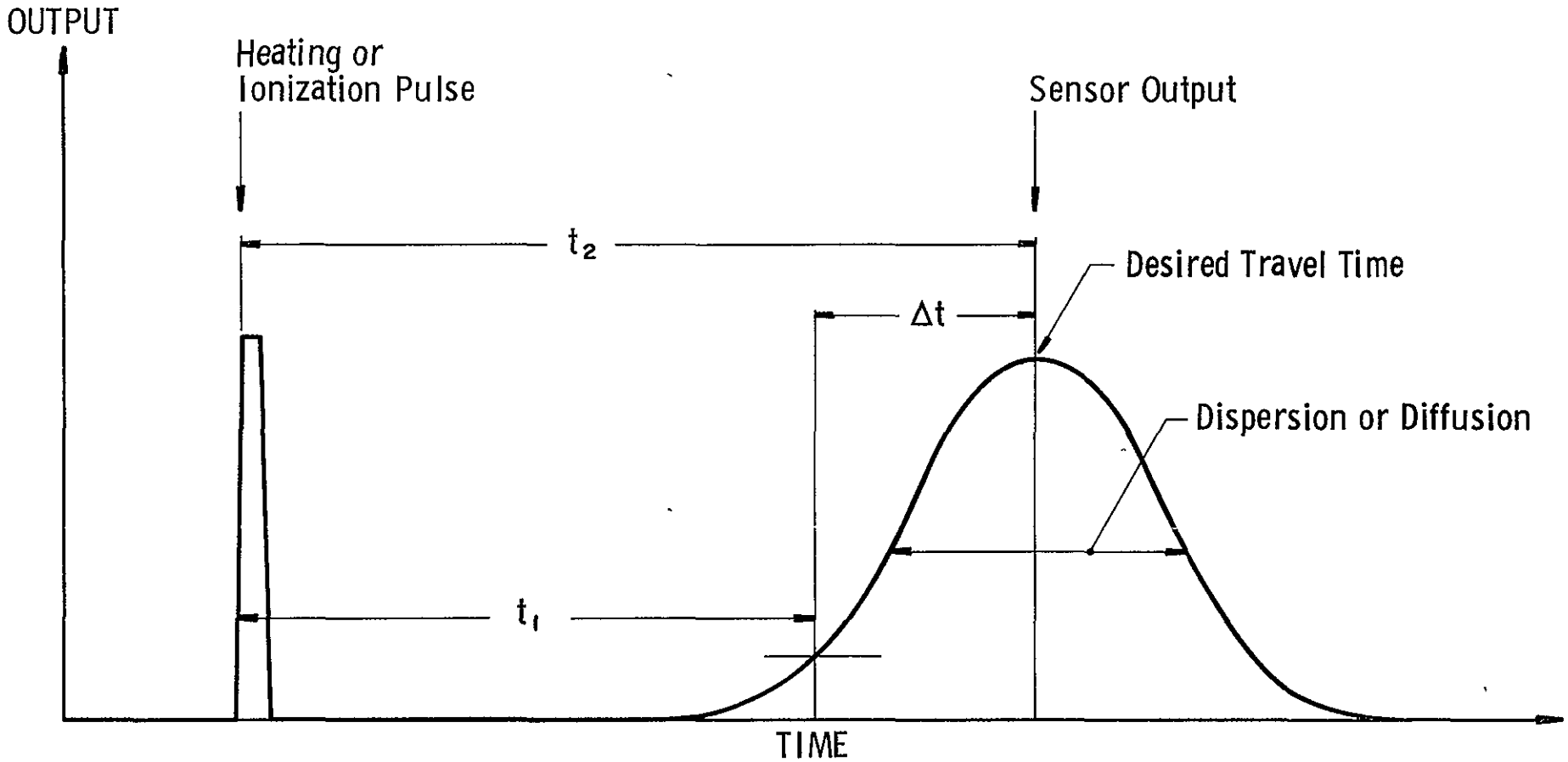

t_1 = Time measured by Kung-Binder electronics (Reference 3)

t_2 = True transient time of hot spot or Ion Cloud

3119

Figure 3. Desired Travel Time with Ion or Hot Gas Tracers

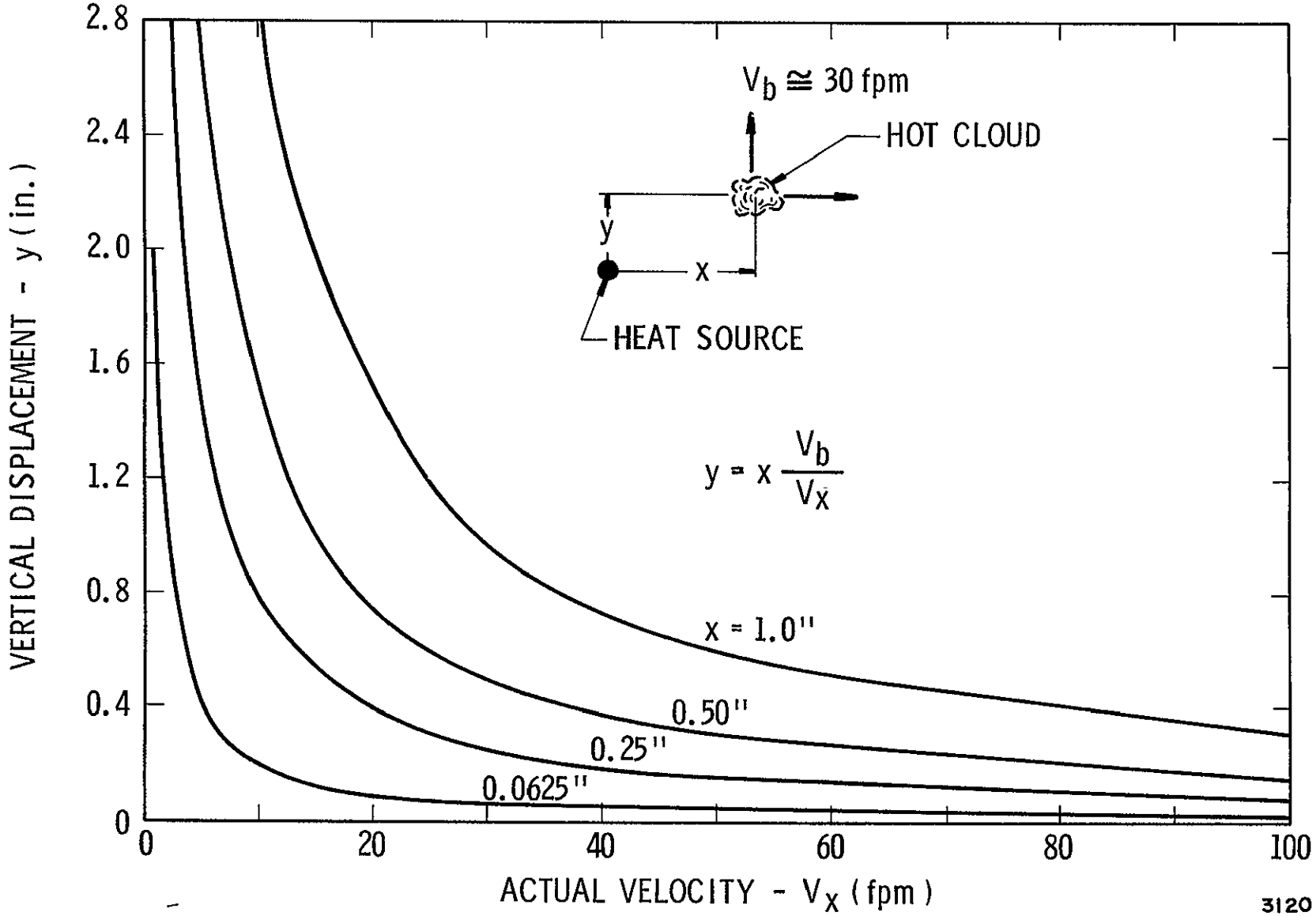

Figure 4. Deflection of Hot Gas Tracer Due to Bouyancy

an electrode gap maintained at high potential, when air flows through the gap altering the ionization characteristics. This technique was found to be greatly affected by pressure and humidity changes, and had poor velocity sensitivity. Since the velocimeter for the present application must operate over a wide range of environmental conditions, and have good velocity sensitivity, this method of utilizing an ion-discharge is considered undesirable.

A second method, which uses ions to determine flow velocity, is based on the principles described in Reference 17. The operational characteristics of an instrument utilizing this technique is determined by the deflection of an ion beam moving between an ion source and a tightly wound resistor.

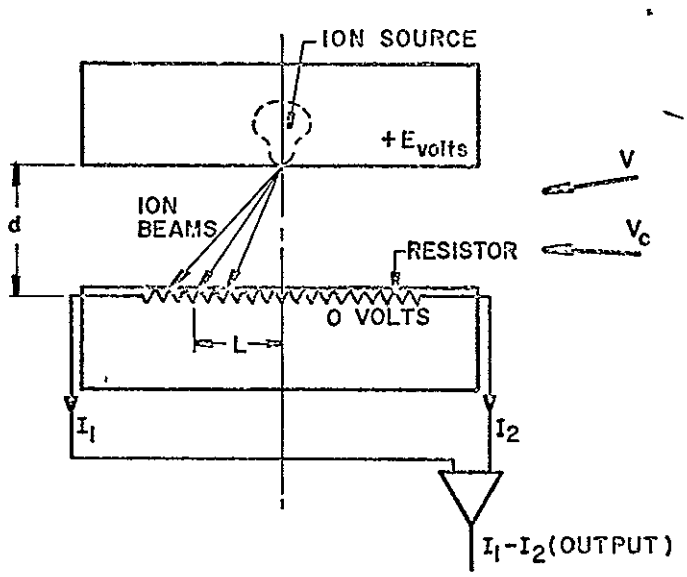

Ion Drift Anemometer

The ion source of this device (see sketch) is located in one wall of a set of parallel plates from which the ions are emitted and then drift under the influence of an electric field to a second plate located at a distance, d , which contains the resistor. A potential is placed across the plates producing a uniform electric field, and the ions move across the gap with a drift velocity given by

$$V_d = Z \frac{E}{d} \tag{10}$$

where Z is the ion mobility, E the gap potential and d the height between the resistor and ion source. Gas flowing between the plates deflects the ion drift velocity vector, and causes the ions to impinge on the resistor at different points when the flow velocity changes. Measuring the difference in microampere current in both legs of the resistor allows the velocity to be determined. The landing distance, L , of the median ion in the ion sheet is given as

$$L = \frac{d^2 V_c}{ZE} \tag{11}$$

where V_c is the longitudinal gas velocity component between the plates.

To ascertain if the ion deflection technique would be practical, at the extremely low velocities for this program, the deflection of the ion beam was calculated for reasonable values of the parameters in Equation 11. The deflection L was calculated to be 2×10^{-4} inches for:

V_c = 1 fpm

d = 3/4 inch

Z = 0.4 m/sec/volt/m

and E = 1 volt.

This extremely small deflection occurs when only 1 volt is applied between the plates. Normally, an instrument of the type described above uses a much greater voltage between the plates (up to 10 KV) which would create an even smaller deflection due to a larger drift velocity relative to the flow velocity. In addition, the deflection is dependent on the ion mobility, Z , which varies with gas properties. It is therefore concluded that this technique is probably undesirable for the present application since, (1) extremely small deflections of the ion beam will occur at the low velocities producing a negligible change in the current flow in the resistor, and (2) compensation for atmospheric changes will be required since the ion deflection is dependent on ion mobility. Also, the technique is essentially unidirectional and would require three components to provide omnidirectional capabilities.

The third method utilizing ionization, is a direct method where ions are used as tracers and velocity is monitored by recording time between a pulsed ion discharge and a detector plate response. The ion

tracer method does not suffer from the buoyancy problems or delicate detector probes required of the hot spot method. This technique has been successfully implemented to measure low density air flow in a high altitude balloon (Reference 18) as well as in atmospheric conditions on the ground (Reference 19). In both cases gas velocities higher than the (0-100) range of this program were measured by monitoring the electrode pulse frequency when the electrode was triggered by the detected signal. Since the ion travel time is only dependent on gas velocity and probe separation distances, the instrument frequency response is independent of environmental changes. Using this technique to determine flow velocity requires (1) detecting the peak of the passing ion cloud to eliminate diffusion effects (Figure 3) and (2) adjusting the discharge electrode voltage to maintain a uniform level of ionization when atmospheric conditions change. This technique appears especially suited to the present application since no lower limit on velocity measurement is imposed by the operational characteristics of the instrument. The only compensation required will be the adjustment of discharge probe voltage to maintain ionization of the gas where large changes in atmospheric conditions occur. Subtle changes in atmospheric conditions (pressure or temperature) will cause a slight change in the density of the detected ion cloud but will not affect its travel time. Therefore, the instrument accuracy will be unhampered. Providing proper ionization of the gas at different atmospheric conditions requires adjustment of the discharge electrode voltage to maintain a constant discharge current. This can be easily accomplished with a constant current power supply which would also eliminate the possible danger of a spark-over hazard by maintaining voltage below the spark breakdown level. The ion-discharge tracer method also lends itself to providing a single head omnidirectional instrument by using a porous spherical detecting surface. Additional information and details on the operational characteristics of this type of instrument are given in the ion-tracer evaluation sections of this report.

II. 8 Initial Candidate Selections for Additional Study

After considering all the advantages and disadvantages of the methods reviewed in the previous sections, the acoustic and ion-tracer techniques appeared to be the best methods to meet the instrument specifications in this program. The acoustic method was chosen because it is inherently independent of gas properties and the ion-tracer method because it provides a direct (tracer) technique also independent of gas properties once proper ionization is established. One-dimensional bread-board laboratory models of both methods were constructed and tested to demonstrate if either or both of these instruments could meet the low velocity measurement requirements. The remainder of the report is devoted to the experimental evaluation of these two techniques.

III. LOW VELOCITY TEST FACILITY

Accurately known air velocities in the range of interest of this program, 0 to 100 fpm are difficult to obtain, especially near zero velocity. One technique reported in the literature, that has been successfully implemented to obtain well defined low velocities, consists of forcing displaced air out of a test section attached to a sealed tank by adding water to the tank reservoir. An experimental test facility based on this principle was constructed for this program. A schematic of this facility along with pertinent test facility information is given in Figure 5 and an overall view of the completed facility is shown in Figure 6. A six inch and a three inch test section are available for testing low velocity measuring techniques. Accurately calibrated rotameters establish the water flow rate into the tank, and the tank reservoir is of such a size that extremely long run times are available at the low test velocities. The average velocity in the test section is given by

$$V_1 = \left(\frac{T_w}{T_1 \quad A_1} \right) \text{ X } (H_2O \text{ Flow Rate}) \tag{12}$$

where A_1 is the test section area, and T_w/T_1 the ratio of water to air temperature. A complete set of thermocouples provide temperature gradient data so thermal effects may be compensated. The velocity profiles in the test section were determined with conventional hot wires before actual testing was initiated. Test section velocity profiles were obtained for both the three inch and six inch test sections. Horizontal and vertical traverses were made four inches from the entrance and at the test section exit for each size test section. The results shown in Figure 7, for the six inch test section, reveal an essentially flat profile over the central portion of the tube and little distortion is apparent between entrance and exit profiles. Calculations based on laminar flow in the entrance of a pipe indicate that for the diameter and length test section chosen, the profiles should be uniform over the majority of the cross section and very little distortion in the axial direction will occur, confirming the experimental results. Also, horizontal and vertical profiles obtained at a given position along the tube axis are identical, indicating a symmetrical flow pattern about the tube axis. The smaller three inch tube exhibits the same profile characteristics as the larger tube.

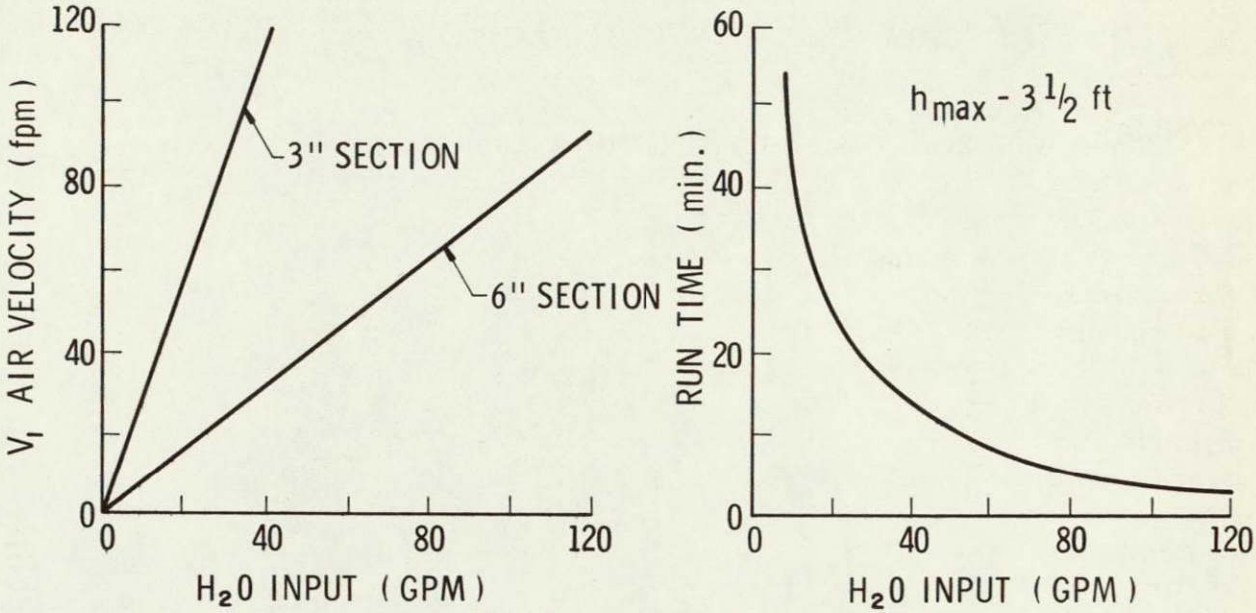

(a) Velocity and Run Time Capabilities

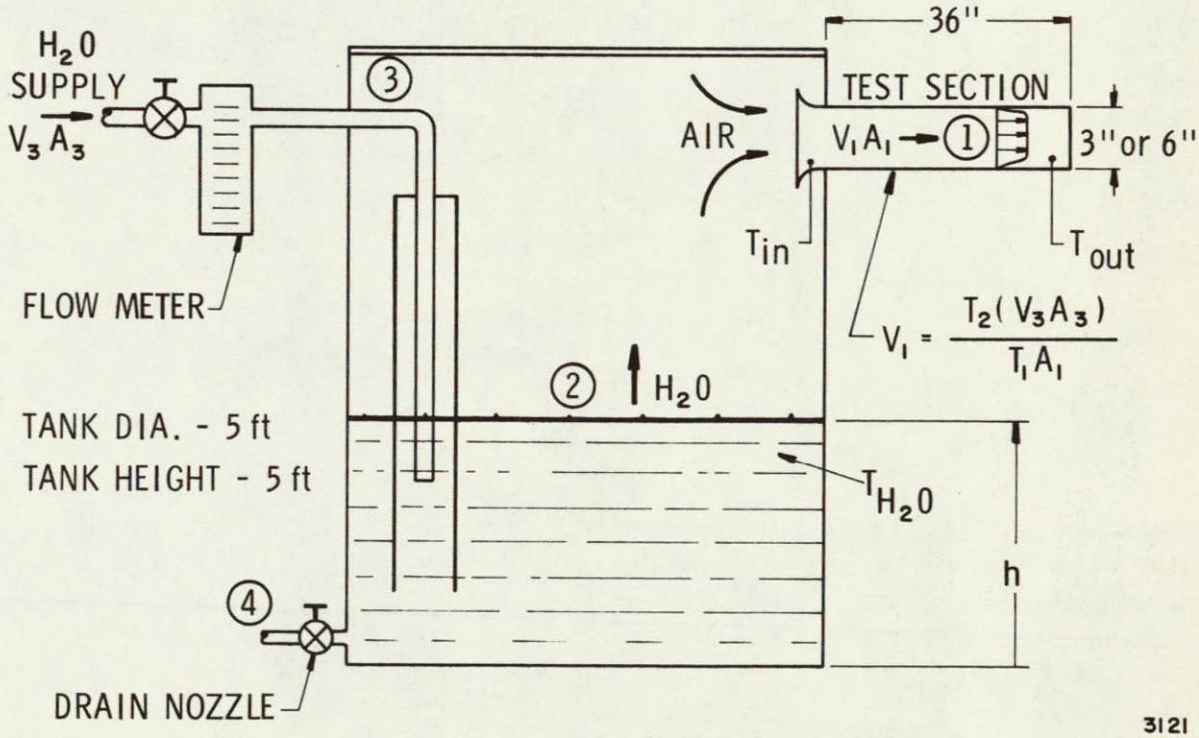

(b) Flow Facility Schematic

Figure 5. Low Velocity Flow Facility Information

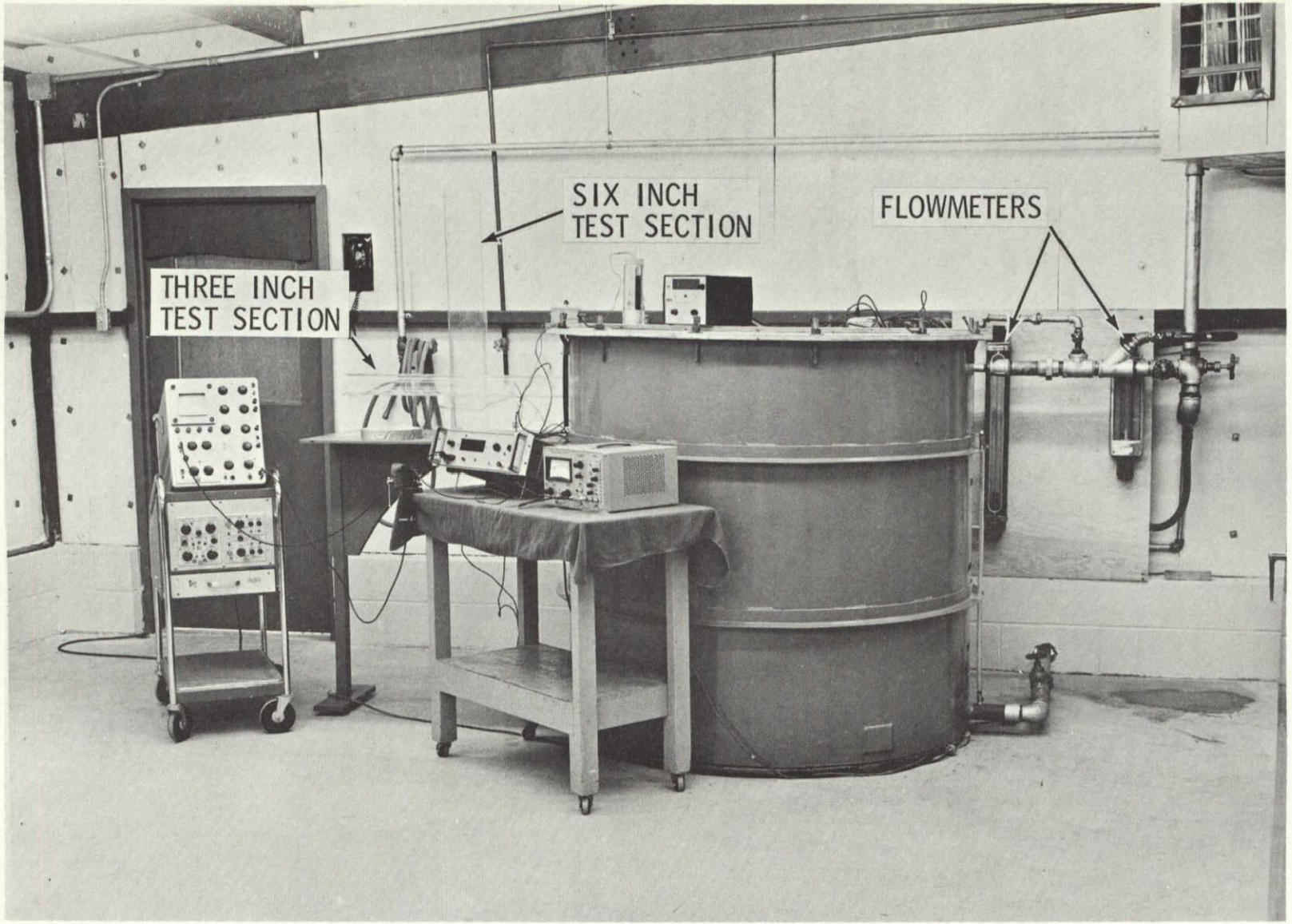

Figure 6. Low Velocity Test Facility

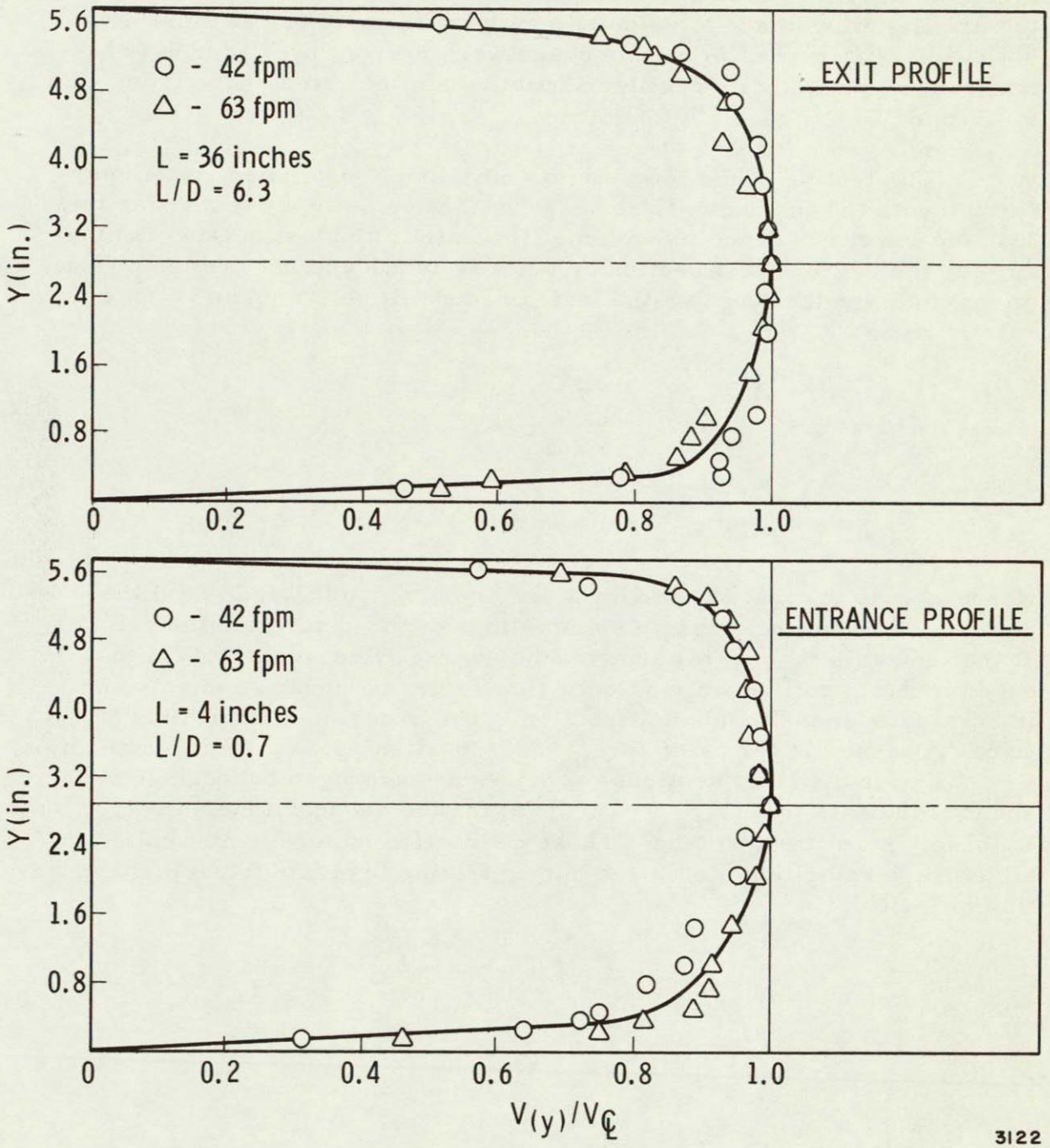

Figure 7. Test Section Velocity Profiles - Large Test Section (Di = 5.72")

The velocity profiles were obtained with a hot-film anemometer whose output was approximately linear over the velocity range measured. Since the hot film would not provide accurate velocity data below 40 fpm, the profiles were made at velocities ranging from 40 to 100 fpm. No noticeable differences in profile shape were present over the 40-100 fpm range, and velocity profiles should retain the same shape from 0-40 fpm.

The testing of the low velocity measuring instruments was performed with the instruments reading the flow velocity along or near the test section axis. Since the volume flow rate to the test section is monitored, the average test section velocity is known and not the center line or maximum velocity which the instruments will sense. The volume flow rate is given by

$$Q = \int_0^r 2\pi y \quad V(y) \quad dy \tag{13}$$

or

$$V_1 = \frac{2\pi}{A_1} \int_0^r y \quad V(y) \quad dy \tag{14}$$

where A_1 is the test section area, r the tube radius and V (y) the velocity distribution across the tube. In order to determine the velocity at the tube axis (V_{max}) in terms of the average flow velocity (V_1) the experimental profiles were fitted with a series of linear segments and integrated over the tube cross section. The experimental profiles (V (y)) were expressed in terms of V_{max} and Equation 14 was used to determine V_{max}/V_1 for both test sections. The results averaged between entrance and exit indicate that ($V_{max}/V_1 = 1.05$) for the six inch tube and ($V_{max}/V_1 = 1.08$) for the three inch tube. These correction factors were applied to all average velocities monitored during testing to obtain the actual sensed flow velocity.

IV. ION-TRACER ANEMOMETER

IV. 1 Introduction

The ion-tracer anemometer (ITA) operates on the principle of measuring the time required for an ion cloud tracer to travel between an ion-source and a detector located a distance d from the source. The average fluid velocity is then determined by the travel time t and separation distance d . The ion-tracers can be provided by various techniques such as radiation, or electric discharge, and the ion detection can be accomplished by induction or ion collection.

The essential requirements for providing a workable system are:

(1) Small transit times to minimize diffusion effects (implies that diffusion velocity is much less than flow velocity);

(2) Large transit time compared with ion-production time;

(3) High density of ionization so detected signal is strong enough to differentiate from system noise;

(4) Small ion collection time compared to transit time;

(5) Ability to detect the peak of the received signal;

(6) A high fidelity of the ions following the gas stream.

The successful implementation of this technique has been reported in References 18 and 19, but for applications considerably different from that of the present efforts. The instrument described in Reference 18 was designed to measure velocities from 15 to 150 fps in low density high altitude air. The instrument described in Reference 19 was designed to measure gas velocities from 30 to 600 fps for normal atmospheric conditions. Ionization in Reference 18 was produced by a glow discharge while Reference 19 utilized a spark breakdown ionization source. In both applications the ionization source was triggered by the detected signal, and the pulse frequency was monitored as a function of flow velocity. Since this technique was proven successful at both low (< 1 psia) and atmospheric pressures,

and no foreseeable limitations on measuring low velocities appeared to exist, the chances of using this technique to meet the specifications in this program appeared excellent. Therefore, an experimental ion-tracer model was constructed and tested in the low velocity flow facility to determine if this technique was practical for measuring velocities from 0 to 100 fpm.

IV.2 Experimental Model

The experimental ion-tracer anemometer (ITA) consists of 2 basic elements, an electric-discharge ionization system and an ion-collection detector system. The experimental ion discharge circuit is illustrated in Figure 8a. This setup consists of (a) an electronic system to provide the pulsed ionization potential, and (b) the ionization probe.

The electronics for the pulsed ionization system include (a) a variable frequency, low voltage ($\sim$5v) pulse source, (b) a pulse amplification and shaping circuit, (c) a power transistor, and (d) a pulse transformer with a winding ratio of about 1000:1. This system provides a variable amplitude, frequency and pulse width ionization current between the electrodes of the ionization probe. Typically, the ionization current may be varied up to about 10 ma, and the pulse frequency may be varied from 0.2 to 1000 pulses per second. The pulse width depends on frequency and shaping employed, but generally is less than 1/100 of the pulsing period. Depending on the probe configuration and spacing, the system current may be adjusted from below the ionization level, up through the spark breakdown point.

The ion detector circuit shown in Figure 8b simply consists of a high input impedance, high gain differential amplifier coupled to the detector probe circuit. The probe circuit contains two metal electrodes with a battery in series on one leg to provide detectable current when the ion cloud passes between the probes.

The circuitry described above provided initial experimental results with a constant pulse rate from the pulse source. The output of this device was the time period from start of the ionization pulse to the peak of the output signal, as observed on an oscilloscope. This initial version allowed the detected signal response to be studied while varying the detector probe voltage, separation distance, discharge electrode geometry and voltage, and signal amplification and processing. Once the received detector signal was optimized and its response to flow velocity determined,

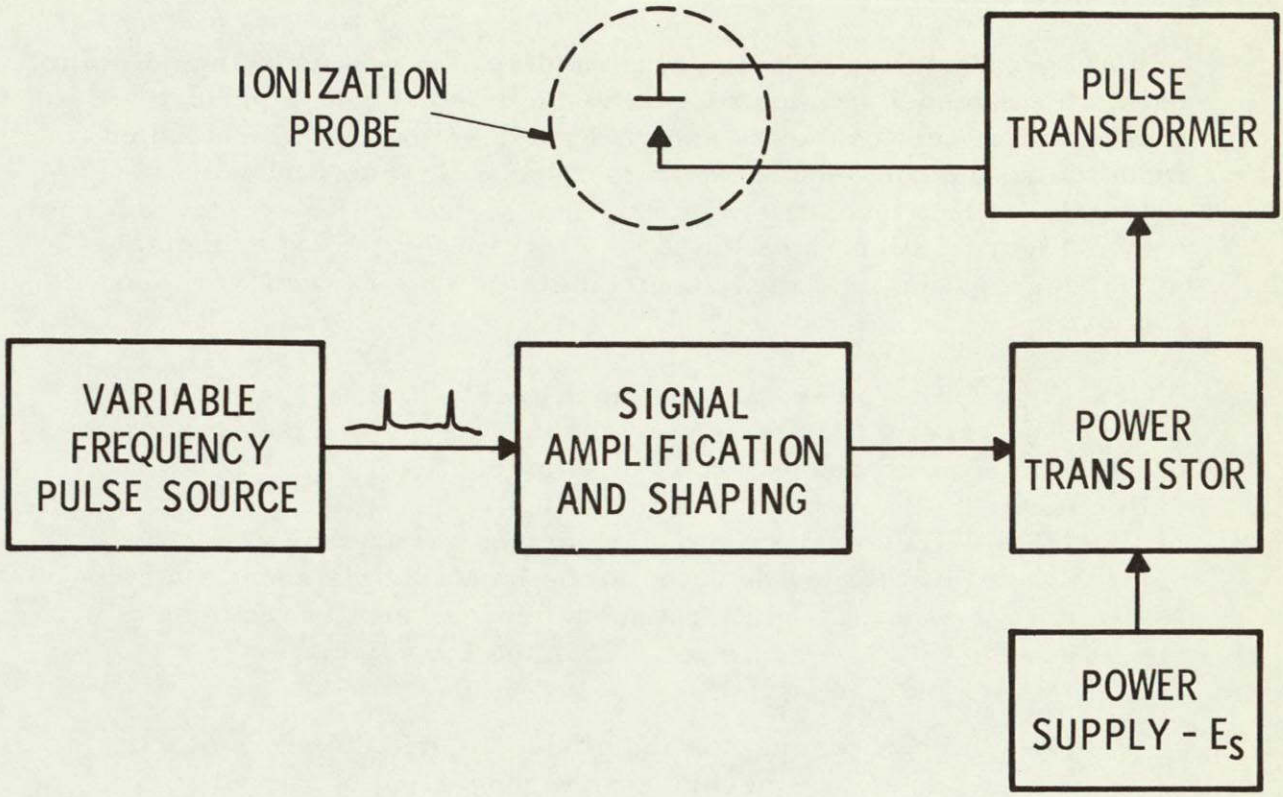

(a) Pulse Ionization Circuit and Ionization Probe

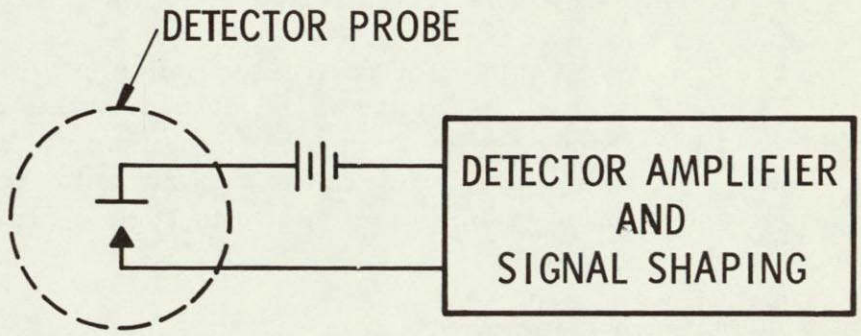

(b) Ionization Detector Circuit

3123

Figure 8. Illustration of Preliminary Laboratory Ion Tracer Device

then a more complicated pulse regenerative ITA was constructed. The basis of this model was to process the detected signal to provide a voltage spike identical to the external pulse source, so the detected signal could then be used to re-trigger the ionization probe.

Figure 9 illustrates the block diagram for the experimental pulse regenerative ion-tracer anemometer. This system works as follows:

(1) The pulse circuit, upon receiving a trigger signal from the starting or shaping circuit, causes the ionization probe to pulse discharge.

(2) The resultant cloud of ionized gas is carried by the flow to the detector probe located a distance d downstream. This transport process ideally requires a time $t = \frac{d}{V_i}$ where V_i is the ion velocity.

(3) Upon sensing the ion cloud, the detector circuit will cause re-triggering or regeneration of the pulse circuit. Hence, a regeneration pulsing frequency $f = V_i/d$ is established.

(4) If the regenerative action is broken, the starting circuit may be used to provide a periodic triggering of the pulse circuit, until the regenerative action is restored.

The breadboard circuitry for the various elements in the block diagram of Figure 9 is given in Figure 10. Obviously, this circuit could be compacted with a proper design to reduce the number of operational amplifiers required. An overall view of the experimental equipment, with the important elements labeled, is shown in Figure 11.

Electrode and Detector Geometry

Ionization of a gas can be accomplished by applying a high electric potential across an electrode gap. Usually one electrode is small compared to the other so that a highly concentrated electric field strength exists in the vicinity of the pointed electrode. This high energy field accelerates electrons and causes the gas in the gap to breakdown into an ionized state.

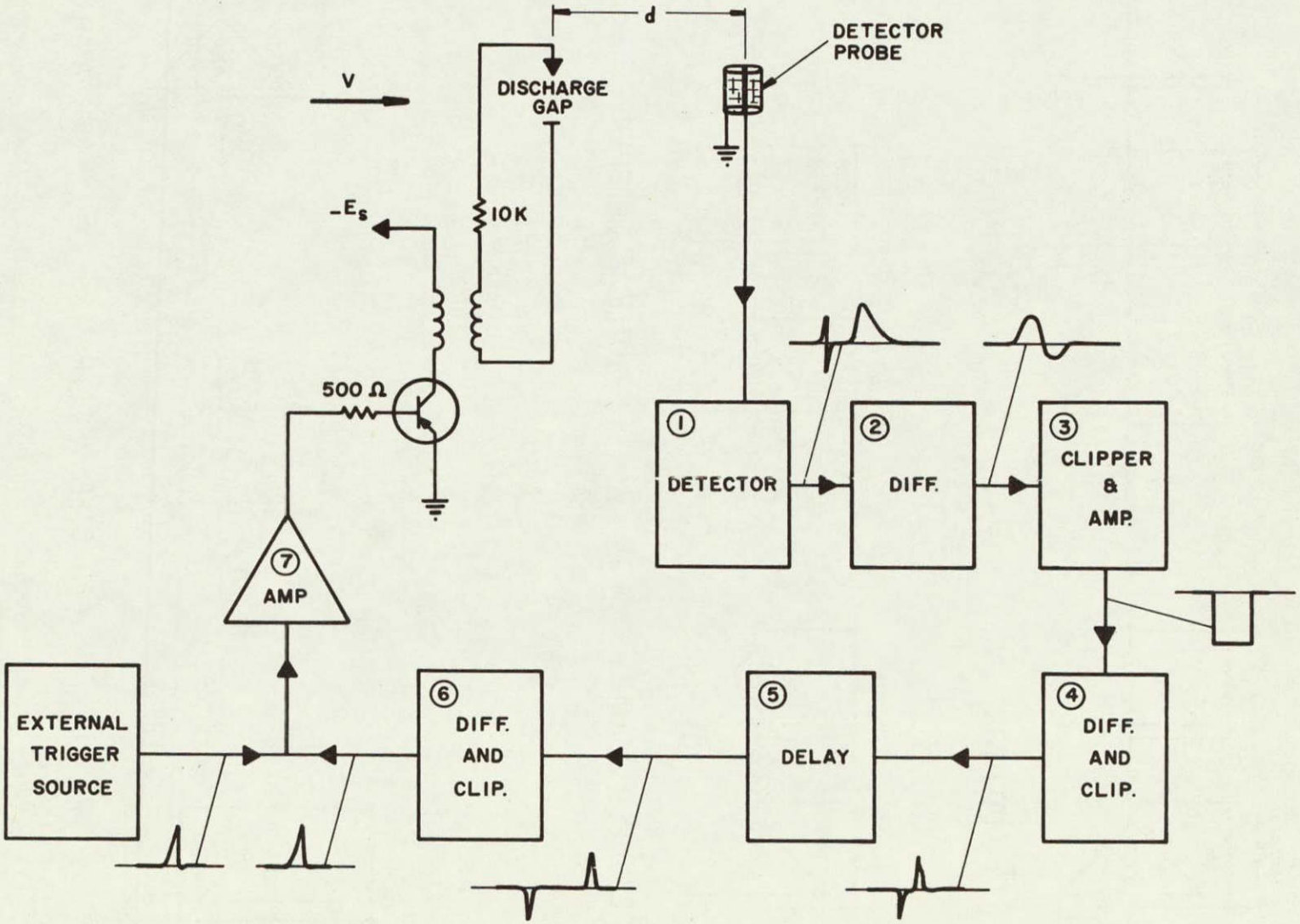

Figure 9. Block Diagram of Pulse-Regenerative ITA

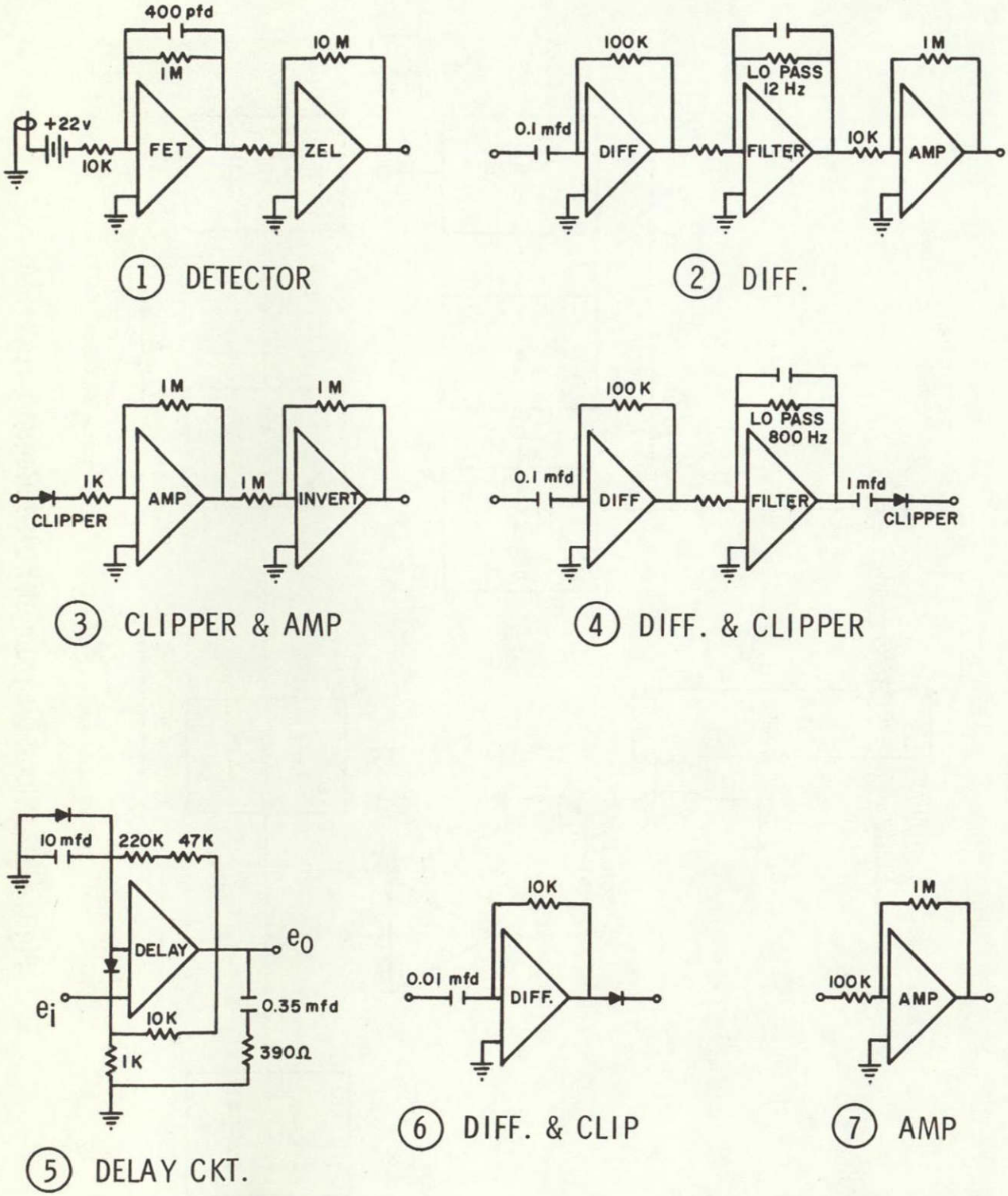

Figure 10. Detector and Signal Processing Circuitry

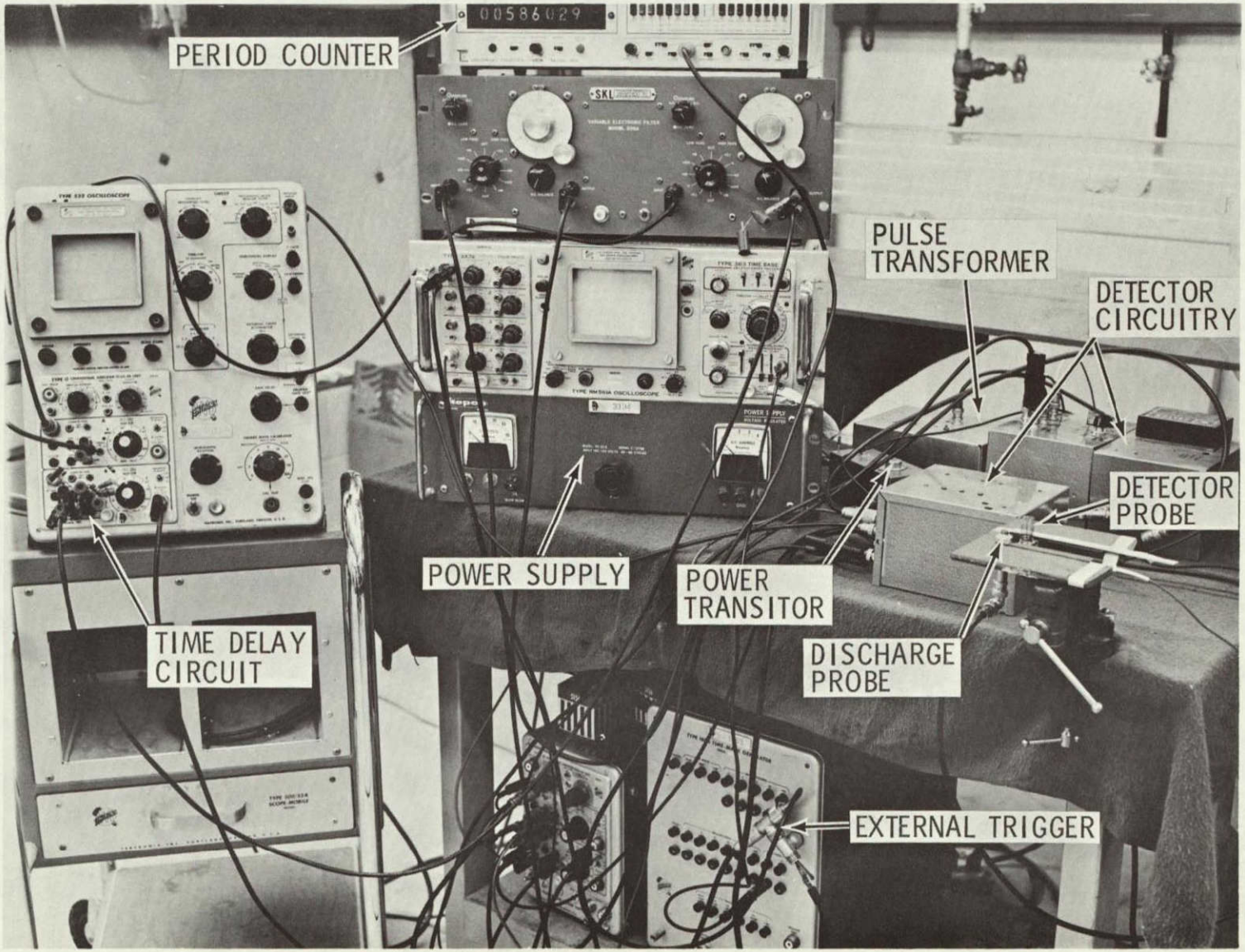

Figure 11. ITA Test Equipment

The detection of these ions can be accomplished by collection or charge induction. If a net charge is present because of an excess of ions of one polarity, the ion cloud passage can be detected by charge induction. With charge induction the ions do not have to physically contact the detector but only need to pass in close proximity. A voltage is induced in the detector circuit because of the net charge in the ion cloud.

If ionization of the gas produces little or no net charge (equal numbers of positive and negative ions) then ion-collection must be used to detect the ion passage. The ions must physically contact the detector surface, and a voltage of a certain polarity is used to attract and collect ions of the opposite sign, thus creating a signal voltage. Both ion collection and induction have been successfully utilized to detect the presence of ions. Ion collection was used in References 18 and 19 since ions of both polarities existed in the ionized gas tracer.

The ionization and detector probes used in this study are shown in Figure 12. A variety of ionization and detector probe geometries were tested to determine the best configurations to provide maximum ionization and detection.

The probe which provided the best ionization (Probe A, Figure 12a) consists of a point-to-cylinder configuration. The point ionization electrode is centered inside of a 0.25 inch cylinder at ground potential with the pointed electrode facing the open end of the cylinder, and recessed slightly from the plane of the opening. When a high potential is applied between the point and the cylinder, air around the point is ionized because of the highly concentrated electric field at the point. The voltage pulse at the electrode is adjusted to provide a corona discharge as evidenced by the purple glow and ticking noise around the electrode tip. Other ionization probe geometries investigated included, point-to-plane, concentric cylinders, and cylinder-to-plane configurations. While these alternate geometries did ionize the gas, the amount of ionization with the same input voltage pulse was not as great as with the point-to-cylinder configuration, and this geometry was chosen for final testing.

The detector probe geometries (Figure 12b) consisted of, Probe D, a cylindrical detector, Probe E, a parallel plate detector, and Probe F a circular epoxy coated disk detector. Probe F was coated with epoxy so that no metal was exposed to the ion cloud. This probe was tested to determine if ion detection by charge induction was possible. Tests with this probe revealed a very weak detected signal compared to the signal with Probes D or E. Therefore, it was concluded that ion-collection

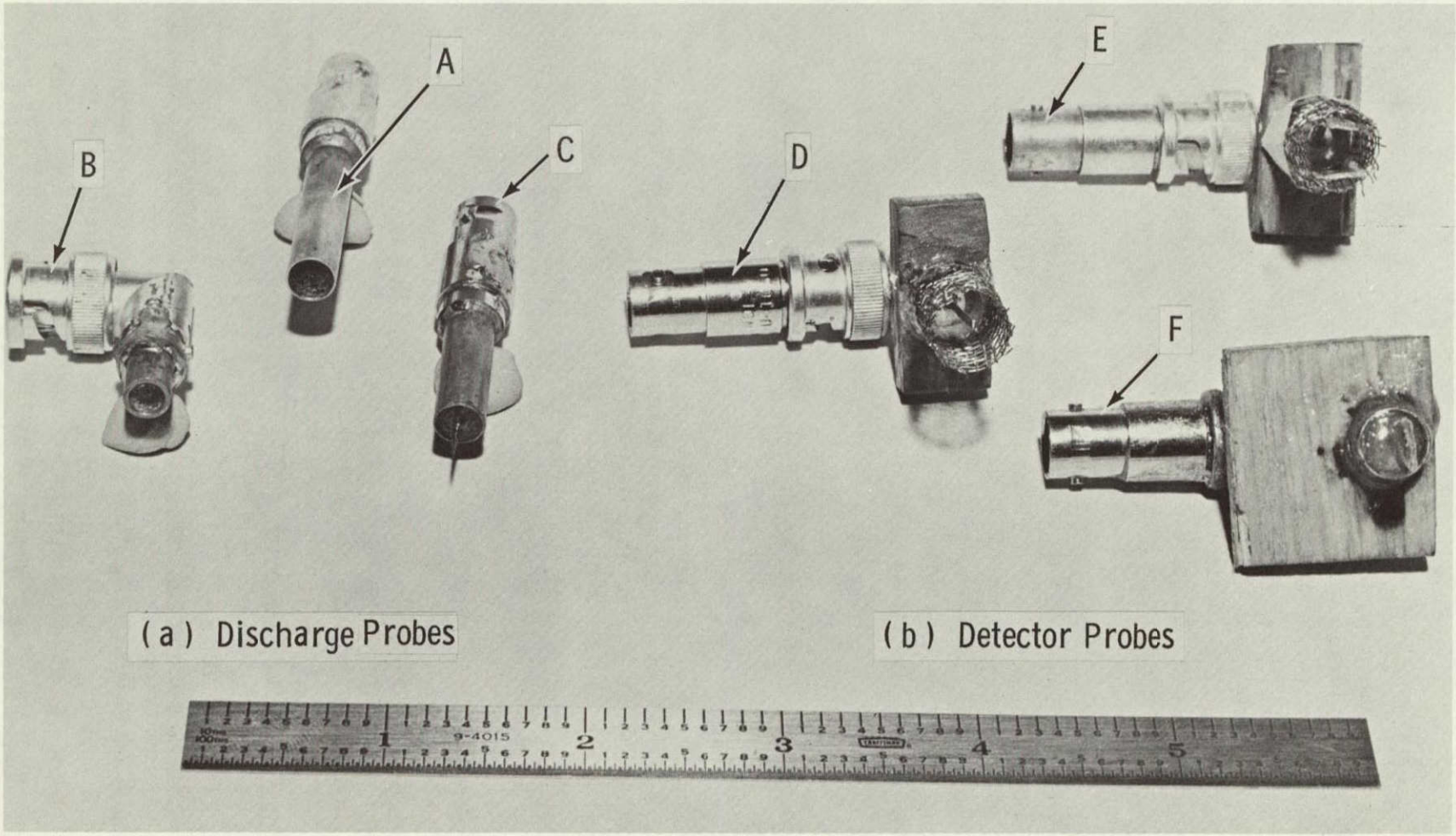

Figure 12. Discharge and Detector Probes

was required as a detection means in the present model. The parallel plate detector probes were designed so the electric field caused by the detector probe voltage would be aligned perpendicular to the direction of gas flow, and therefore ion-acceleration, caused by the detector probe voltage, could be eliminated. The signal responses of Probes D and E were equivalent, but the larger surface area of the parallel plate detector created more noise in the detected signal. Both detector Probes D and E required a wire mesh shield to eliminate 60 Hz noise in the detected signal. Probe D was chosen as the best detector design, and was used in all subsequent testing.

Detector Probe D consists of a 1/16 inch cylindrical rod surrounded by a wire mesh at ground potential. The detector probe voltage, necessary to obtain a sharp signal from the passing ion cloud, can be varied from 0 to $\pm$ 22 VDC. The discharge and detector probes are arranged on a support frame and the separation distance, d can be varied from 0.5 to six inches to establish the effects of probe separation distance.

IV.3 Experimental Results

Detected Signal

The objective of the initial testing of the ITA model was to oscillographically observe the detector response, and adjust the various ITA parameters until a strong detected signal was realized over the 0-100 fpm range. The strength of the detected signal was dependent on the transit time required for the ions to travel from the discharge to detector probe. Increased transit times created a greater diffusion of the ion cloud, resulting in a lowering of the peak signal voltage and a spreading of the detection time interval. Increased transit times occurred when the flow velocity was decreased, or the probe separation distance increased. The effects of flow velocity on signal response for a given separation distance are shown in Figure 13a. The effects of separation distance at a given velocity are shown in Figure 13b. In Figure 13 the signal response curves are actual traces taken from oscilloscope photographs, and the effects of increased ion diffusion with decreasing velocity, or increasing separation distance, are evident.

In addition to the expected effects of velocity and separation distance on detected signal shape, there was an unexpected response (curve d in Figure 13a) at zero flow velocity. At a given separation distance, the strength of the zero velocity signal was found to depend on the detector probe voltage, E_p. It was initially assumed that the signal was the result of ion attraction by an electric field between the detector probe and discharge

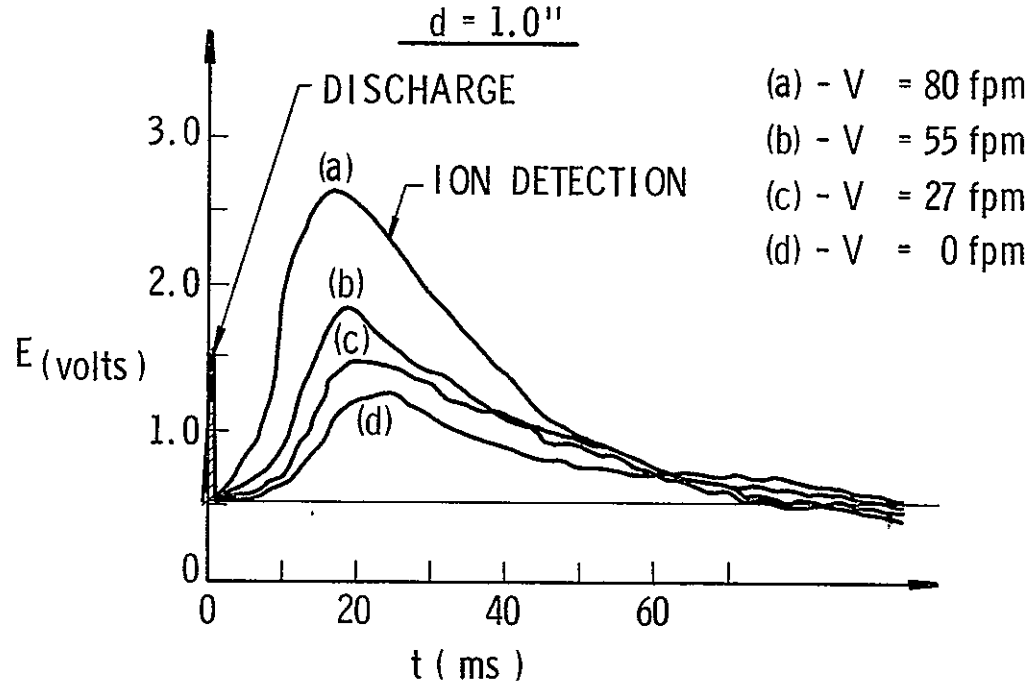

(a) Detected Signal with Flow Velocity Change (d = cons.)

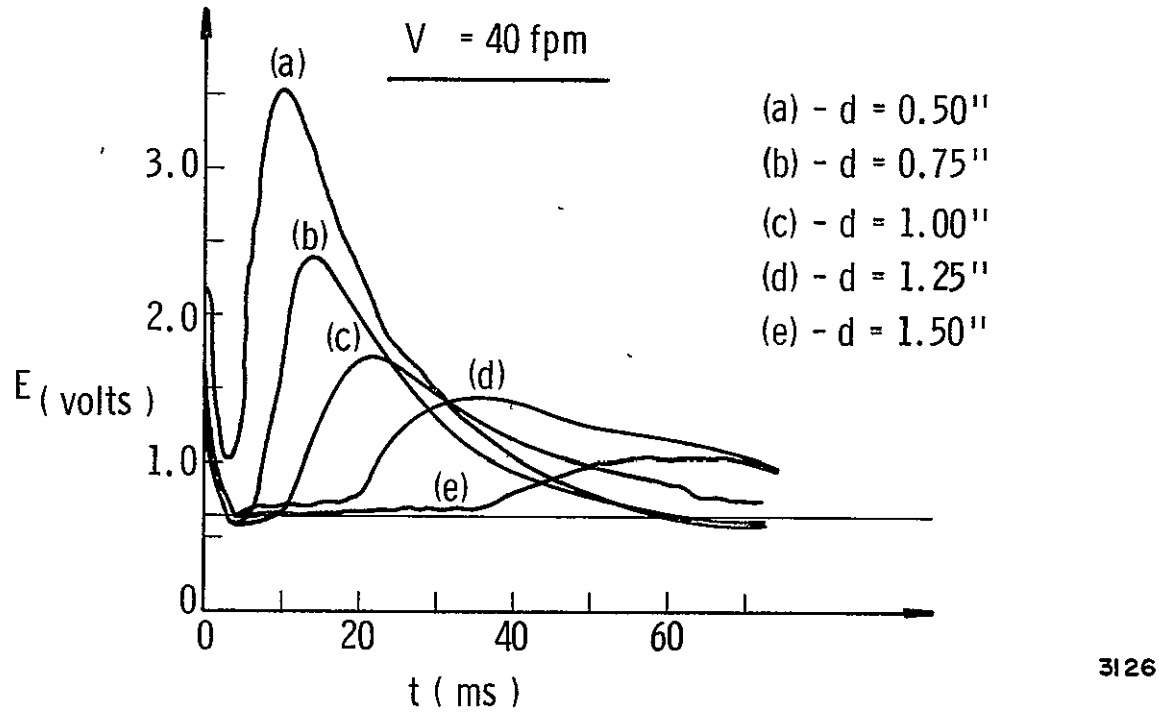

(b) Detected Signal with Separation Distance Change (V = cons.)

Figure 13. ITA Detected Signals Reproduced from Actual Oscilloscope Traces

probe, created only by the detector probe voltage. However, the same ion drift was observed with the parallel plate detector when the detector probe field was aligned perpendicular to the flow direction. Therefore, it was concluded that the ion drift at zero velocity was the result of a stray field that exists between the high potential discharge electrode and the detector probe, and that the detector probe field alone is not responsible for the drift. The signal response at zero flow velocity only occurs at close discharge-detector separation distances. At distances greater than 2 inches no signal is detected at zero velocity with the present model.

Ion Drift Velocity

The ion-drift at zero flow velocity results in some finite velocity being recorded with no flow. This drift velocity is

$$V_d = Z\varepsilon$$

where Z is the ion-mobility and ε the electric field strength. Since the field responsible for the ion drift is of an unknown nature, its strength can not be calculated directly. Therefore, the ion drift velocities were determined experimentally by measuring the transit time between the pulse discharge and the detected signal at zero flow velocity. The results in Figure 14 show the resulting drift velocities as a function of detector probe voltage and separation distance. Typical drift velocities ranged from 0 up to 250 fpm at the smallest separation distance and largest probe voltage.

Peak Signal Voltage

The basis of operation of an ITA is the change in travel time of the ion-tracer with flow velocity. However, examination of the detector signal response reveals that the peak signal voltage, as well as transit time, can be used to monitor flow velocity. The peak detected voltage versus actual flow velocity is given in Figures 15 and 16 for various separation distances d. The curves appear linear with flow velocity over the majority of the 0-100 fpm velocity range. The nonlinear response near zero velocity can be explained by examining the effects of diffusion on signal magnitude. The peak detected voltage will depend on the density of the ion-tracer as it passes the detector probe. The ion density (Reference 20) at the signal peak is shown to vary with time as

$$N = \frac{N_o}{(4\pi Dt)^{3/2}} \qquad (15)$$

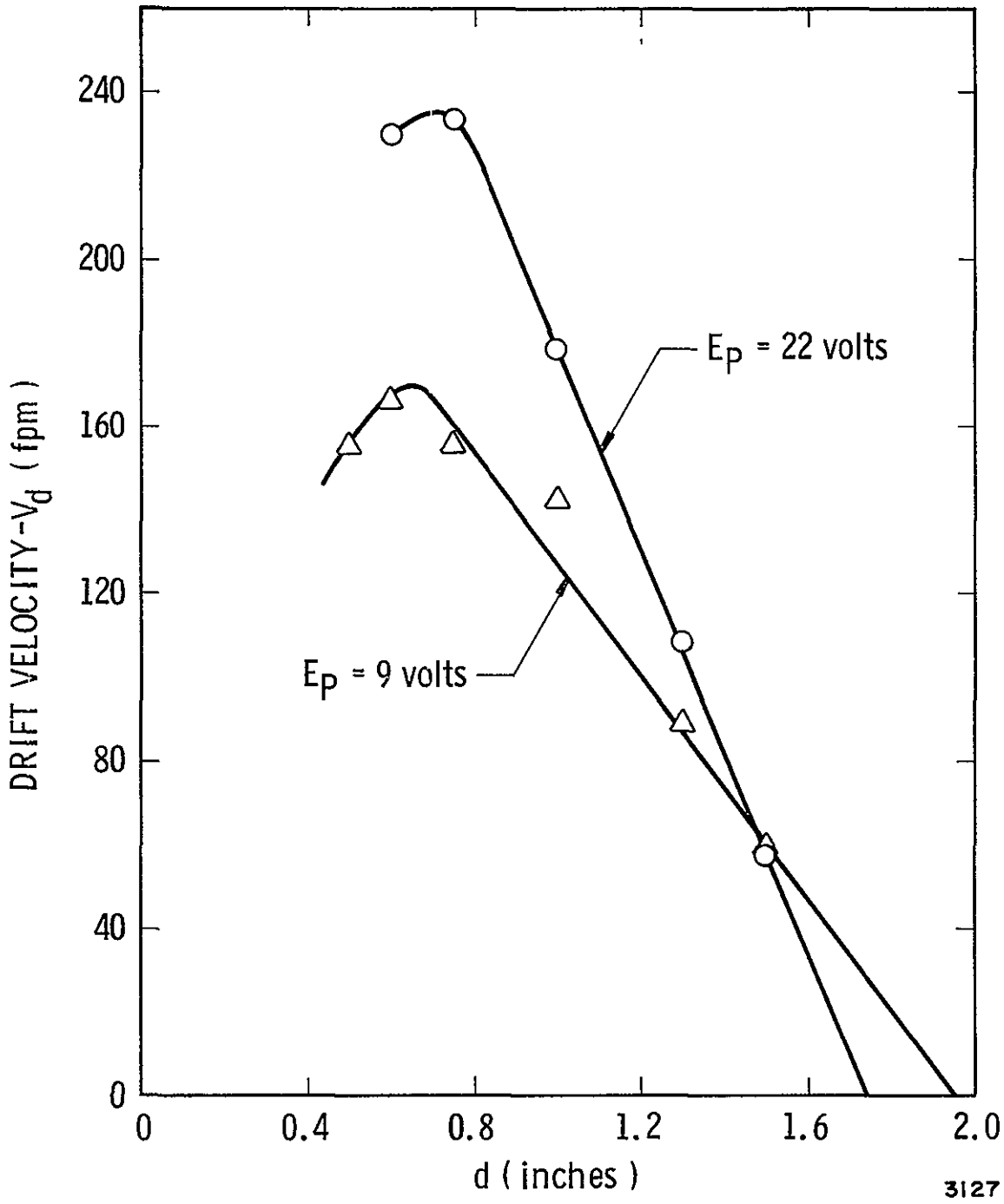

Figure 14. Ion Drift Velocity vs Separation Distance

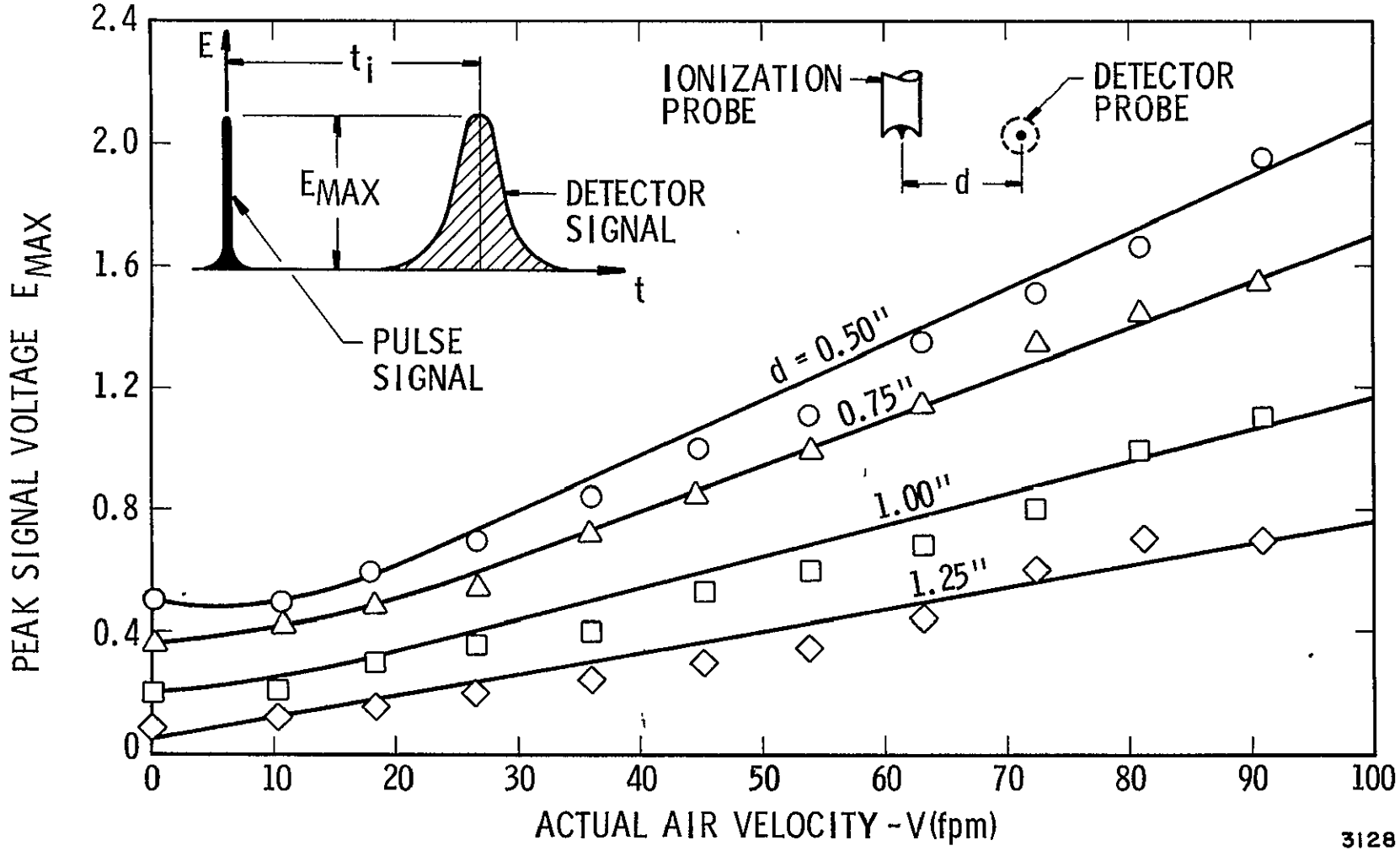

Figure 15. Peak Signal Voltage vs Actual Air Velocity (E_P = 9 volts)

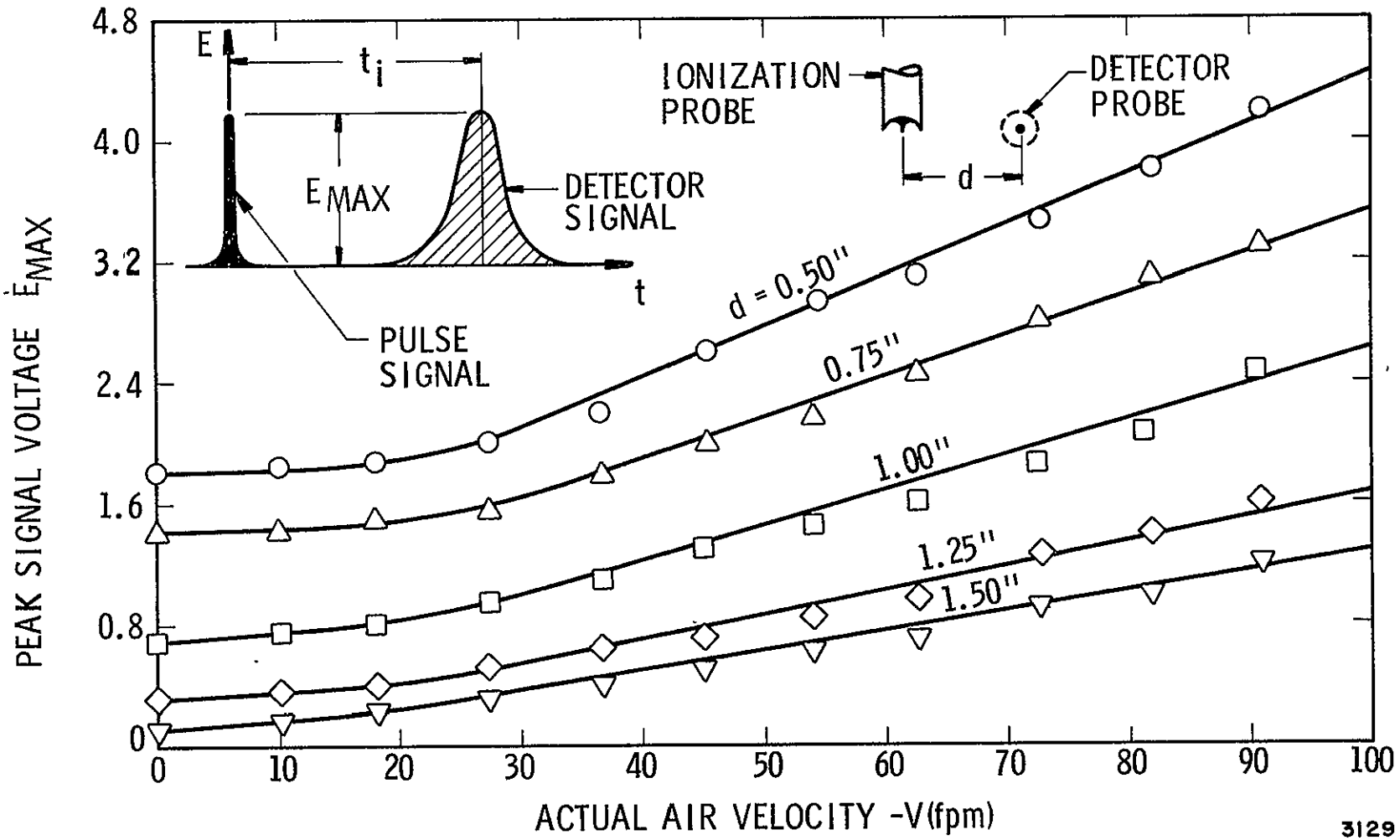

Figure 16. Peak Signal Voltage vs Actual Air Velocity (E_P = 22 volts)

where N_o is the ion density at $t = 0$, N the density at time t and D the coefficient of diffusion. Assuming that the peak voltage varies directly with ion-density yields

$$E_{max} = \frac{E_{max_o}}{(4 \pi Dt)^{3/2}} \tag{16}$$

Inserting the transit time t in terms of ion velocity V_i and separation distance d gives

$$E_{max} = E_{max_o} \left(\frac{V_i}{4 \pi D d} \right)^{3/2} \tag{17}$$

showing a nonlinear change in peak voltage with flow velocity. The results in Figures 15 and 16 indicate that the parameters V_i, d and D in Equation 17 are of such a magnitude that the response of peak voltage to flow velocity is approximately linear over the range of interest. The nonlinear response of peak signal voltage with flow velocity is an undesirable feature. The results presented in this section are given to show the effects of gas flow on the detected signal, and that an alternate method of implementing the ion-tracer anemometer is available. However, since the tracer technique intended for this instrument inherently yields a linear response, the tracer method is the most attractive. Results in the next section confirm this statement.

Pulse-Regenerative Operation

A working model of a pulse-regenerative ITA requires the processing of the detected ion cloud to provide a re-triggering of the ionization probe with the peak of the detected signal.

The detector signal and subsequent processing to provide a pulse-regenerative operation is shown in Figure 17. The basic detected signal is shown in Figure 17a along with the desired point (P) for re-triggering. The subsequent steps in processing this signal are shown in Figures 17b-f. The time delay shown in Figure 17e is required to allow sufficient time elapse in order that the detected signal will diminish before subsequent pulses are detected. Since the detected signal width can approach 100 ms at low velocities, with transit times of 20 to 40 ms, the delay is necessary so signal superposition will not alter the pulse regenerative operation. The re-triggering signal shown in Figure 17 is shaped to provide the proper voltage spike to trigger the ionization probes. The oscillograph traces shown in Figure 17 were taken at zero flow velocity with a discharge-detector separation distance of 0.5 inch and with

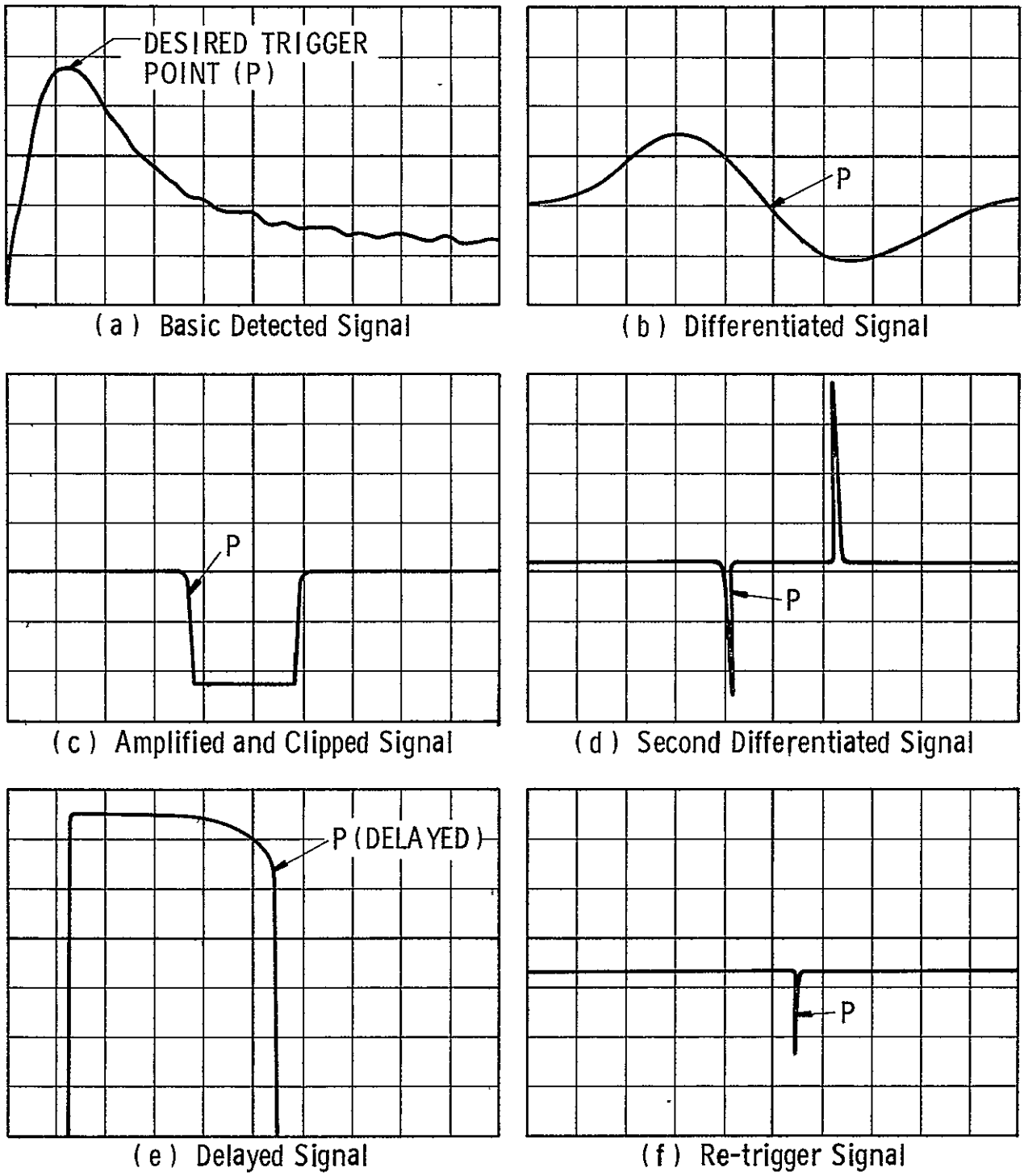

(a) Basic Detected Signal

(b) Differentiated Signal

(c) Amplified and Clipped Signal

(d) Second Differentiated Signal

(e) Delayed Signal

(f) Re-trigger Signal

3130

Figure 17. Signal Processing for Pulse-Regenerative Ion-Tracer Anemometer (From Actual Oscilloscope Traces)

+22 VDC on the detector probe. The signal shown in Figure 17a is the result of the ion-drift velocity. This drift velocity provides a signal for the instrument to "sing around" at zero flow velocity and no external re-triggering is necessary. The circuitry required to provide the processing steps shown in Figure 17 is given in Figure 10.

Pulse Frequency vs Velocity

The pulse regenerative ITA was tested in the low velocity facility Pulse frequency response versus flow velocity was obtained. Since the pulse regeneration period in the present model is delayed from the ion travel time, the total period between pulses is

$$t = t_i + t_d \tag{18}$$

where t_i = ion travel time and t_d = delay time (includes time delay and electronic processing delays). The ion travel time is determined by the drift velocity, flow velocity and probe separation distance by

$$t_i = \frac{d}{V_d + V} = \frac{d}{V_i} \tag{19}$$

The pulse regenerative frequency based on the total time period t is given by

$$f_t = \frac{1}{t_i + t_d} = \frac{1}{t_d + \frac{d}{V_d + V}} \tag{20}$$

a nonlinear function of the gas velocity, V. To obtain a linear frequency response to flow velocity requires subtracting the delay time from the pulse period before the frequency is determined. The resulting frequency response is a linear function of the gas velocity and is given by

$$f_i = \frac{1}{t_i} = \frac{V_d + V}{d} \tag{21}$$

The two velocity components in Equation 21 can be separated into separate frequencies such that

$$f_i = f_d + f \tag{22}$$

where f_d is the drift frequency at zero velocity, and f is the frequency due to gas velocity. The results of the drift velocity can be seen as only an addition of a constant drift frequency to the gas flow frequency response. Therefore, the drift frequency determines the y-intercept of the frequency versus flow velocity curve and not the slope. The drift frequency response for separation distances and drift velocities typical of the present ITA model are given in Figure 18a. The expected gas velocity frequency response for the 0-100 fpm flow velocity and typical separation distances are given in Figure 18b. The expected response of the ITA can be determined from Figure 18 as follows.

(1) For a given separation distance d and probe voltage E_p, the drift velocity is determined experimentally (Figure 14).

(2) The drift frequency, f_d, corresponding to this drift velocity is determined in Figure 18a.

(3) The frequency shift from 0-100 fpm is given in Figure 18b.

(4) The frequency response versus flow velocity is predicted as varying linearly from f_d @ V = 0 to $f_d + f_{100}$ at 100 fpm.

The results of the frequency response versus flow velocity of the ITA are given in Figures 19 and 20. The period between pulses was measured with an electronic period counter and the time delay subtracted from the total period count. The resulting ion travel time t_i was then used to determine the frequency response shown in Figures 19 and 20. These curves exhibit the expected response as predicted by the previous analysis. At the larger separation distances the drift frequency is lower, as predicted, and the total frequency change smaller. The data was taken at intervals of 10 fpm from 20 to 100 fpm and every 2 fpm from 0 to 20 fpm. Each run was repeated to determine repeatability and the results indicate essentially the same response for repeat runs. Near zero velocity, some of the data exhibit a non-linear response. However, the points where nonlinear response occur exhibit no distinct trend, and in some cases the response was linear down to zero flow velocity while on repeat runs a

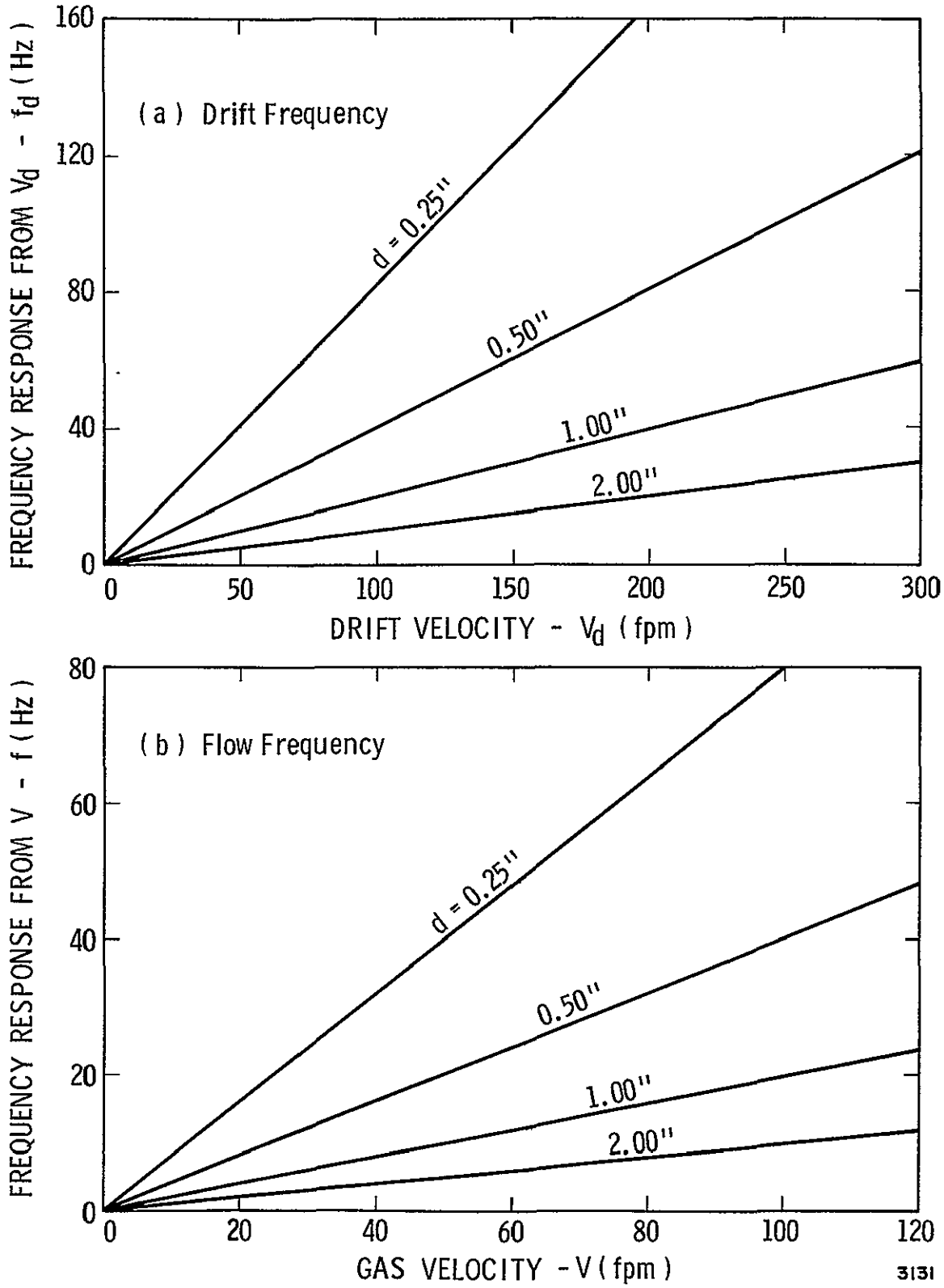

Figure 18. Predicted Frequency Response of ITA for Different Separation Distances

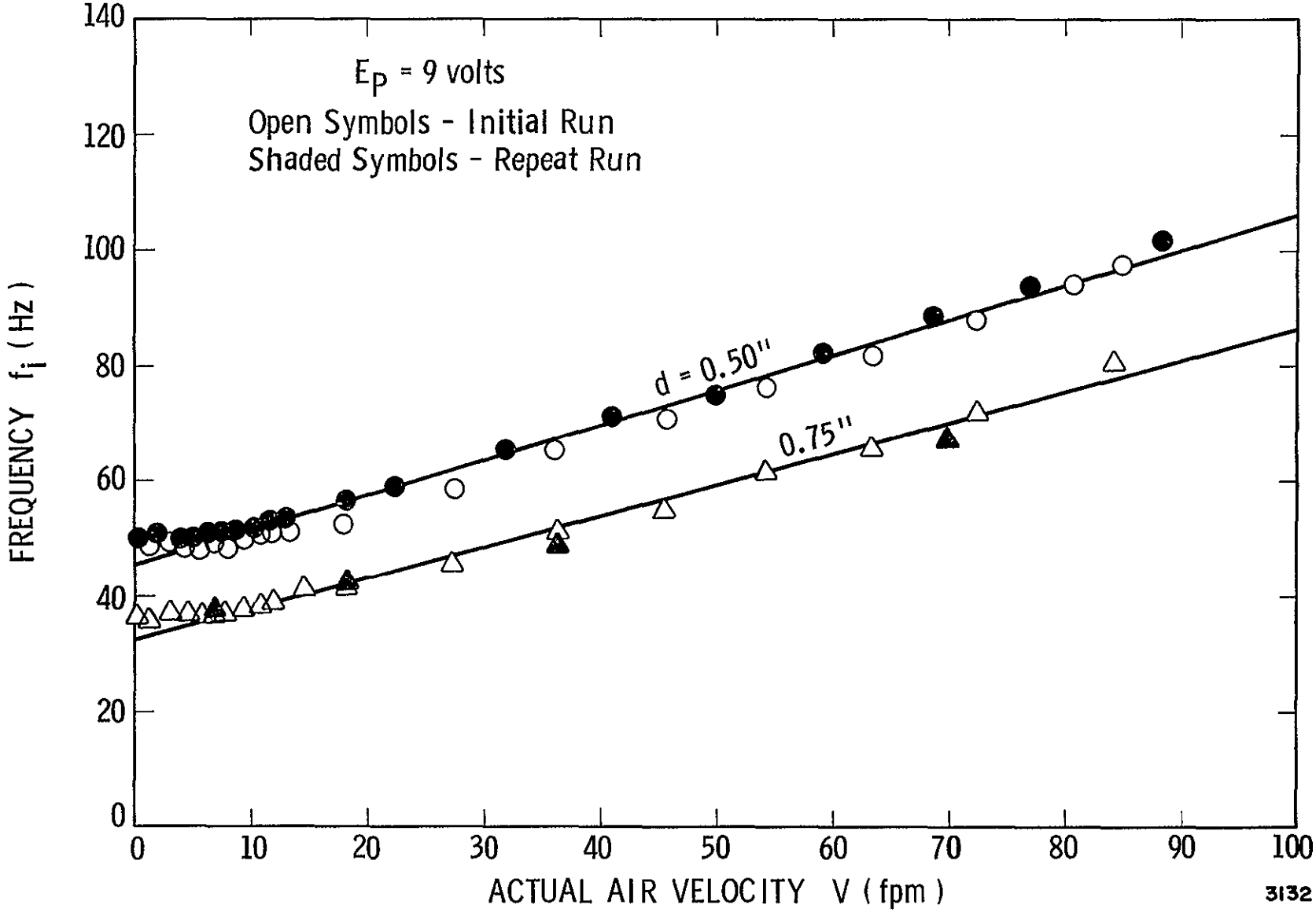

Figure 19. Frequency Response of Pulse-Regenerative ITA (E_P = 9 volts)

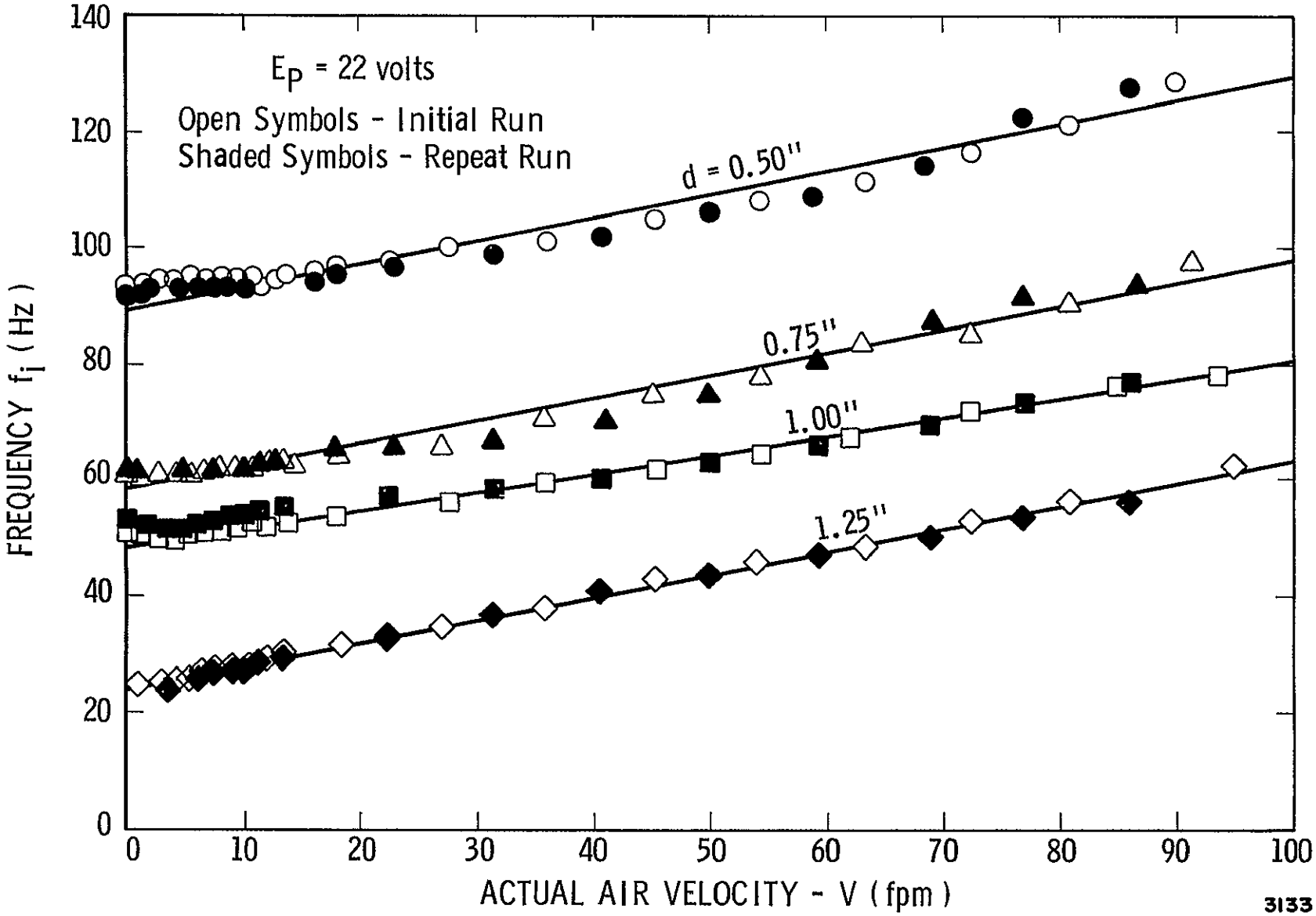

Figure 20. Frequency Response of Pulse-Regenerative ITA (E_P = 22 volts)

nonlinearity was observed. This is believed to be the result of the difficulty of establishing consistent flow conditions at the extreme low end of the velocity range with the present test facility. This problem occurs because of the water displacement technique used to provide the gas flow. When the tank is drained, dry air from the room is pulled into the tank. As the testing proceeds, the air evacuated from the tank becomes more humid, and the humidity changes from the beginning to end of each test run. The net effect of this humidity change is a change in the zero drift frequency since ion mobility is affected by humidity, the change in drift travel time relative to the gas travel is large at velocities near zero flow. Therefore, when conditions of approximately constant humidity were maintained, while testing from 0-100 fpm, the resulting frequency response exhibited linear characteristics over the entire range. Where conditions changed, the nonlinear characteristics near zero velocity were observed.

This humidity effect on the frequency response points out the major drawback of having a drift velocity exist at zero flow velocity. This resulting drift frequency in terms of the field and ion mobility is given by

$$f_d = \frac{Z\varepsilon}{d} \tag{23}$$

The ion mobility, Z, will not only be affected by humidity changes but also gas density changes. A more general expression for f_d taking into account density variation is

$$f_d = \frac{\rho_o Z_o \varepsilon}{\rho_d} \tag{24}$$

where the subscript, o, refers to atmospheric conditions. Thus, if a final instrument design included a zero drift frequency, this frequency would have to be nulled out before testing under different atmospheric conditions. This could easily be accomplished with a null screw and dead air chamber.

Advantages do exist however, when a drift velocity exists. These include (1) an available signal at zero flow velocity to maintain the pulse-regenerative action of the instrument, and (2) shorter transit times to provide more pulses per second and better instrument response. If no drift velocity is present, an extremely small separation distance is required to yield small transit times at velocities below 10 fpm. Present results indicate that transit times greater than 40 ms result in too weak a signal, caused from ion-diffusion, to be properly detected. With no drift velocity a separation distance of 0.008 inch is required for a transit time of 40 ms at 1 fpm. It would be difficult to provide a detector-discharge separation distance of 0.008 inch where no electric field was created over this distance

by the high voltage ionization probe. Therefore, a nulling of a drift frequency will probably be required of the final instrument design. It should be noted, however, that the velocity-frequency relationship, following drift frequency nulling, will be independent of atmospheric conditions.

IV. 4 Final Evaluation of ITA

The experimental results from the testing of the laboratory model of the ion-tracer anemometer support the paper evaluations, indicating that this technique of low velocity gas flow measurement has high potential for meeting the specifications of this program. A final evaluation of the ITA is given below for each specification category listed in the program objectives.

Range

Test results of output frequency versus flow velocity in Figures 19 and 20 show that the instrument response for the ITA covers the 0-100 (fpm) specifications of this program. Adequate response from the instrument is observed at the lower end of this range between 0 and 20 fpm. Other techniques uncovered in the literature for measuring low velocity have a lower cut-off point of approximately 10-20 fpm at best. However, no lower cut-off point is present with the ITA, and our results show that it should provide accurate readings over the 0-100 fpm required range. In addition, the upper limit on velocity measurement can easily be extended to provide a much wider measurement range if desired.

Accuracy

No statistical analysis of the data scatter present in Figures 19 and 20 was performed to determine instrument velocity accuracy. The data spread in these figures indicates that instrument accuracy for most of the test conditions is within $\pm$ 5 fpm and in some cases approach the $\pm$ 1 fpm requirements of the program. The accuracy observed was a function primarily of the ion generator-detector separation distance, and the collector voltage. The results show that these parameters can be properly selected to optimize the accuracy for a given flow range. Considering that the present laboratory model consisted of rather crudely constructed detector and discharge probes, and that no optimization of the pulse-regenerative detector circuitry was performed, the chances of providing $\pm$ 1 ft per minute accuracy in a final instrument design appear good.

Output

The output of the present laboratory model was a digital reading of the pulse period between pulse discharges on the ionization probe. This digital readout can easily be converted to provide the 0-5 VDC output in a final instrument. The final instrument could electronically subtract the pre-determined time delay of the time delay circuit from the total pulse period, take the reciprocal of the resultant period, and convert this to a digital 0-5 volt output. The resulting output would be linear with velocity over a 0-100 fpm range, as indicated by the data in Figures 19 and 20, and the final output could be made to read directly in fpm.

Environmental Pressure and Temperature

Compensation for changes in environmental pressure from 3 to 15 psia, and temperature from 60-80°F, will be required of this instrument to (1) maintain the integrity of the ion-tracer by allowing for changes in ionization characteristics, and (2) allow for changes in the zero velocity drift frequency. Proper ionization can be obtained over a reduced pressure range by adjusting the ionization probe voltage to maintain the same current as at atmospheric conditions The most difficult condition to produce ionization was that of the present test program, i.e., with a normal environmental (high) pressure, and a high humidity. Ionization is much more easily accomplished under conditions of low pressure and/or low humidity, or under circumstances most likely for the present application. The effects of an atmospheric pressure change on the zero drift frequency can easily be compensated by nulling out the zero drift frequency with a nullmeter. It should be emphasized that changes in instrument frequency between zero and 100 fpm will not be affected by atmospheric pressure changes, since this frequency change is dependent only on the travel time between the discharge and the detector probes, and not atmospheric conditions. Thus, once the instrument has been nulled to compensate for atmospheric pressure changes, the frequency-velocity calibration will remain constant.

The 60-80°F temperature range required of this instrument will produce little change, if any, in the operational characteristics of this device at a given pressure. This range of temperature change could have a small effect on the drift frequency at zero velocity. Again, this can be compensated by zero null before testing. In summary, the effects of environmental changes such as pressure, temperature or gas composition on instrument operation are (1) a change in ionization characteristics at the discharge probe, and (2) a change in drift frequency at zero velocity.

The instrument response between 0 and 100 fpm is independent of environmental conditions.

Frequency Response

The frequency response of this instrument should meet the 1 HZ requirements listed in the program specifications. With the present laboratory model, a regenerative frequency of approximately 5 HZ was recorded. Therefore, at least 5 samplings per second of gas velocity were available over the entire velocity range measured. Reducing the time delay in the signal processing circuit would provide additional pulses per second for even greater instrument response.

Omnidirectional Capabilities

Testing of the current laboratory model was accomplished with a unidirectional instrument. The operation of this instrument is based on the travel time of the ions between the discharge and detector probes, thus an omnidirectional instrument can easily be constructed using porous spherical detector surfaces. The gas flow from any direction would result in the ions traveling from a center electrode to the spherical detector surface in a time dependent on the flow velocity and detector radius. This type of device would indicate velocity magnitude but not vector direction, and would not require three separate discharge-detector pairs with vector addition to obtain velocity.

Design

Test results indicate that successful operation of this instrument requires small separation distances in order that the detected signal will re-trigger the ionization electrode. A small sensor head is therefore required, and a compact instrument should be readily attained. The detector and discharge probes do not require delicate elements, and are much more rugged in construction than the sensing heads of hot wire or hot film probes. Because of the open nature of the discharge and detector probes, the instrument should cause little restriction of the gas flow. All components in the instrument circuitry can be made into a compact form using readily available solid state components. It is anticipated that the final size of the electronics instrument package could be put in a volume the size of a shoe box. The sensing head would be of such a size that it could easily be hand held, and the power supply could either be a battery or an external power supply source. Therefore, it appears that this instrument could be built as either a portable instrument with a

self-contained power supply, or as a telephone version with a control box and power supply built into a wall.

IV. 5 Specifications and Scope of Work for ITA Development

The development program required to provide a final deliverable instrument, meeting the low velocity measurement requirements of the present application, should consist of two program phases. The suggested scope of work for these two phases, and the estimated time and man-hours required for each is:

Phase	Description	Estimated Period	Estimated Man-Hours
I	Develop miniature omnidirectional discharge and detector probes. Improve the electronic circuitry to include a current limiting function, a compact power supply, and a DC readout. Also, study possible elimination or reduction of the zero-velocity ion drift. Lastly, evaluate a final model ITA.	8 months	2000
II	Design, construct, test and calibrate a final prototype instrument for delivery to NASA.	4 months	1200

The task details required to meet the objectives of these two phases are outlined below.

Task I 1 - Development of Sensing Heads

The objectives of this task should be (a) to determine an optimum sensing head which provides an omnidirectional capability, and (b) to select the materials for the head construction.

In this task the various geometries which could provide omnidirectional capabilities for this instrument should be defined. It is anticipated that one of the geometries that could possibly meet this qualification is a porous spherical detecting head. However, other geometries could provide omnidirectional capabilities, also. Examples of two and three-dimensional heads are shown in Figure 21. This study should consider

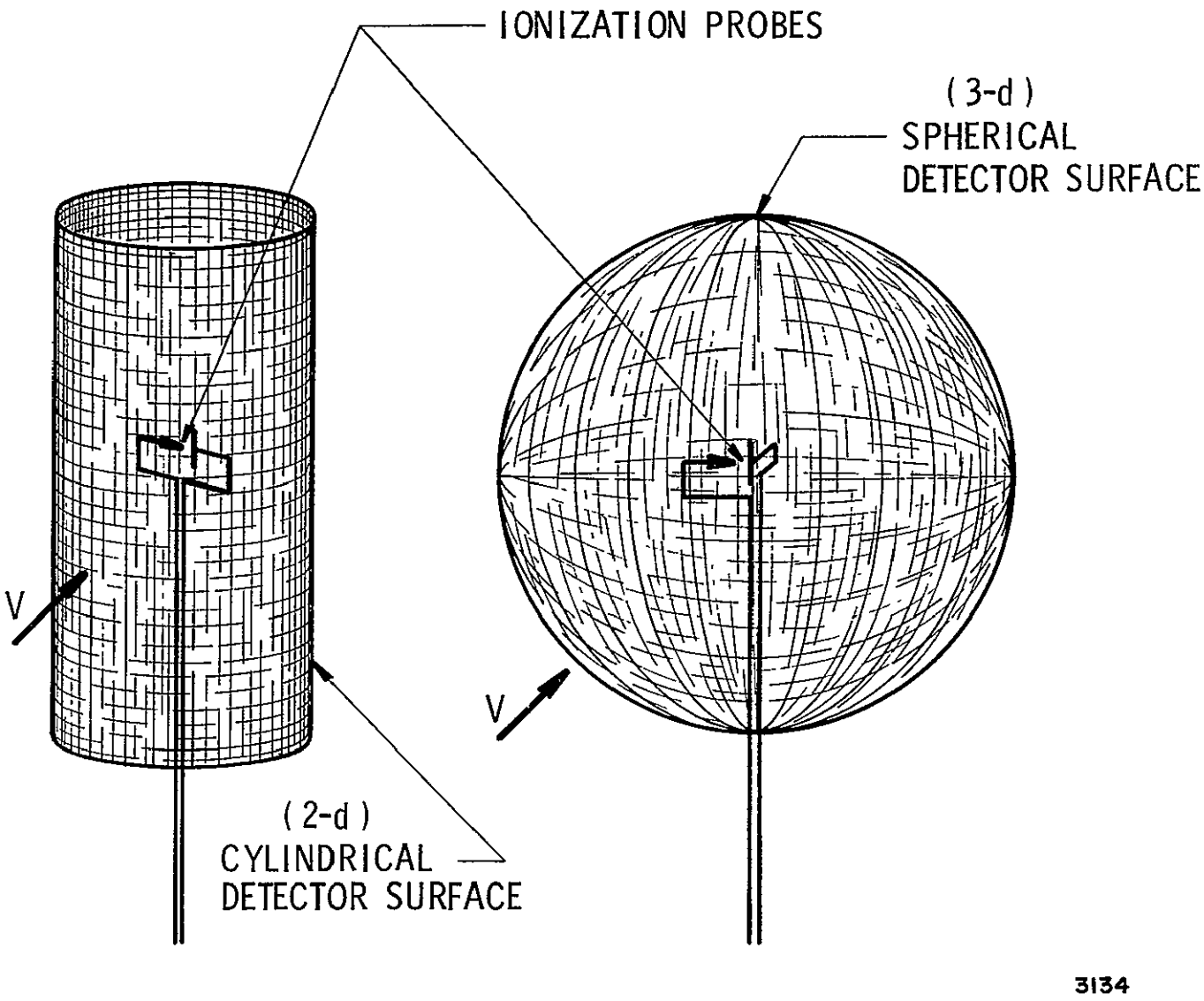

Figure 21. Omni-directional Detector Concepts

carefully all aspects of an omnidirectional sensing head and their effects on instrument operation.

This task should also attempt to provide definition of the types of material that may be used in the construction of the discharge and detector probes. Continual useage of this type of instrument over a long period of time could cause some probe contamination, which would reduce the ionization characteristics and change the instrument response. It is anticipated that a material such as platinum or other non-corrosive alloys might be used for the discharge electrodes, and for the detector probes. In addition, discharge probe geometries should be defined that will be compatible with an omnidirectional sensing head. This would entail miniaturization of the discharge probes so that they could be contained in the center of a spherical-type detector. Studies of geometries other than the point-cylinder arrangement used in the present investigation should be conducted to define the optimum design for a small compact omnidirectional unit.

The last aspect of this task should be the construction of a final model of the selected sensing head. This would then be used for an evaluation, along with the finished model electronics, of the optimized ITA.

Task I. 2 - Electronic Circuitry Optimization

The objective of this task should be to develop final bread-board electronic circuitry. Work is needed to provide an ionization current limiting means, to design a compact power supply, to provide a DC readout capability, and to determine if the zero velocity drift frequency can be eliminated.

In the present study a zero velocity drift frequency was present because of an existing electric field between discharge and detector probes. One purpose of this task should be to determine if an instrument can be built without a zero drift frequency, or if a zero drift frequency is desirable. In conjunction with Task I. 1, this would include a study of discharge detector geometries that would provide predictable electric fields between the two probes. Detector and discharge probes based on these studies would then be constructed, and the drift velocities between the probes measured as in the present study. Results of this study would determine if the drift velocities could be predicted from known electrode geometries and voltages. Thus, a desired frequency could be built into the final instrument design and instrument response could be optimized with respect to this drift frequency. Total elimination of the zero velocity drift frequency would necessitate addition of an automatic restart circuit,

since the system would then cease to "sing-around", or self-re-trigger when the velocity went to zero.

Another aspect of this task would be to define the circuitry for the final model instrument design. This will include a study of the final power supply design, the final detector circuitry components and all component simplification required to produce a small packaged instrument. In addition, the final readout circuitry will also be designed. It is anticipated that a constant current power supply could be utilized in this device; therefore, an estimate of the expected voltage change required to keep a constant discharge current over the 3 to 15 psi environmental change will be made. A power supply will then be designed to maintain a constant discharge current over this voltage range. The detector circuitry utilized in the present application was designed to seek the peak of the passing ion cloud signal and to re-trigger the ionization probe. An additional study will be performed to determine if this detector circuitry can be improved such that a better definition of the peak of the passing ion cloud could be obtained. Such an improved design would lead to better instrument accuracy. To provide a small compact instrument, a study would be performed to determine if any of the components in the present circuits can be eliminated, reduced in size, or combined with other circuit elements.

Task I. 3 - Evaluation of Final ITA Model

The objective of this task will be to perform a series of evaluation experiments on the final ITA model configuration, as evolved from the previous two tasks.

The instruments will be tested over the 0-100 fpm velocity range of interest. This testing will include positioning the omnidirectional heads at various angles to the flow direction and monitoring flow velocity versus angle of inclination. Also, readout from the output circuitry will be recorded versus actual flow velocity. Instrument tests on the discharge head will also be conducted on the 3-15 psi environmental pressure range. This will be accomplished by placing the head inside a vacuum box where pressures can be provided in the 3-15 psi range. Output signals on the detector probe will be observed over this range to determine if any change in output signal over this 3-15 psi environmental range is present. If the current limiting power supply is operating correctly, then no change in the detector probe signal should be evident. In addition, tests in an oxygen environment should be performed to determine the effects of a change in gas composition, from air to O_2,

on the ionization characteristics of the discharge probe. The sensing heads should be tested in O_2 and air under identical conditions, and the detector signals compared to indicate differences in the ionization process in the two gases. If the detected signals differ appreciably, then the voltage to the discharge probe should be adjusted until equal ionization is accomplished.

Task II. 1

The purpose of this task is to evaluate all results of the Phase I studies and to determine a final ITA prototype design. This would include a statistical analysis of all the data obtained in this study to determine the final instrument accuracy. In addition, the instrument response versus flow angle data would be evaluated to determine if there was any orientation in the neighborhood of the support shaft where the instrument accuracy was affected.

Any modifications from the geometries or designs tested in Phase II would be made, and the instrument retested for final results.

Task II. 2

A final prototype low velocity measuring ion-tracer anemometer (ITA) would be built for delivery to NASA. This instrument would be tested in the low velocity flow facility to determine a final instrument response. Final characteristics of this instrument would be recorded and included along with the prototype unit.

V. ACOUSTIC GAS FLOWMETER

V. 1 Introduction

Acoustic techniques have been developed in the past to measure air or gas transport effects in meteorology (anemometry), and under confined flow conditions such as in gas transfer pipelines, air ducts, and wind tunnels. Similar methods have been developed for liquid flow measurements in the ocean, in rivers and streams, in liquid transfer pipelines, and in confined hydraulic channels. Methods based on both single-path and two-way sound transmission have been used in these applications. Single path methods require an accurate knowledge of the speed of sound in the gas (or indirectly a knowledge of the gas constituents and temperature). Dual path methods usually operate on a differential measurement principle and do not require information on the gas constituents, temperature, etc. In either case, certain assumptions are made to facilitate the analysis and interpretation of the acoustic travel times measured by the instrument. These assumptions will restrict the predicted performance to conditions of homogeneous gas mixtures and steady laminar flow conditions during the measurement time interval required by the instrument. Such assumed conditions will generally prevail for the space cabin circulation measurements and flowmeter specifications for this program, thereby lending reasonable validity to the analysis results.

The discussions to follow show theoretically that the small gas flow velocities found in manned spacecraft cabins can be feasibly measured using the acoustic sing-around method. An array of such acoustic sensors can be used to measure and derive the three-dimensional vectorial flow velocity, if required.

V. 2 Description of the Proposed Acoustic Flowmeter Method

The acoustic flowmeter principle is one in which mass transport (or flow) perturbations in a sound propagation medium introduce variations in sound wave travel times between source and receiver combinations oriented in a known manner in the flow. Since sound propagation depends upon molecular collisions between the constituents of the medium, any physical motion of the medium will readily affect the apparent propagation of sound in the medium An analysis of the transit times can reveal the flow component of the medium along the sound propagation path between the sound source and receiver combination.

Consider an omnidirectional sound source located at the origin of an x, y, z coordinate frame in a uniform velocity field. If an acoustic pulse is radiated from the source at a speed, c, it is transported in the direction of flow at the flow velocity, v. The wavefront of the acoustic pulse with respect to a stationary coordinate system is expressed by

$$(x - v_x t)^2 + (y - v_y t)^2 + (z - v_z t)^2 = c^2 t^2 \tag{25}$$

where (v_x, v_y, v_z) are the velocity components of v and t is the elapsed time after pulse transmission. Equation (25) describes a spherical wavefront expanding uniformly with time and having its origin at ($v_x t$, $v_y t$, $v_z t$). In an arbitrary gas flow environment in which only time and coordinate positions are known, Equation (25) contains four unknowns, (v_x, v_y, v_z and c). With four separate source and receiver combinations, it would be possible to experimentally derive the three-dimensional flow velocity components and sound velocity from experimentally measured pulse transit times. With a knowledge of the speed of sound in the medium, it would be possible to derive the three-dimensional flow components from only three sources and receiver combinations.

In order to avoid the inaccuracies associated with the technique in which three relatively small variables, (v_x, v_y, v_z), and one relatively large variable, c, are involved, and to circumvent the need for collateral knowledge of the speed of sound in the medium, a two-directional measurement arrangement can be used.

Considering only the flow component along the x-axis for the moment, if two receivers are located on the x-axis at +x and -x, then two different transit times will be observed: (1) the transit time resulting from propagation velocity aided by v_x in one case, and (2) the transit time resulting from propagation velocity retarded by v_x in the other. When these conditions are substituted into Equation (25), two quadratic equations in t_1 and t_2 result,

$$(v_x^2 + v_y^2 + v_z^2 - c^2)\ t_1^2 - 2 x v_x t_1 + x^2 = 0 \tag{26}$$

$$(v_x^2 + v_y^2 + v_z^2 - c^2)\ t_2^2 + 2 x v_x t_2 + x^2 = 0 \tag{27}$$

where t_1 and t_2 are the acoustic travel times from the origin to +x and -x, respectively. Solving Equations (26) and (27) for t_1 and t_2 and taking

the difference of their reciprocals yields

$$v_x = \frac{x}{2} \left(\frac{1}{t_1} - \frac{1}{t_2} \right) \tag{28}$$

Thus, if the separation distance, x , is known and the two transit times, t_1 and t_2, between the source and each receiver are measured, then the x-component of the flow velocity can be computed. It should be noted from Equation (28) that this relationship does not require any knowledge of the gas constituents, gas temperature, or speed of sound. With other pairs of receivers located on the y- and z-axis, similar measurements can yield the y- and z- components of the total air circulation flow vector

In interpreting Equation (28), it is convenient to recognize the reciprocal travel times, $1/t_1$ and $1/t_2$, as frequencies associated with the transit time periods, t_1 and t_2. In a practical embodiment of this measurement method, the transit times can actually be used as the delays in two repetitive-pulse feedback systems, thereby deriving the quantities $1/t_1$ and $1/t_2$ directly from the system operation. Thus, when frequencies are measured directly, Equation (28) becomes

$$v_x = \frac{x}{2} (f_1 - f_2) \tag{29}$$

where $f_1 = 1/t_1$ and $f_2 = 1/t_2$. This result shows that, in the theoretically ideal case, the measured flow velocity is directly proportional to the difference in pulse repetition rates in the two acoustic feedback oscillator channels, with the constant of proportionality dependent only upon the transducer separation distance, x .

The measured parameters in this instrument arrangement are the "sing-around" frequencies in each channel and the separation distance between the transducer pairs. Since frequency is the measured variable, the inaccuracies usually associated with taking the difference between two large numbers such as $1/t_1$ and $1/t_2$ are minimized by using electronic counting techniques to derive average values of f_1 and f_2 over the allowable response time of the instrument system before computing the difference, $(f_1 - f_2)$. For example, in the case of an acoustic flowmeter having a transducer separation distance of one foot in an air medium (speed of sound = 1200 fps), the frequencies, f_1 and f_2, will be in the order of 1200 pulses per second. Therefore, if the frequency measurement is accomplished over a period of one second, then about 1200 sing-around pulse events are averaged together in each channel. Further, if a flow velocity

of v_x = 60 fpm is being measured, the difference frequency between the two sing-around channels will be 1201-1199 = 2 pulses per second. In order to resolve this difference frequency with greater precision, especially for lower flow velocities in the order of 1 fpm, it will be convenient to multiply the sing-around frequency in each channel by an integral factor in the range of about 20 or 30 before performing the frequency measurements and taking the difference. By this electronic leverage technique, the measurement time required to derive the difference frequency to within the desired accuracy is significantly reduced.

Figure 22 shows a simplified block diagram of a two-channel acoustic flowmeter based on the operating principle discussed above. Operation of this system is described as follows:

(a) Start, Enable, and Reset commands are initiated by the Control.

(b) Each regenerative channel transmits a short acoustic pulse at separate frequencies (f_1 and f_2) which, when received at the appropriate receiver, re-initiates another acoustic pulse from the transmitter in the same channel.

(c) This action continues, producing a pulse repetition frequency of f_1 in the upper channel and f_2 in the lower channel until the Control resets the Enable line.

(d) During this two-channel sing-around process, the Counters have been accumulating a count equal to n times the number of pulses repeated in each channel.

(e) At the end of the measurement response time, the Control issues a Subtract command which results in a digital output proportional to the flow velocity component and clears the counters.

(f) The complete measurement sequence is then repeated.

The two-channel acoustic sing-around system described here has been simplified in some respects by the assumptions of homogeneous gas mixtures, steady laminar flow, and a one-dimensional transducer alignment along the direction of flow. These simplifications are generally

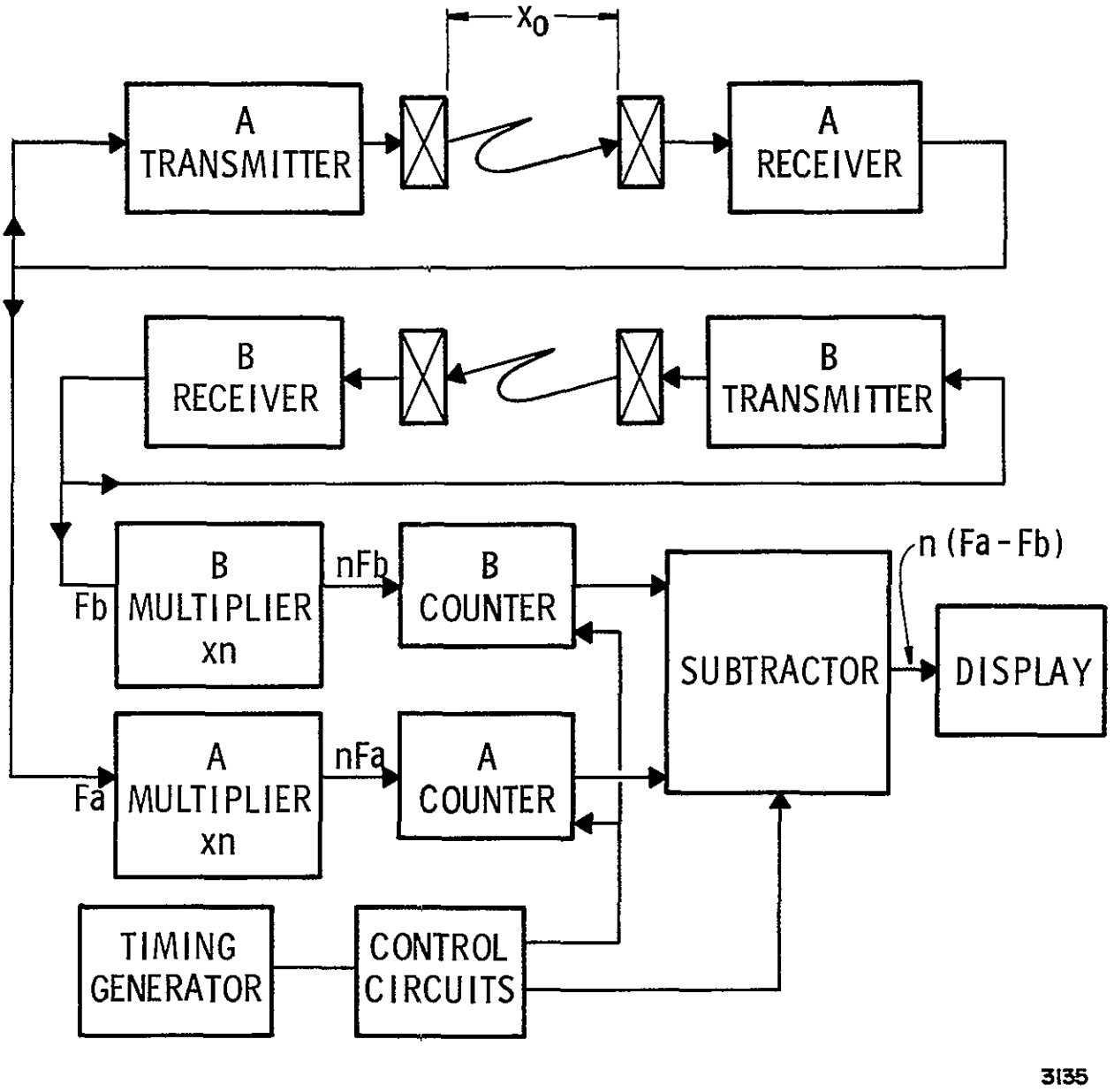

Figure 22. Block Diagram of Two-Channel Acoustic Flowmeter

appropriate for space cabin circulation measurements and form a reasonable basis for a mathematical model of the concept. The analyses in the next section will expand the consideration of the technique to include the measurement errors introduced in a practical implementation of the method.

V.3 System Error Analysis

A detailed "worst-case" error analysis has been made to determine the applicability of the acoustic sing-around flowmeter to the present application. This analysis is presented in the Appendix, and the significant results may be summarized as follows:

(a) Fixed dimensional errors and fixed time delay errors produce significant velocity measurement errors but can be adjusted mechanically or electrically so as to mutually cancel between channels.

(b) The most significant electronic error results from discrete time jitter in each sing-around channel, and may typically produce a flow measurement error of the order of 10 ft/minute.

(c) Variable errors associated with the transducer mounting structure include thermal expansion, mechanical vibration, and flow obstructions. The latter appears to be most significant, and will typically produce errors of about 2.5 percent for a transducer separation of 6 inches, with a structural support diameter of 0.15 inches.

V.4 Experimental Model

Selection of Acoustic Flowmeter Operating Frequencies

The primary considerations in developing an experimental model acoustic flowmeter which can approach the theoretical concepts analyzed earlier are: (1) fast acoustic pulse rise time, and (2) good received signal-to-noise ratio. The first of these requirements implies a wide bandwidth acoustic signal and, hence, one of relative high frequency; the second requirement implies high transducer sensitivity and minimum ambient noise and system noise effects. These requirements are in

conflict with one another because of certain limitations in practical high frequency transducer materials and components and the acoustic absorption properties of air. A compromise design approach must, therefore, be taken which will tend to provide the most desirable practical model.

The transducer frequencies are selected to be the highest practical values which will simultaneously:

(1) Allow the low frequency channel bandwidth to be a maximum for an assumed transducer mechanical Q of 5;

(2) Limit the maximum frequency distortion resulting from sound absorption in air to be 10 db or less in the high frequency channel at the widest transducer separation distance of 1 foot.

The coefficient of sound absorption in air for sound frequencies greater than about 150 kHz is essentially governed by the viscosity effects rather than the relaxation effects of air molecules (Reference 21). Above 150 kHz the absorption coefficient is

$$\alpha = 0.01721 \ f^2 \ \text{db / cm} \qquad (30)$$

where f is expressed in hundreds of kilo-Hertz.

Using this relation for sound absorption loss and an assumed transducer Q of 5, the following table of information can be calculated:

TABLE I. SOUND ABSORPTION IN AIR AT HIGH FREQUENCIES

Frequency (kHz)	Absorption Rate (dB/cm)	Attenuation over 12-in Path (dB)	Bandwidth $BW = f/Q$ (kHz)	Rise Time $T = 1/BW$ (μ sec)
150	0.0388	1.18	30	33
200	0.0689	2.08	40	25
300	0.155	4.67	60	16.7
400	0.277	8.36	80	12.5
500	0.431	13.05	100	10
600	0.619	18.75	120	8.3
700	0.843	25.6	140	7.2
800	1.110	33.5	160	6.3

For a 10-dB absorption shading across the transducer bandwidth, the highest center operating frequency for a one foot transducer separation can be found from

$$(\alpha)_{low} x_o = (\alpha)_{high} x_o - 10 \qquad (31)$$

where:

$$(\alpha)_{low} = 0.01721 \left(f_o - \frac{BW}{2}\right)$$

$$= 0.01721 \left(f_o - \frac{f_o}{10}\right) \text{ dB/cm}$$

$$(\alpha)_{high} = 0.01721 \left(f_o + \frac{f_o}{10}\right)$$

f_o = center frequency (kHz x 100)

x_o = 1 ft.

$$BW = \frac{f_o}{Q} = \frac{f_o}{5}$$

Substituting these conditions into Equation (31) gives

$$f_o^2 = \frac{10}{30.28\ (0.01721)\quad (1.1)^2 - (0\ 9)^2} = 48.6$$

which yields a center frequency of 695 kHz. Thus, it should be possible to operate one channel of the acoustic flowmeter at a center frequency of about 700 kHz and the other channel at a lower frequency. The separation of the two acoustic frequencies must be sufficient to prevent sound pulses in one channel from interfering with the operation of the other channel. The bandwidth of the high frequency channel will be larger than that of the low frequency channel; however, the high frequency bandwidth should be made equal to that of the low frequency channel in order that the rise times in each channel will be equal.

If the low frequency channel is operated at a sound frequency of 500 kHz, the bandwidth will be 500/5 = 100 kHz and the two channels will be separated by a guard band of (700 - 50) - (500 + 50) = 100 kHz which should be adequate to minimize the possibility of inter-channel interference.

A third lower frequency of operation was also selected by this same analysis procedure as a precaution toward the availability of the necessary transducer elements, and the possibility of operating difficulties with the relatively high sound absorption conditions at 700 kHz. If the highest frequency of operation is considered to be 500 kHz, a low frequency of 350 kHz can be selected for use in the second channel, thereby providing an operating bandwidth of 70 kHz and a separating guard band of (500-35)-(350+35) = 80 kHz.

Any pair of the frequencies derived above can be used in the experimental acoustic flowmeter without inter-channel interference. To consider the use of any lower frequencies in the design of the instrument would cause an unnecessary constraint on the rise time of the sound pulses because of the practical bandwidth which can be achieved with piezoelectric transducers. In this general range of frequencies, the operating bandwidth of ceramic elements is approximately constant and equal to about 20 percent of the center frequency of the transducer crystal element.

Piezoelectric crystals of a lead metaniobate composition were selected for this application because of their relatively low mechanical Q and, consequently, their wider bandwidth. These elements were obtained from Gulton Industries, Metuchen, New Jersey (Glennite G-200 piezoceramic material) in the form of D-shaped half-discs cut from single initial discs to insure matched frequencies in the source and receiver transducers.

Transducer Assembly Design

One of the basic premises of the dual sing-around flowmeter is that the speed of sound is the same in each of the channels at any given instant. This infers that the two acoustic propagation paths occupy the same volume. This, of course, is not physically possible but necessitates that these crystals be mounted as close together as possible so that the two ultrasonic beams probe the same column of air

Since the sound pulses are traveling in opposite directions along parallel paths, the transmitting crystal for one channel is adjacent to the receiving crystal of the other channel at each end of the transducer fixture. As shown in the sketch below, the undesirable coupling between the channels can take two forms: (1) the electrostatic capacity (Cc) between the adjacent crystals which can electrically couple a portion of the transmitter voltage from one channel directly into the receiver of the other; and (2) the acoustic radiation paths (Ac) between the

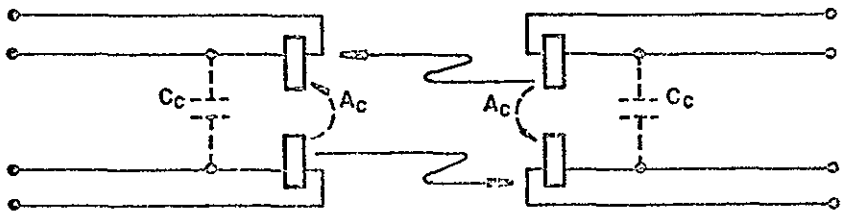

Electrical Configuration - Two Channel Acoustic Flowmeter

transmitter crystal and the receiver crystal. There is an acoustical path between adjacent crystals through the supporting structure, and another through the air. The fixture holding these crystals must provide the maximum possible attenuation to these cross coupled signals and yet must be small and streamlined to produce a minimum of air turbulence. Additionally, the support must be designed to prevent mechanical vibration of the transducers.

Figure 23 is a drawing of the crystal housing fixture used in the experimental evaluation of the acoustic flowmeter. The cavity in the face of the housing was lined with Corprene for mounting the crystals and a "blinder" or divider was installed between the crystals. The divider consisted of a sandwich of brass shim stock electrical shielding covered on each side with a layer of Corprene. The shim stock was electrically connected to the housing and served to reduce the capacitive coupling between the channels. The Corprene lining and blinder served to reduce the acoustic coupling. Lead wires were brought in through separate openings behind the crystals from a common passageway through the vertical support tube. These wires were twisted pairs with electrostatic shields. The shields were insulated from the housing, being terminated at the transmitter and receiver ends of the lead wires.

In the initial electronic system tests the transducer fixtures were mounted on an optical bench. During final system tests in the low velocity flow facility, the fixtures were initially mounted on plexiglas and later on asbestos board plates. Figure 24 is a photograph of the pair of transducer fixtures mounted on the plexiglas plate. Note that there is provision for spacing the transducers at separation distances of 12, 6, 4, and 2 inches.

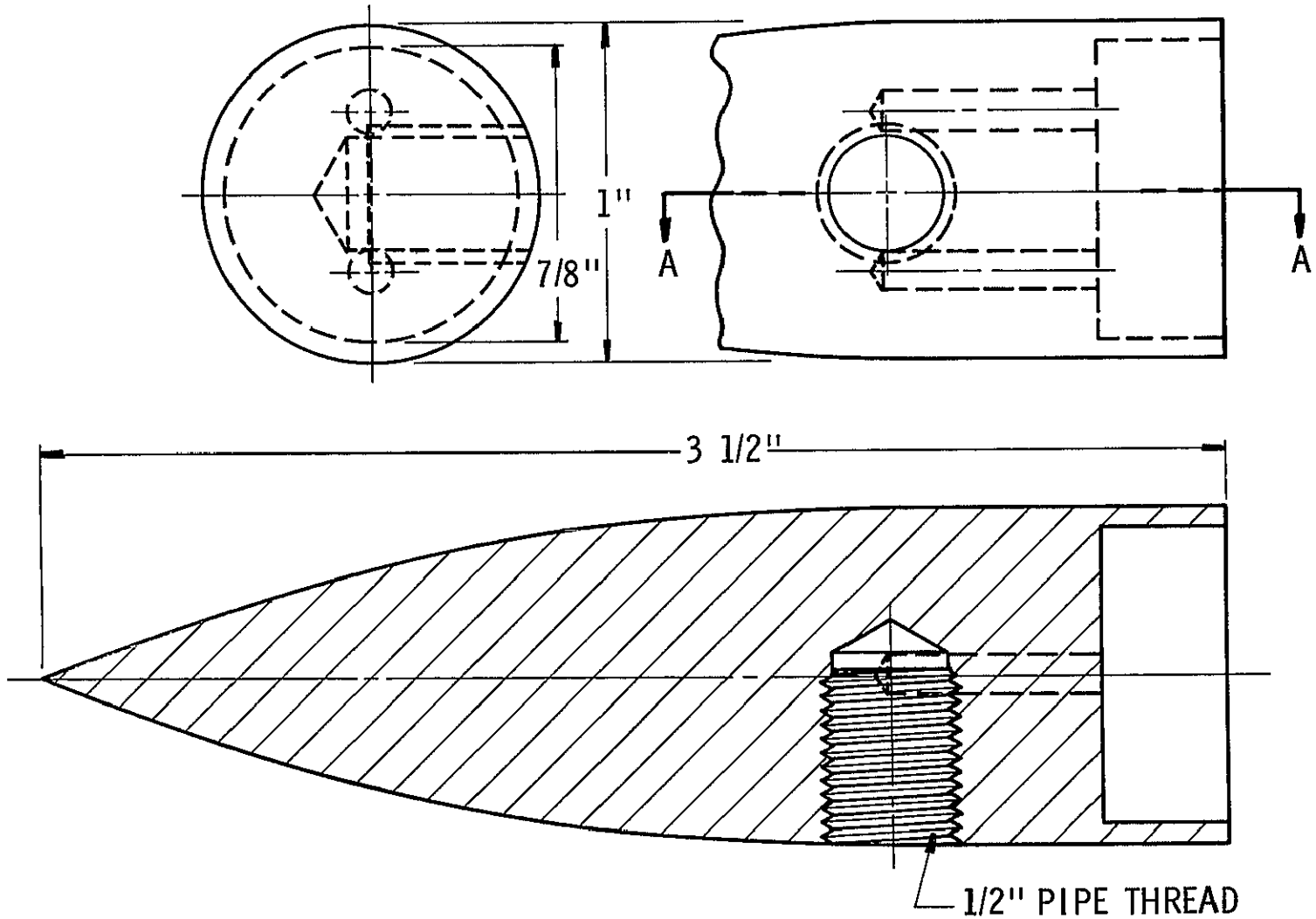

Figure 23. Crystal Transducer Housing

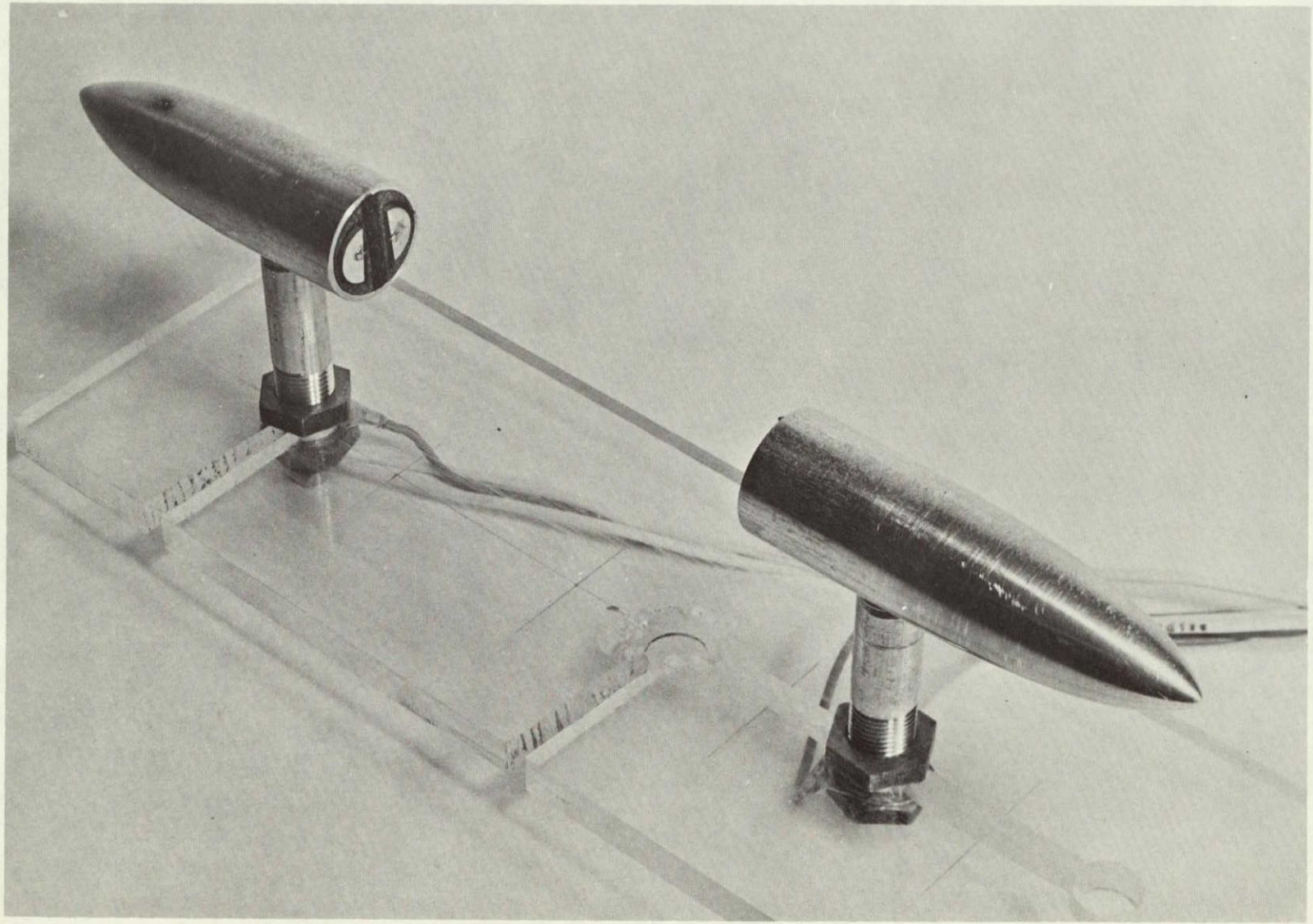

Figure 24. Acoustic Flowmeter Transducer Texture, Four Inch Spacing

Electronic System

a. Overall System Operation

Referring to Figure 22, the Flowmeter Block Diagram, it can be seen that the system is composed of two basic sections: (1) the sing-around oscillators; and (2) the frequency measuring components. The following paragraphs describe these sections and their operating characteristics.

b. Sing-Around Oscillators

As described earlier, the sing-around oscillators are of the pulse feedback type where the period of oscillation is determined by the acoustic travel time between the transmitting and receiving crystals. The two channels are identical with the exception that the ultrasonic transducer frequencies are different. In the final tests, one channel was operated with crystals resonant at 345 kHz and the other channel crystals were resonant at 510 kHz.

The transmitter circuit shown in Figure 25 is a modified "Firestone" circuit. In the description which follows, it is assumed that the ultrasonic pulses are being received, amplified and applied to the primary terminals of transformer, T1, as re-trigger pulses. Prior to the reception of this pulse the silicon controlled rectifier (SCR), Q1, is in the non-conducting state. C2 and the transmitting crystal capacitance are charged to 400 volts through R2 and L1.

When the trigger pulse is received, it is coupled through transformer, T1, and coupling capacitor, C1, to the gate of the SCR, Q1. The SCR is switched to the conducting state by the pulse, discharging C2 immediately. Inductor, L1, along with the crystal capacitance forms a resonant discharge circuit at the same frequency as the mechanical resonance of the crystal. The SCR reverts to the blocking state at the end of the first oscillation in the crystal circuit; however, C2 provides a low impedance path for the circulating current in the resonant circuit. The oscillations die down at a rate set by the electrical and mechanical "Q" of the circuit and crystal. The crystal launches an ultrasonic pulse into the air of the same waveform as the voltage across the crystal. The duration of the ultrasonic pulse is short with respect to the period between pulses. As the oscillations die down, the capacitors recharge and await the next trigger pulse.

The receiving section of the sing-around oscillator consists of an AC amplifier, a rectifier or envelope detector, a level detector and

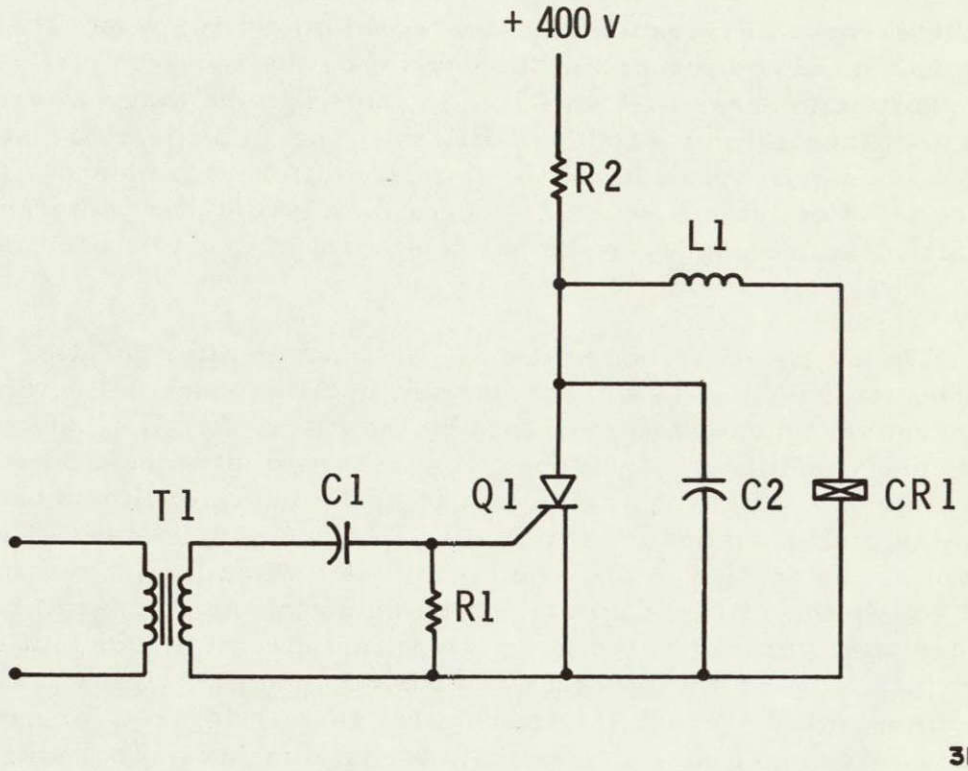

Figure 25. Acoustic Flowmeter Transmitter Schematic Diagram

a pulse transformer driver. The simplified diagram of the basic receiver/circuits is given in Figure 26.

Referring to the simplified schematic, the inductor, Lc, is shown shunting the receiving crystal. This inductance serves to tune out the crystal capacitance which would otherwise seriously attenuate the voltage induced in the crystal by the received ultrasonic pulse. The amplifiers labeled A1, A2, and A3 in the diagram are field effect transistor cascode amplifiers. The amplifiers are stagger tuned, i.e., each circuit tuned to a slightly different frequency, to produce an effective bandwidth of approximately 100 kHz centered on the resonant frequency of the particular set of crystals used in that channel.

The output of A3 is rectified in the base-emitter junction of Q1. The rectified pulses of base current in Q1 produce collector current pulses which when smoothed by the filter, R1C1, produce a voltage equivalent to the envelope of the received ultrasonic pulse. This voltage waveform is applied to one of the input terminals of the integrated circuit comparator amplifier, A4. An adjustable DC reference voltage is applied to the other terminal. When the increasing signal equals the reference voltage, the output of the comparator changes state. Amplifier A5 is an integrated circuit driver unit used to interface between the receiver comparator and the trigger transformer in the transmitter. Thus, the transmitter is re-triggered for each received pulse and a new ultrasonic pulse is launched. This sing-around process continues at a rate determined by the travel time of the ultrasonic pulse from transmitter to receiver plus the delay time through the electronic portion of the loop. This electronic delay is small compared to the travel time and is constant and independent of air velocity. This fixed time delay offset can be accounted for in the instrument calibration and does not seriously affect the inherent accuracy of the concept.

c. Frequency Measuring Components

This section of the system includes the frequency multipliers and their associated frequency counters and arithmetic logic units which produce a binary number equal to the difference of the counter contents and the display section. Simplified diagrams are given with the description of each of these circuits in the paragraphs which follow.

The frequency multiplier circuitry was designed to accommodate the four different transducer spacings of 12, 6, 4, and 2 inches. The

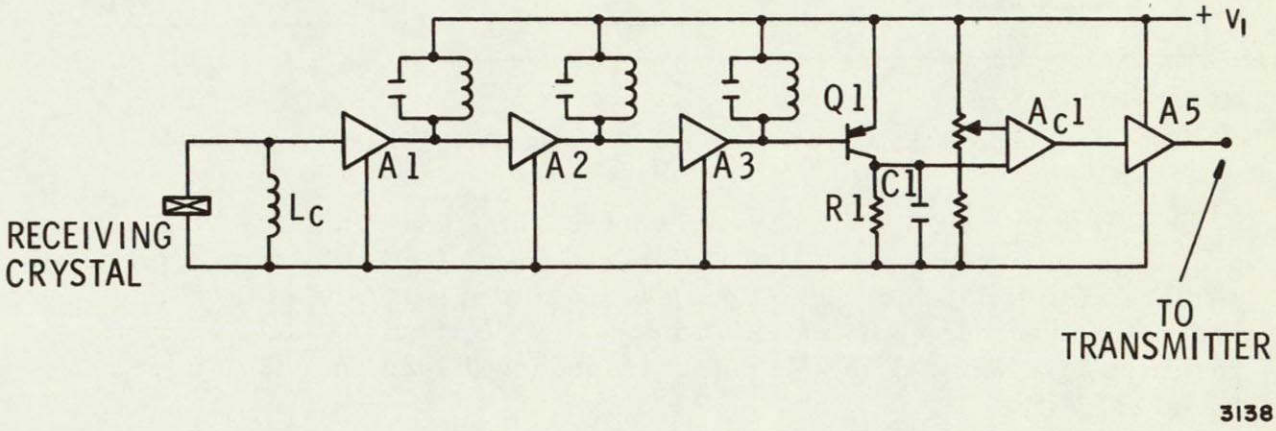

Figure 26. Acoustic Flowmeter Receiver Simplified Diagram

nominal sing-around frequencies at these spacings would be 1200 hz, 2400 hz, 3600 hz and 7200 hz, respectively, and hence the required multiplying factors at each spacing are 30, 15, 10, and 5 as discussed previously in the error analysis (Appendix). The block diagram below indicates the arrangement of the switch and the multipliers required to achieve these various multiplication ratios.

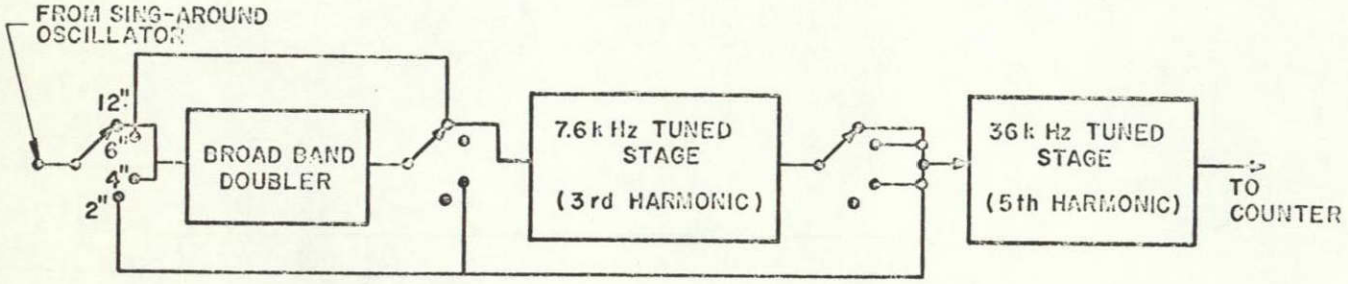

Acoustic Flowmeter - Multiplication Stages

In the position of the switch shown, the signal from the sing-around oscillator is first doubled, then tripled, then multiplied by five to produce a total multiplication of 30. Other switch settings use the multiplier sections in various combinations to produce the required factor always resulting in a nominal 36 kHz output frequency (based on a 1200 ft/sec sound velocity).

Each multiplier output is fed through a gate to an eight state counter as shown in Figure 27. The counters are allowed to accumulate counts, i.e., the gates are "on" for exactly one second. Since there are approximately 36,000 counts per second, all but the last 256 counts (the capacity of an 8-stage binary counter) in each channel are discarded as overflow. This is possible because it is the difference of the two frequencies that indicate flow velocity in a one to one correspondence, i.e., one foot per minute flow for each cycle per second difference in the two multiplied frequencies.

After the one second counting period, the outputs of the counters are held steady at the final count for 0.9 seconds. The eight binary bit outputs of each counter are connected to an 8-bit subtractor. This subtractor circuit consists of two 4-bit arithmetic logic units programmed to produce the (a-b) function.

In order to display the output of the subtractor on an illuminated decimal display it was also necessary to convert the binary difference

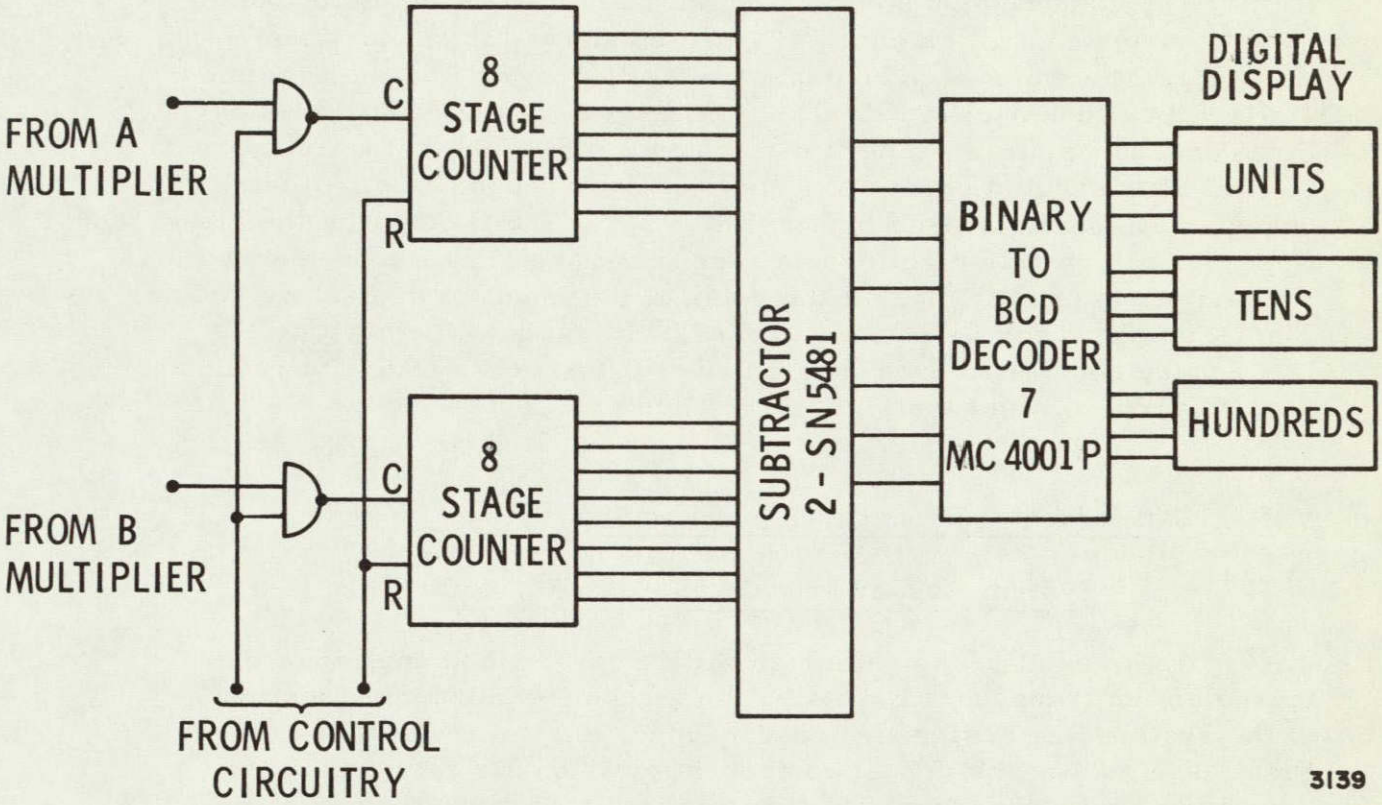

Figure 27. Frequency Measuring Components

to a binary-coded decimal number. This decoding process was performed by seven MC4001P decoders. The outputs of the decoder were connected to a Monsanto MDA-3 alphanumeric display. Thus, for approximately 0.9 seconds, the display readout is steady and indicates the flow velocity numerically in feet per minute. At the end of the readout period, the counters are reset and the count accumulation process and display period is repeated.

The counter inputs and reset lines are controlled by the timing generator and control circuits. Figure 28 shows the connections of these circuit elements. The basic timing is provided by the precision 1 kHz tuning fork oscillator. The 1 kHz signal is divided by 1000 by three decade counters. The flip-flop connected to the output of the last counter is connected so as to toggle once each second, i.e., it will change state once for each input. This causes the Q output of the flip-flop to be alternately high for one second and then low for one second. This output is used to control the gates at the input to the 8-stage counters. The $\overline{Q}$ output of the flip-flop is "anded" with outputs from within the last decade counter to produce a pulse at 0.9 seconds after the readout period starts to reset the eight stage counters.

V.5 Experimental Procedures and Results

System Assembly and Laboratory Results

As a result of the rather slow delivery by the supplier of the piezoelectric transducer crystals, the frequency measuring section of the system was designed, breadboarded, and assembled first. Final assembly of the digital components was on a semipermanent breadboard wiring system. In final test, this section of the system performed satisfactorily. Tests were performed with precision oscillators to determine accuracy and correctness of the logic design. After final debugging and checkout of the frequency measuring components, the assembly of the sing-around oscillator was begun. Preliminary laboratory tests were performed on the acoustic sing-around system using the transducer mechanical fixture and the transmitter circuits described earlier. The receiver components used in these tests were commercial amplifiers and filters.

Experiments indicated that the early estimates of the electromechanical efficiency of the low -Q lead metaniobate crystals were somewhat optimistic. The low level of the received ultrasonic pulses

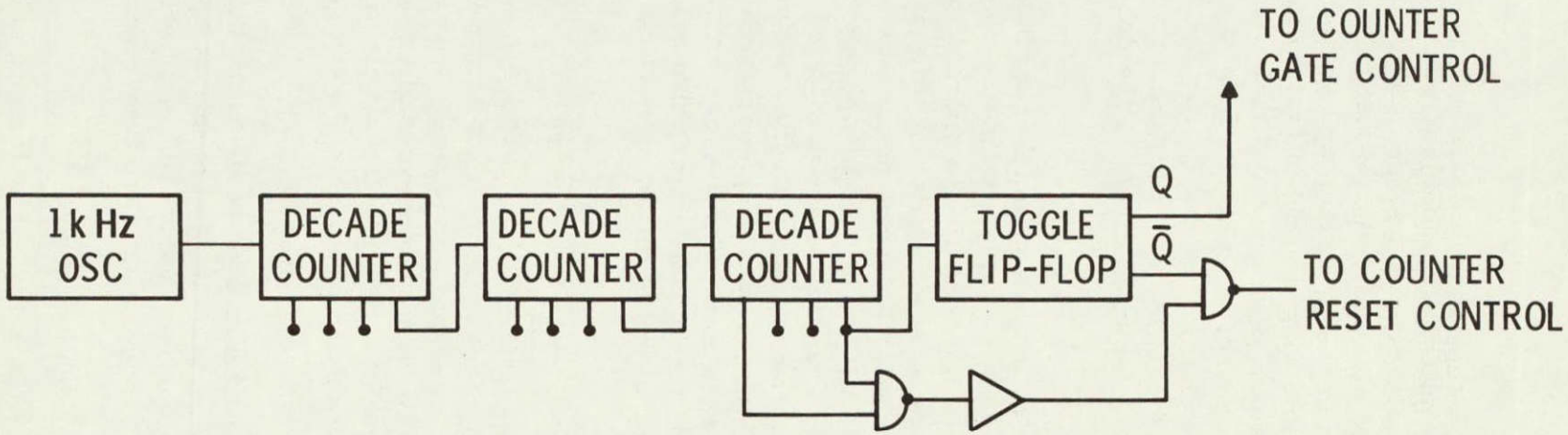

Figure 28. Timing and Control Circuits

required that higher gain low noise amplifiers be constructed. The additional gain requirement of the amplifiers, of course, compounded the problem of rejecting the undesired electrical and acoustical feedover. With extreme care and careful design of the grounding and shielding circuits, it was possible to obtain stable sing-around operation in either channel. However, when both oscillators were operated simultaneously as conceived, and the sing-around frequencies adjusted close to one another, as required in the system zero adjustment, the two oscillators invariably tended to synchronize together. In this condition, it was not possible to accurately detect air flow velocity in terms of the difference frequency.

It was obvious that a redesign of the two-channel transducer assembly and modification of the electronics system would be required to achieve sufficient channel separation and stability to operate the two channels simultaneously. As there was not sufficient time or funds remaining to perform these modifications, it became necessary to test the system in the flow test facility using a non-simultaneous operating mode. In this mode of test operation, readings of the multiplied sing-around frequency of each channel were recorded with only one sing-around oscillator operating at a time. Two sing-around frequency readings were made as quickly as possible at each flow velocity, one for the "up-stream" channel and the other for the "downstream" channel. The results of these measurements are given in the following section.

Low Velocity Flow Facility Tests and Results

The transducer assembly was installed in the test section of the low velocity flow facility and the equipment assembled as shown in Figure 29. Since only one sing-around oscillator operated at any time, only one frequency multiplier was required. The input to the multiplier was switched between each of the sing-around oscillators as required. To disable the unused oscillator, power was removed from the trigger amplifier.

A commercial electronic counter was used to measure the multiplied frequency. The oscillators were adjusted to operate at approximately the same sing-around frequency; however, no attempt was made to adjust them to precisely the same frequency at zero flow velocity.

Data was taken in the following manner:

a) Flow in the test section was adjusted to the highest expected level and allowed to stabilize;

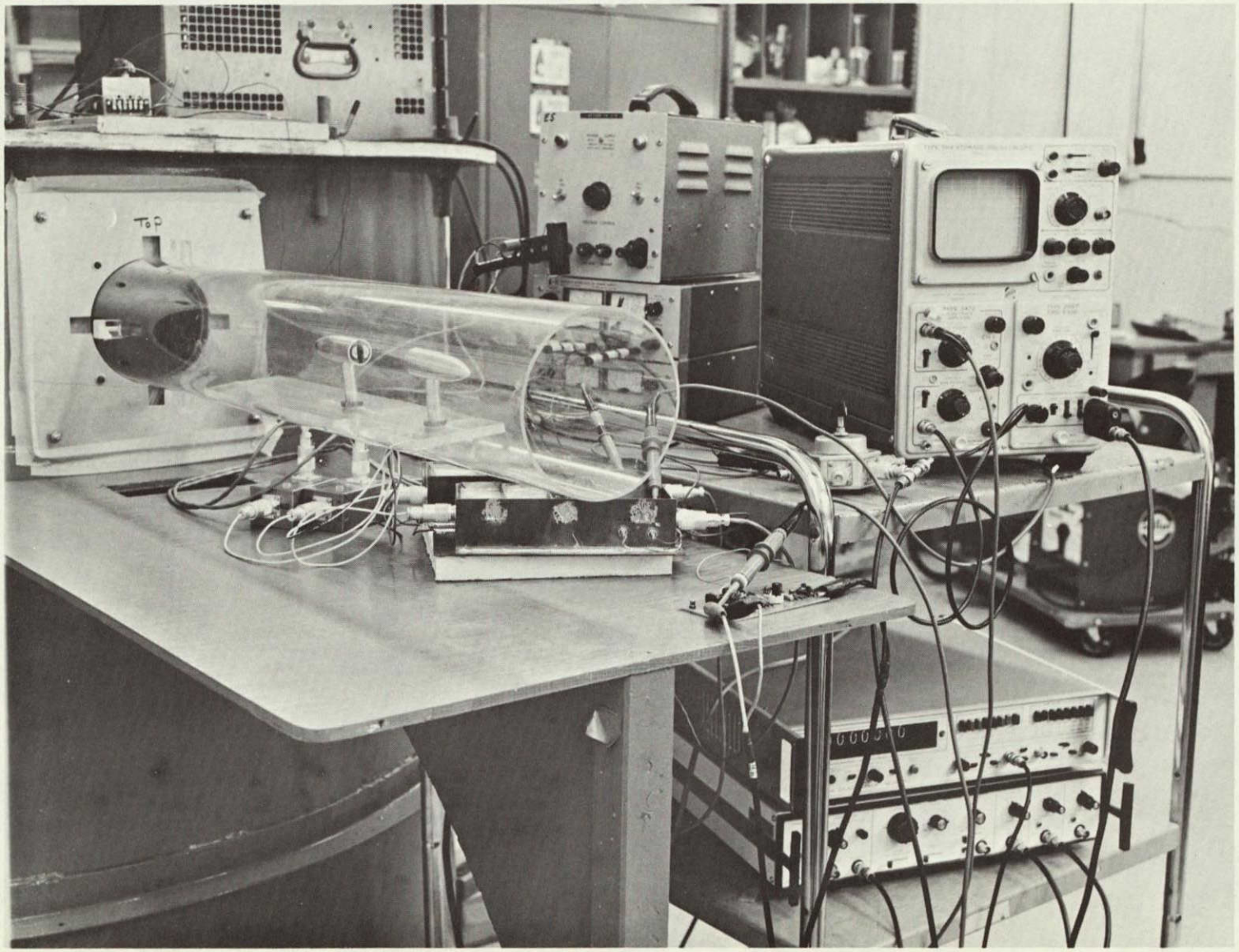

Figure 29. Acoustic Flowmeter Equipment Assembly At Low Velocity Test Facility

b) Frequency of each sing-around channel was recorded, switching between channels as quickly as possible;

c) Flow was then reduced to the next lower level and stabilized;

d) Data was again taken. The steps above were repeated down to the lowest flow level desired;

e) Frequencies of the oscillators were finally recorded at zero flow.

A number of such runs were made with several frequency readings recorded during each run at each flow level. Data from several of these runs were discarded as useless when the run was aborted for any reason before completion. For example, the experiments were prematurely terminated whenever the frequency of either oscillator became unstable or varied more than two or three hertz in consecutive one second periods.

Whenever a frequency instability developed, it was almost invariably caused by a change in the amplitude of the received pulse. Often this amplitude change appeared as a fluctuation probably resulting from turbulent conditions in the wake of the transducer. Figure 30 presents the results of four flow calibration test runs. The curves are a plot of difference frequency at the particular flow velocity less the difference frequency at zero flow as a function of flow velocity. All of these data were obtained using a transducer separation distance of 4 inches. Wider separation distances were not used because of instabilities in the high frequency sing-around channel.

V.6 Evaluation of Experimental Model Acoustic Flowmeter

The test results reported in the previous section represent a compromise in the operating concept of the two-channel sing-around flowmeter because of the necessity to operate each channel sequentially rather than simultaneously. This necessity, although required for these particular tests, is not a fundamental necessity and can be overcome by equipment design modifications.

Since a compromise in the operation of the present acoustic model was required, the evaluation of this technique is based on data obtained from an acoustic model with limited operational capabilities. Therefore, no detail breakdown evaluation for each of the specification categories is presented, as was done for the ion-tracer anemometer,

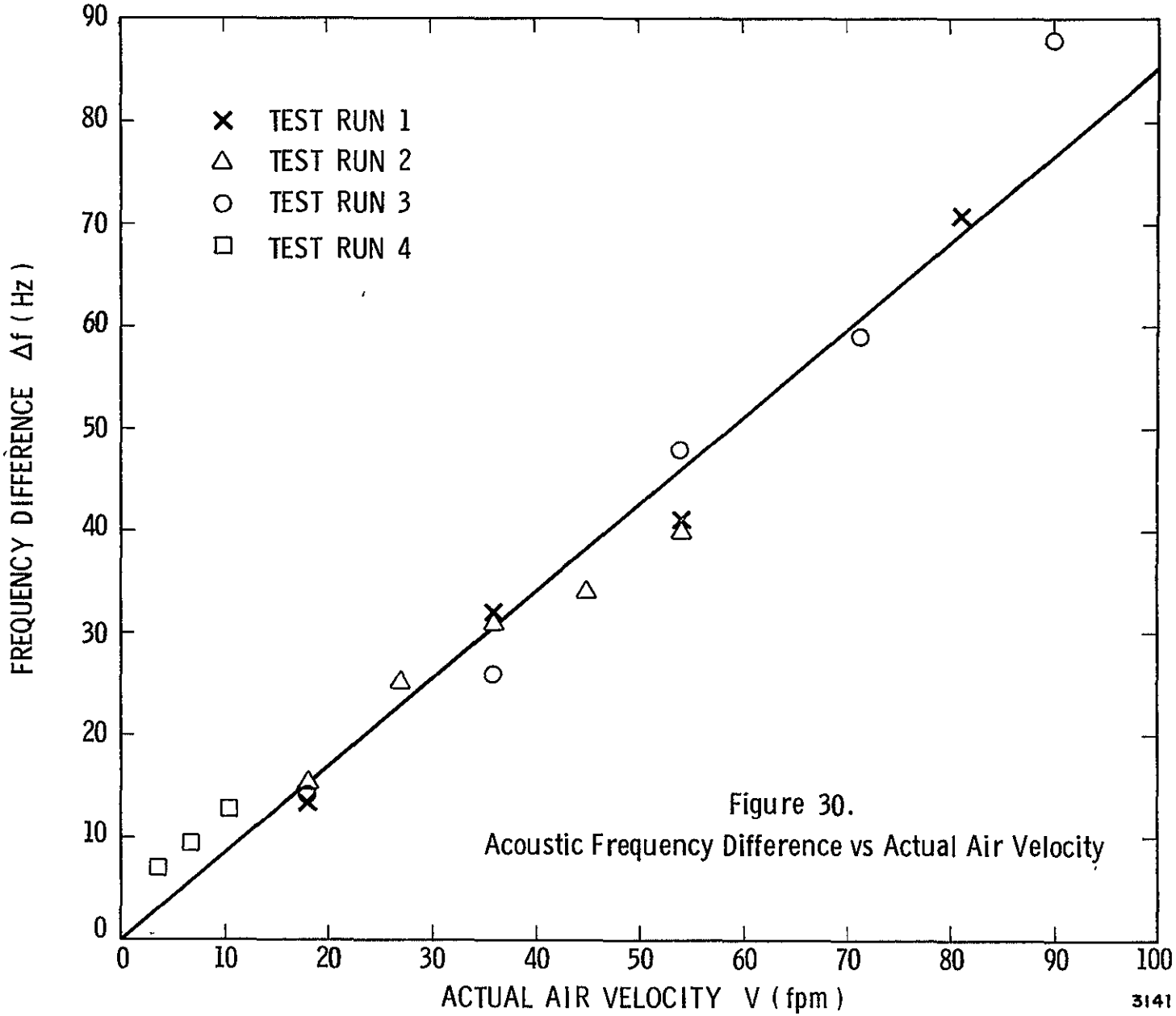

Figure 30.
Acoustic Frequency Difference vs Actual Air Velocity

and the evaluation is restricted to discussing the present acoustic test results and their implications. A final evaluation would require the testing of an updated acoustic model with simultaneous channel operation.

Overall, the limited calibration tests in the low velocity test facility indicate that the acoustic flowmeter technique could detect air motions at velocities down to about 3 ft/min with a linear response characteristic between sing-around difference frequency and flow velocity. Measurements over the 3 ft/min to 100 ft/min velocity range indicate that the measurements were usually within $\pm$ 5 ft/min with the least data scatter occurring over the 3-10 fpm range.

The necessity for sequential operation of the two sing-around channels introduced several limitations in testing the full capabilities of the acoustic flowmeter. The major limitation was that the measurements in the second channel were not made on the same parcel of air as that of the first channel. This limitation allowed for the possibility of slight differences in air temperature, humidity, flow fluctuations and turbulence to affect the two measurements. Sequential operation of the two channels also prevented the use of the direct numerical readout feature built into the overall electronic system and made it impossible to obtain a complete flow measurement reading within the 1-second response time ultimately required of the system concept.

These limitations and difficulties with the experimental model notwithstanding, several series of careful test measurements demonstrated that the performance of the basic system concept approached the final system requirements with reasonable success. The compromising limitations of the sequential sing-around frequency measurements, if anything, must be considered to introduce greater operating errors than would be expected with simultaneous channel operation.

The repeatability of the measurement technique is illustrated by the bounded scatter of the data points shown in the calibration curve shown earlier. The variations in the projected zero flow intercept from the various test runs is generally within the experimental error range of the measurements. However, where such offsets are pronounced and where the slope of the response curve deviates from the one-to-one proportionality, these effects are attributed to the "drift" in the zero flow condition used in the final scaling of the sequentially measured sing-around frequencies obtained during the course of the experiment. The zero flow reading used to correct all of the various readings obtained during a test run, lasting several minutes, was taken only once at the end of the run.

At the higher flow levels, similar shifts in the slope of the calibration curve as well as the wider scatter in the measured points is a result of incremental time delay changes and time jitter in either or both sing-around channels. Turbulent flow effects in the acoustic propagation path introduced significant amplitude fluctuations in the received sound pulses. These fluctuations, in turn, cause uncorrectable shifts in the sing-around frequencies. While simultaneous operation of the two sing-around channels would not be expected to fully nullify such fluctuations, it should provide the most optimum conditions for minimizing these errors. The primary approach to minimizing turbulence-associated errors would be the modification of the acoustic transducer fixtures to make them as small as possible for minimum disturbance of the flow. In conclusion, an experimental acoustic flow anemometer with simultaneous operation of both acoustic transducer-receiver pairs is required before a final evaluation of this technique can be given. The results from the present model, tested with sequential channel operation, indicate that an accurate low velocity anemometer based on the acoustic principle could be constructed.

V.7 Scope of Work for Additional Development of Acoustic Flowmeter

Several operational and design problems arose during the design and test phases of work on the acoustic flowmeter, some of which ultimately compromised the testing of the instrument concept as originally proposed. Therefore, the scope of work for development of a final instrument package is not given. Instead, the scope of work for additional development effort required to provide an acoustic model from which a final evaluation of the acoustic technique could be made is given.

Assessment of Problem Areas

a. Frequency Measuring Section

No serious defects in the design of the frequency measuring circuits were detected, however, in the present concept, the counting period was one second and the display period was 0.9 seconds. During the counting period, the visual display was active and indicated the accumulating count. A change in design to eliminate this annoyance could be readily achieved.

A reduction in the component count and complexity of the digital subtracting circuits would be desirable. In addition, the adjustability of the averaging time, and a full scale range changing capability could also be considered.

b. Transmitter and Receive Sections

There are several areas in the design of the acoustic source and receiver circuits which require consideration. Reduction of parts count and complexity is, of course, always desirable. Reduction of interchannel crosstalk and frequency response improvements are necessary. Improvements in the rise time of the transmitted pulse is also a requirement if the accuracy and resolution is to be further improved.

c. Transducers and Mounting Fixture

The ultrasonic transducer devices require the greatest amount of additional development work Transducers with fast rise time and greater sensitivity are required. Flow turbulence obviously occurred in the wake of the transducer housings. Also, because of the size of the mounting fixture, there is a possibility that the full flow velocity was not experienced between the transducer housing particularly at close spacing. To take full advantage of the sound velocity cancelling properties of the concept, it is important that the two sound beams probe the same column of air to the maximum extent possible. For these reasons, as well as others associated with electrical crosstalk, a full redesign of the transducer housing is required.

Conceptual Improvements in Problem Areas

In general, the proposed concept of the flowmeter has been shown to be basically correct with no conceptual flaws. The experimental tests, even though compromising below the ultimate mode of system operation, have borne this result reasonably well. Improvements in the problem areas outlined above are necessary in the continued development of the acoustic flowmeter. The following paragraphs present solutions, improvements or indicate a possible new design in the specific problem areas given.

a. Frequency Measuring Section

One major improvement is possible in the sing-around signal processor. The use of a nonlinear mixer to produce the difference frequency continuously rather than accumulating counts for a fixed time interval will add flexibility to the instrument averaging time setting, would eliminate a large portion of the electronic circuitry and would, in principle, provide a flow measurement based primarily on instantaneous sing-around data. Further, since the difference frequency would be available continuously, the frequency could be counted by decade

counters rather than straight binary counters thus eliminating the binary to binary coded decimal conversion. The annoyance of watching the new count accumulate can be eliminated by adding a storage-register and a nominal amount of gating logic.

b. Transmitter and Receiver Sections

The basic transmitter circuit was found to be adequate; however, it should be possible to eliminate the requirement for a high voltage power supply by the use of step-up autotransformers to produce the high voltage transducer driving pulse.

In the receiver, integrated circuit amplifiers and advanced design interstage filtering should produce a more stable and properly shaped frequency response.

c. Transducers

The basic cause of the relative insensitivity of piezoelectric crystals operating in a thickness vibration mode is the extreme acoustic impedance mismatch when coupling into air. Impedance matching techniques generally lead to high Q to poor rise time devices. However, there are other transducer concepts which should maintain adequate rise time characteristics while improving the basic transducer sensitivity. One concept would be to use a bimorphic bender crystal configuration in conjunction with a metal diaphragm to obtain a flexure mode vibrator. This is normally a rather high Q device; however, proper selection of a backing material could possibly provide the required damping to give the required rise time.

There is also the possibility of employing a capacitor microphone concept for the source or receiver or both which uses a metalized plastic film stretched over a porous or sintered metal backing. The porous structure of the backing allows nonresonant flexure vibration of the many small diaphragm areas thus formed.

d. Transducer Housing and Associated Structure

Two basic problems are involved in any redesign of the transducer structure:

(1) The reduction of turbulence in the air column between the transducers; and (2) crosstalk reduction while maintaining intimacy

of the sound beams. A suggested redesign which should greatly reduce both of the problems involves separating each of the transducers into individual smaller housings. Separating the housings to allow free passage of air between them should also reduce turbulence. Further, the sound beams could cross at the center of the air column rather than being aimed parallel to one another. This would have the effect of forcing the sound beams to probe more of the same column of air. The small fixed error introduced by the slight angle of the beams with the air velocity vector would be easily sealed out in the readout.

VI. CONCLUSIONS AND RECOMMENDATIONS

In the present study, many techniques for measuring low velocity gas flows were examined. Acoustic and ion-tracer methods were chosen as having the best potential in meeting the specifications in this program. Laboratory models based on these two techniques were constructed and tested over the velocity range of interest. As a result of this study we can conclude that the ion-tracer technique has the greatest potential in meeting all the instrument requirements specified in this program. Based on the test results, it appears that the ion-tracer anemometer (ITA) can be built into a compact, omnidirectional instrument which can accurately measure gas flows over the 0-100 fpm range under environmental conditions ranging from 3-15 psia and 60-80°F. The only undesirable feature discovered for this technique is the need for adjusting the ionization probe power input to maintain uniform ionization when large environmental changes occur and to null out the zero drift frequency at zero gas velocity. However, neither of these two requirements effect the instrument response between 0-100 fpm which is independent of environmental conditions.

The acoustic technique requires a larger instrument than the (ITA) and is inherently a unidirectional instrument. Therefore, a three component unit would be required to provide omnidirectional capabilities, further adding to the instrument size. Difficulties experienced in the present program in testing the acoustic model basically stem from the difficulties in differentiating between flow velocities of 1 fpm and the much larger speed of sound in a gas. This feature requires rather complex electronics to provide the frequency multiplication and processing necessary to detect small frequency differences at low velocities. However, it is believed that current difficulties with the present model can be overcome and test results indicate that an accurate instrument can be built to measure gas velocity from 0-100 fpm. The major advantage of the dual-path acoustic technique is its inherent independence of environmental temperature, pressure or gas constituents. If this advantage is of primary concern, and if a large instrument could be tolerated, then additional work on the acoustic technique would be warranted.

The final recommendation, based on the results of the present program, is that the ion-tracer technique be developed into a final low velocity gas measurement instrument capable of meeting all the specifications in this program. An outline of a recommended development program for the ion-tracer technique was presented in Section IV. 5.

VII. ACKNOWLEDGMENTS

The authors of this report wish to express their gratitude to Mr. R. F. Roemer and Mr. W. B. Pratt for their help and skill in building the low velocity flow facility. Moreover, special thanks are extended to Mr. C. M. Wood for his efforts and ingenuity in assembling the ITA electronic circuitry.

In addition, appreciation is extended to Mr. V. J. Hernandez for his skillful work on the figures and to Mrs. M. A. Stark who typed the text.

APPENDIX
Acoustic Gas Flowmeter System Error Analysis

ACOUSTIC GAS FLOWMETER SYSTEM ERROR ANALYSIS

To demonstrate the applicability of the acoustic sing-around flowmeter to low-velocity air circulation measurements, error analyses are developed below which provide a theoretical prediction of the measurement accuracy, the useful low-velocity threshold, and the design parameters required in an appropriate measurement configuration. The measurement errors will be derived for the "worst-case" conditions where the various independent errors are compounded in a root-mean-square manner. Consequently, it should be expected that the measurement accuracy would meet or exceed the performance predicted by the analysis results presented.

Several sources of error can influence the operation of the two-channel acoustic sing-around flowmeter. The nature of these error sources and the categories in which they can be grouped are:

1. Electronics - associated:

   a. Time delays resulting from electronic rise time and and bandwidth limitations;

   b. Digital counter errors resulting from lowest significant digit resolution;

   c. Digital counter time base accuracy and stability;

   d. Electronic circuit noise affecting sing-around pulse trigger time;

2. Structure - associated:

   a. Acoustic path length, geometric uncertainties and dimensional stability;

   b. Flow-induced wakes in the acoustic propagation paths; and

3. Three-dimensional flow vector determination.

The physical configuration of a practical acoustic flowmeter capable of measuring a three-dimensional flow vector will contain three orthogonally-oriented, two-channel sing-around systems. The mounting of the six transducers required in this configuration must necessarily be on a dimensionally stable open-frame structure which could produce minimum air flow disturbances in the acoustic paths. Further, the size of

the air volume used in the flow measurement will directly influence the threshold sensitivity and accuracy of the system because of acoustic travel time dependencies and volumetric flow stability variations.

The differential characteristic of the two-channel flowmeter technique has the inherent feature of cancelling any error effects common to both sing-around channels. Thus, the sources of error arise from the differences in the physical and electronic parameters in each channel. Consequently, it should not be unreasonable to consider the possibility of balancing out many of the overall system errors by certain electronic or mechanical adjustments affecting only one channel at a time. Also, since the sing-around frequency is the measured parameter, digital counter averaging during the response time interval of the instrument will smooth out much of the anticipated random fluctuation noise associated with each sing-around pulse.

Electronic System Errors

Electronic system errors can be reduced basically in inaccuracies, or differential variations, in apparent acoustic travel times in each sing-around channel. Electronic circuit rise time delays and acoustic path length variations are both responsible for these error effects.

If small electronic delays, t_1 and t_2, are assumed to exist in each sing-around channel and if the path length in each channel is presented by $x_1 = x_0 + \Delta x_1$ and $x_2 = x_0 + \Delta x_2$ then Equations 26 and 27 may be used to calculate the sing-around and repetition times, t_1' and t_2'. Next, taking the difference of the reciprocals of the times t_2' and t_2', and substituting into Equation (28), an expression for the apparent x-component of flow velocity, v_x', may be derived. For small incremental perturbations and for the condition, $c \gg v_x$, the apparent x-component of flow may then be simplified to the expression

$$v_x' = v_x + \frac{c}{2\gamma_0}\left[(\Delta\gamma_2 - \Delta\gamma_1) + c(\Delta t_2 - \Delta t_1)\right] \qquad \text{A.1}$$

The error term in the bracketed term is comprised of only the differential path length discrepancy, $(\Delta x_2 - \Delta x_1)$, and the differential electronic time delay, $(\Delta t_2 - \Delta t_1)$, between the two acoustic sing-around channels. The root-mean-square error between the apparent and actual flow velocities is given by

$$\Delta v = (v_x' - v_x)_{rms} = \frac{c}{2\gamma_0}\left\{(\Delta\gamma_2 - \Delta\gamma_1)^2 + c^2(\Delta t_2 - \Delta t_1)^2\right\}^{1/2} \qquad \text{A.2}$$

It should be noted that the derivation of v_x' discussed above showed that the flow-dependent error terms are negligible by a factor of v_x/c in comparison to the fixed system errors given in Equation A.1. Also from Equation A.2 it should be noted that steady state electronic timing adjustments in either one of the sing-around channels (which can be readily implemented) can, therefore, approximately compensate for steady state acoustic path length discrepancies and time delay sources of error.

The rms system errors arising from differential path length discrepancies and from differential time delays in the sing-around electronic circuits are given by Equation A.2. This equation can be rewritten as

$$\left(\frac{x_o \Delta v}{30c}\right)^2 = \left(\frac{\Delta x}{12}\right)^2 \times 10^{-6} + (c\Delta t)^2 \times 10^{-12}$$

for:

$\Delta x = (\Delta x_2 - \Delta x_1)$ in mils
$\Delta t = (\Delta t_2 - \Delta t_1)$ in microseconds
c in ft/sec
x_o in feet
Δv in ft/min.

Figures A.1 and A.2 illustrate the sensitivity of the flow velocity error equation to small changes in acoustic path length and electronic time delay. These results pertain to the static errors resulting from improper balance between the two sing-around channels. The errors expected from time dependent effects (assuming a statically balanced system) are discussed later.

The application of electronic leverage to the individual sing-around frequencies prior to determining the difference frequency and flow velocity has no effect on the accuracy of the system. This can be readily observed from an extended error relationship obtained from Equation A.1 which can be reduced to a form showing that the final difference frequency measured pulse by pulse will be

$$N \Delta f' = \frac{2N}{x_o}\left\{v_x + \frac{c}{2x_o}\left[(\Delta x_2 - \Delta x_1) + c(\Delta t_2 - \Delta t_1)\right]\right\} \qquad \text{A.3}$$

In the practical case where the difference frequency is measured by a counter averaging over a continuous sequence of pulses, or more precisely in the present measurement concept, each sing-around frequency is measured over a relatively large number of pulses and then subtracted, the final measured value of the difference frequency is (approximately)

$$\overline{N \Delta f'} = \frac{N}{K}\sum_{i=1}^{k}\left\{(f_1 - f_2) + \frac{c}{x_o}\left(\frac{\Delta x_2 - \Delta x_1}{x_o}\right) + \left(\frac{c}{x_o}\right)^2 (\Delta t_2 - \Delta t_1)_i\right\} \qquad \text{A.4}$$

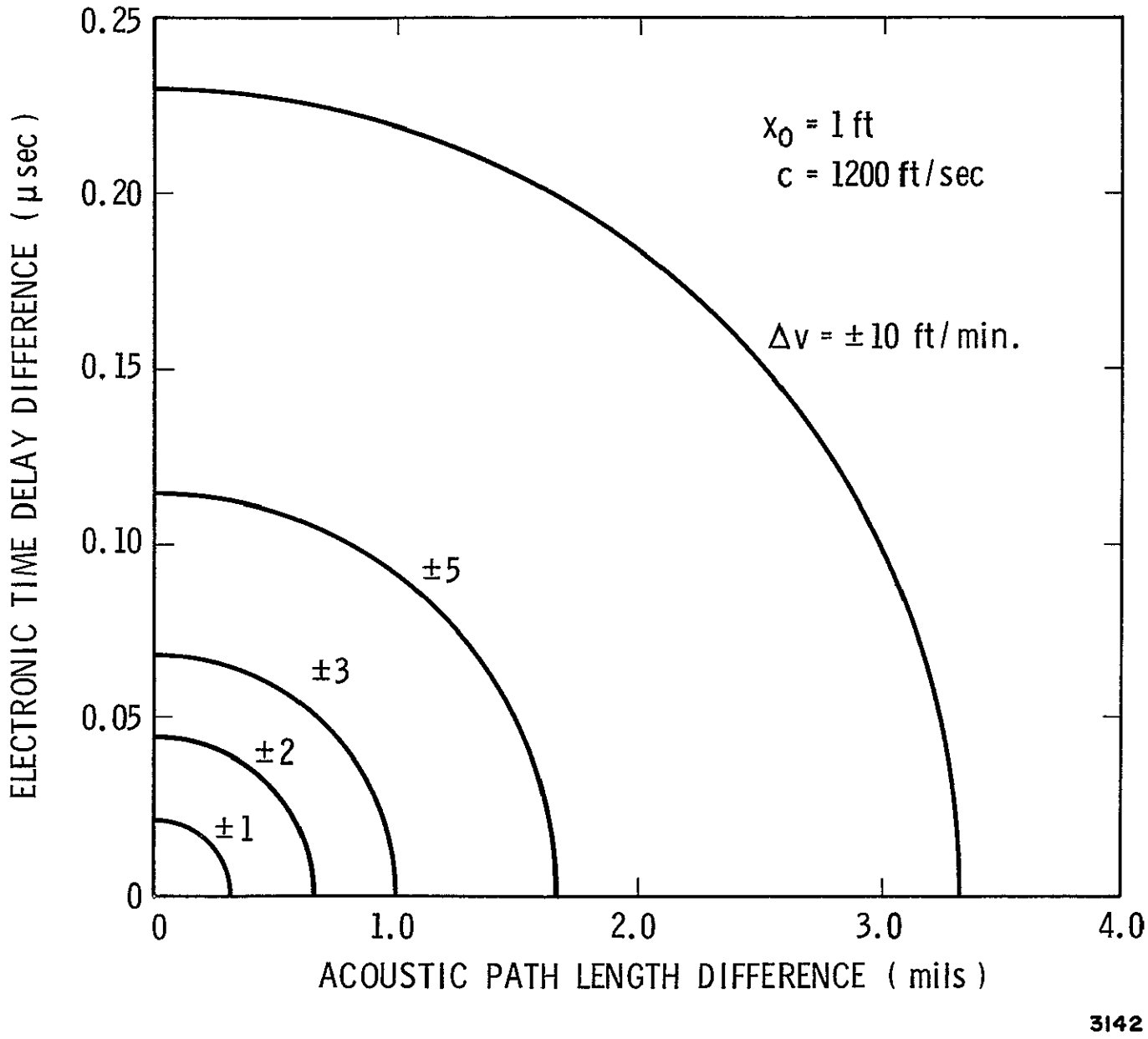

Figure A.1 Acoustic Flowmeter RMS Error Sensitivity - Constant Transducer Separation Distance

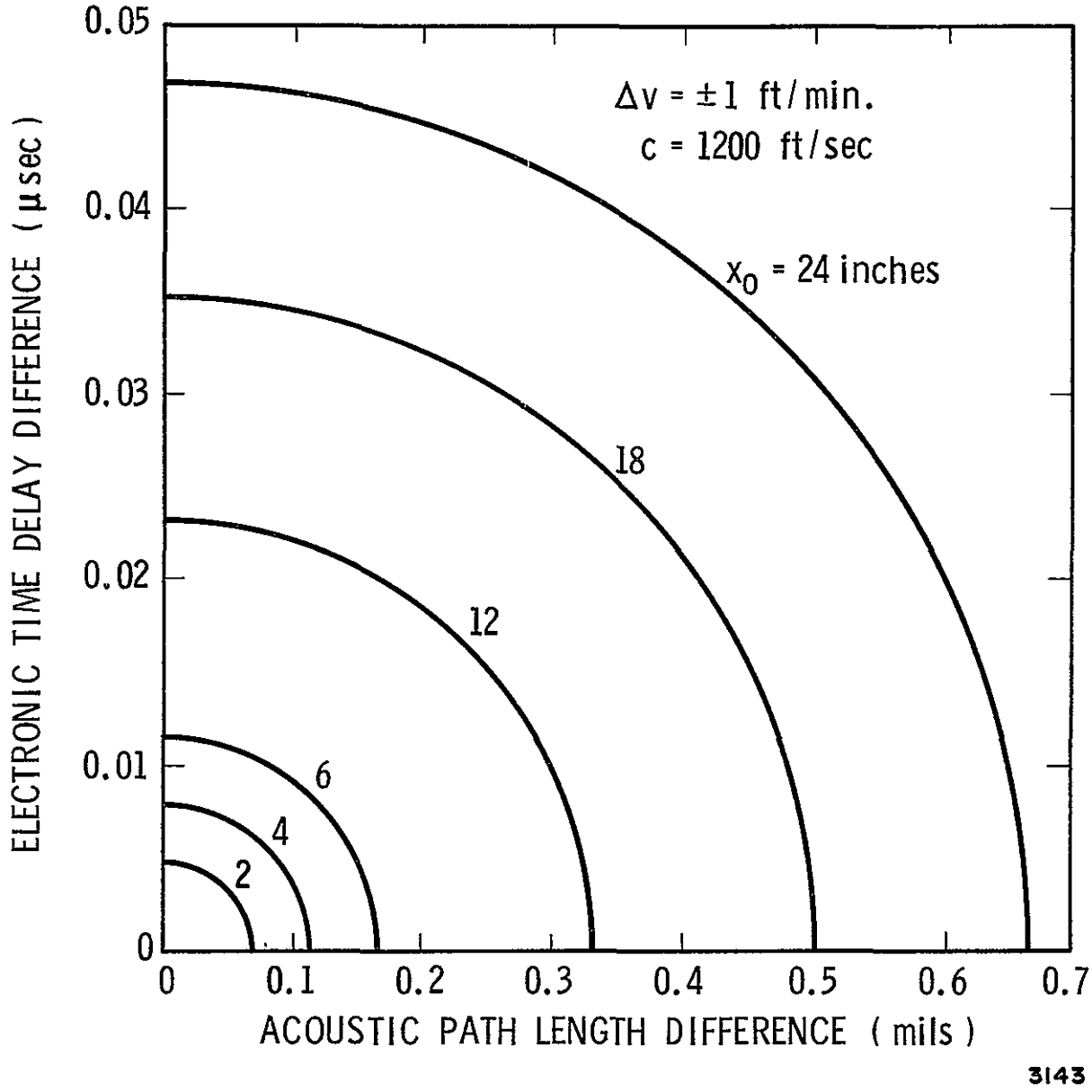

Figure A.2 Acoustic Flowmeter RMS Error Sensitivity - Variable Transducer Separation Distance

where:

K = number of pulses over which the counter reading is averaged.

The term $(\Delta t_2 - \Delta t_1)i$, is the only term considered susceptable to time varying conditions of a system origin. The differential path length, $(\Delta x_2 - \Delta x_1)$, is, of course, subject to vibration effects; however, this is considered as an ambient influence rather than a system effect. Equation A.4 is an approximation in the sense that the averaging process is forced to involve K pulses in each sing-around channel when in reality the averages will be made over a common time interval. The effects of this approximation are negligible since, for each channel the number of pulses within a time, T, are

$$K_1 = \left(\frac{c+v_x}{x_o}\right)T \approx \frac{cT}{x_o} \quad \text{for } c \gg v_x$$

$$K_2 = \left(\frac{c-v_x}{x_o}\right)T \approx \frac{cT}{x_o} \quad \text{for } c \gg v_x$$

The time period, T, is typically the response time of the instrument, or less. Also, when electronic leverage is employed, the number of pulses over which the average is derived is multiplied by the leverage factor, N. Thus, to a good approximation, $K = \frac{NcT}{x_o}$ when electronic leverage is used.

A convenient interrelationship can be chosen between the electronic leverage factor, N, and x_o in order to give a direct digital readout of v_x in units of, say, feet per minute directly from the counter reading of N f'. For example, if x_o is chosen to be one foot then, for N f' in Hz and v_x in feet per minute, the ratio, $2N/x_o$, must be 60 and hence N=30. Thus, the use of an electronic leverage factor of 30 with an acoustic path length of one foot will allow a direct numerical counter indication of the flow velocity in feet per minute. Similarly, for other separation distances the electronic leverage factors for direct numerical readout in feet per minute are:

x_o		N
inches	feet	
18	1.5	45
12	1.0	30
6	0.5	15
4	0.333	10
2	0.167	5

From these relationships, it can be observed that for a directly calibrated velocity readout in feet per minute, the ratio, N/x_o, is a constant scale factor of 30 $\frac{\text{sec}}{\text{ft-min}}$.

Based on the above, plus several other assumptions, we may now derive an expression for the electronic system error in terms of the various time delays and fluctuations in each sing-around channel. The assumptions are:

1. The time delays and fluctuations in each channel can be represented by combinations of fixed and time varying functions of the form

$$\Delta t_1 = \Delta t_{o_1} + g_1(t)$$

$$\Delta t_2 = \Delta t_{o_2} + g_2(t)$$

where Δt_{o_1} and Δt_{o_2} are the fixed time delays and $g_1(t)$ and $g_2(t)$ are the time dependent fluctuations.

2. The fixed time delay errors can be conveniently adjusted electrically to cancel one another.

3. There is an inherent ± 1 count error, typical of all digital counting circuits which have a one-to-one match between the pulsed data input sample length and the counter recycle time interval.

Based on the above, the instrument error may be expressed as

$$\overline{\Delta v_x'} = \frac{c}{2T}\left\{\left[\sum_{i=1}^{Nc T/x_o} g_2(t_i)\right] \pm 1 - \left[\sum_{i=1}^{Nc T/x_o} g_1(t_i)\right] \pm 1\right\} \qquad \text{A.5}$$

where $g_1(t_i)$ and $g_2(t_1)$ describe deterministic time variations which occur on each of the i sing-around cycles. Similarly, when $g_1(t_i)$ and $g_2(t_i)$ are random variables

$$\overline{\Delta v_x'} = \frac{Nc^2}{2x_o}\left\{\left[\langle g_2(t_i)\rangle \pm 1\right] - \left[\langle g_1(t_i)\rangle \pm 1\right]\right\} \qquad \text{A.6}$$

in which $\langle\ \rangle$ denotes the time average over period, T.

The time dependent functions causing errors in each sing-around channel result from several effects which can be classified as: (1) time drift of sing-around pulse trigger threshold due to system component and power supply voltage changes; (2) additive

noise on the propagated acoustic signal resulting either from ambient acoustic effects or receiver circuits; and (3) discrete time 'jitter' in the processed sing-around trigger pulses resulting from amplitude fluctuations in the propagated sound pulses in which the time increments are integral multiples of the propagated acoustic signal period. For well designed electronic systems, the drift and receiver noise sources can be made negligible compared with ambient acoustic noise and propagation fluctuation effects. Therefore, a worst-case analysis can be restricted only to considerations of the discrete time jitter in each sing-around channel.

Time jitter errors can be characterized by the random variables

$$g_1(t_1) = \begin{cases} 0, & \text{with probability } p \\ +\frac{a}{fa_1}, & \text{with probability } q \\ -\frac{b}{fa_1}, & \text{with probability } r \end{cases} \qquad \text{A.7}$$

$$g_2(t_1) = \begin{cases} 0, & \text{with probability } p' \\ +\frac{a'}{fa_2}, & \text{with probability } q' \\ -\frac{b'}{fa_2}, & \text{with probability } r' \end{cases}$$

where a, b, and a', b' are positive integers and the t_i represent the sequence of sing-around pulse periods occurring during the averaging period, T.

Obviously, if $q = r = q' = r' = 0$, then the error expressed by Equation A.7 is zero. On the other hand, if it is assumed that the fluctuations, $g_1(t_i)$ and $g_2(t_i)$ are only between two adjacent cycles of the sound pulse signal, i.e. $a = a' = 1$ and $r = r' = 0$ in Equations A.7 then the mean values of $g_1(t_1)$ and $g_2(t_i)$ can be derived from consideration of the random variable illustrated in the following sketch:

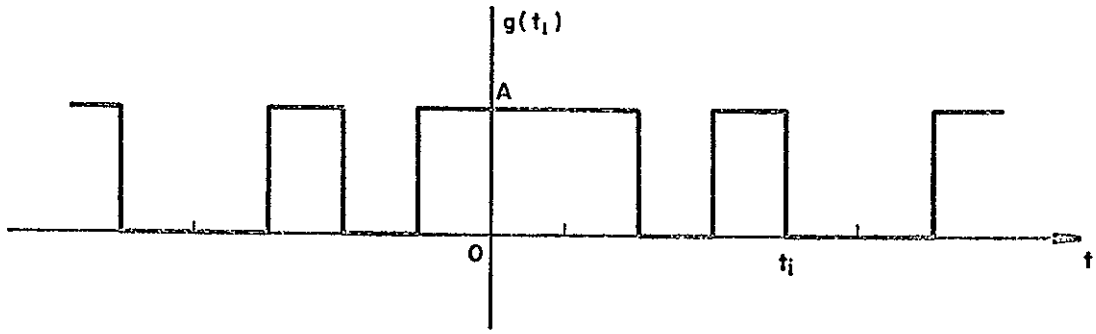

Random Variable Representing the
Worst Case Time Jitter Characteristic

In this sketch it can be noted that the values A and zero are mutually exclusive of one another. They are also assumed to be independent of one another at all incremental sing-around periods, t_i. The value of $g(t_1)$ after time T is either A or zero depending upon whether the number of transitions in the time interval, T, were even or odd. Assuming that the probability of k transitions in time, T, is given by a Poisson distribution then the probability of k = even is

$$P(k = \text{even}) = P\left\{g(t_i) = A\right\} = \frac{1}{2}\left(1 + e^{-2\alpha T}\right) \qquad \text{A.8}$$

The quantity, α, represents the average number of transitions per unit time in the interval, T, and is generally a large number corresponding to $\frac{NcT}{x_o}$ of Equation A.6 in its maximum. Thus, the mean value given by Equation A.8 is essentially $E\left\{g(t_i)\right\} = \frac{A}{2}$ and is equivalent to the time average values demoted in Equation A.6. Thus, the flow measurement error for

$$\frac{N}{x_o} = 30 \text{ sec/ft-min}$$

$$c = 1200 \text{ ft/sec}$$

$$A_2 = \frac{1}{f_{a_2}} = \text{channel 2 sound frequency (740 kHz)}$$

$$A_1 = \frac{1}{f_{a1}} = \text{channel 1 sound frequency (350 kHz)}$$

is

$$\overline{\Delta v_k'} = 8.9 \pm 2 \text{ ft/min} \qquad \text{A.9}$$

For the case where the time jitter effects include some variations in both the positive and negative directions relative to a nominal sing-around trigger point, the time average error is reduced from the value given by Equation A.8. Therefore, the error in Equation A.9 also decreases.

2. Structure - Associated Errors

Structure - associated errors arise from three major sources or effects: (1) thermal expansion or contraction of the mechanical assembly; (2) vibration of the mechanical assembly; and (3) air flow alterations and turbulence resulting from the flow obstruction effects of the assembly. The first two sources of error are associated primarily with choices of materials and physical configurations of the structural design which are flexible enough to allow minimization of their errors. The flow perturbations produced by the structure itself are a more fundamental form of error and are examined in closer detail below to provide preliminary information on structural assembly design concepts.

Flow perturbations will produce vortex turbulence downstream of the ultrasonic transducer supports. For small Reynolds numbers ($N \leq 60$), the velocity defects will be laminar, whereas at higher Reynolds numbers ($60 \leq N \leq 500$), the velocity defects will consist of moving periodic vortex patterns. In this range of flow ($60 \leq N \leq 500$), the dimensionless frequency Strouhal number, S, serves as a measure of the periodicity of the vortex disturbances. The Strouhal number if given by

$$S = \frac{f_s D}{V} \qquad \text{A.10}$$

f_s = frequency of oscillation

D = diameter of the structural body

V = free stream velocity

As a result of the flow perturbations and turbulent wakes around the structural mountings, the observed flow velocity will be less than the free stream velocity.

The range of flow velocities in this application correspond to Reynolds numbers in the range $0 \leq N \leq 500$. For typical transducer and support structure dimensions the vortex oscillation frequencies will be in the range of $0 < f_s \leq 50$Hz.

For small Reynolds numbers ($N \leq 60$) the effect of the wake may be estimated from laminar flow theory. The worst case condition is where the flow velocity defect lies directly between acoustic source and receiver transducers integrally installed in a cylindrical support mounting oriented normal to the flow. For two support cylinders of radius, a, separated by a distance, x_o, the average flow velocity error ratio is found to be

$$\frac{|\overline{v_{x_o}} - v_o|}{v_o} = \frac{2a}{x_o} \qquad \text{A.11}$$

Thus, for a measurement error of 2.5 percent at a transducer seperation of, say, 6 inches, the structural supports should have a radius of 0.075 inch, or a diameter of 0.15 inch.

For larger Reynolds numbers ($60 \leq N \leq 500$), the flow disturbances depart from the laminar characteristics described above. In this case the average downstream velocity behind the supporting cylinders will be more strongly modified from the free stream velocity as the flow increases, and, consequently the measurements will be in greater error at the higher flow rates. In prior investigations of acoustic anemometers designed for meteorological applications, this error has been estimated to be as great as 15 percent. However, verification of this degree of error can only be confirmed through experimental results.

It can be concluded from this brief analysis of disturbed flow conditions that wake effects from transducer supporting structures can introduce considerable errors in the observed flow measurements if the downstream transducer is enveloped by the wake of the upstream transducer. For other orientations of the source and receiver transducer pairs, the support structure wakes occupy a smaller percentage of the sound transmission path and will introduce proportionately less flow disturbance.

3. Vector Computational Error

Another source of error arises when the vector sum of three orthogonal flow components is computed. This error is attributed to two effects: (1) the combination of three orthogonal components each having a small error; and (2) structural misalignments modifying the orthogonality of the measured components.

To estimate the error in the vector sum of three measured flow components under these circumstances let v_i (i = 1, 2, 3) be the true velocity components, Δv_i (i = 1, 2, 3) the respective flow component errors, and $\Delta \theta_i$ (i = 1, 2, 3) the angular deviations from orthogonality. Assuming that Δv_i and $\Delta \theta_i$ have the same magnitude, and are small errors, the relative error in vector flow magnitude is

$$\frac{|\Delta v_a|}{|\vec{v}|} = \frac{3}{2}\left(2\frac{\Delta v_i}{v_i} + \Delta\theta_i^2\right) \qquad \text{A.12}$$

For $\left|\frac{v_1}{v_1}\right| = 0.05$ and $\Delta\theta_i = 0.05$ radian, the error is

$$\left|\frac{\Delta v_a}{\vec{v}}\right| = \frac{3}{2}\left[0.10 + 0.0025\right]$$

$$= 15 \text{ percent}$$

Note that the orthogonality alignment error will generally be negligible for angles up to about 0.15 radian or about 8 degrees.

REFERENCES

1. Head, M. R., and Surrey, N. B., "Low Speed Anemometer," J. Sci, Instruments, Vol. 42, 1965, pg. 349.

2. Head, M. R., and Thorp, R. R., "Direct Reading Low Speed Anemometer," J. Sci. Instrum., Vol. 42, 1965, pg. 811.

3. Kung, R. J., and Binder, G. J., "Ultra Low-Speed Anemometry," Colorado State Univ., Grant DA-AMC-28-043-65-G20, AD 658172, June 1967.

4 Griffiths, R. T., and Nicol, A. A., "A Fibre Flowmeter Suitable for Very Low Flow Rates," J. Sci. Instrum., Vol. 42, 1965, pp. 797-799.

5. Trokhan, A. M., "Velocity Measurements," Measurement Techniques, June 1968, pp. 764-767.

6. Odar, Fuat, "A High-Response Triaxial Strain-Gage Anemometer," Research Report 254, U.S. Army Materiel Command, Terrestrail Sciences Center, Cold Regions Research & Engineering Laboratory, Hanover, New Hampshire, Jan. 1969.

7. Wasan, D. T., Davis, R. M., and Wilke, C. R., "Measurement of the Velocity of Gases with Variable Fluid Properties," AIChE Journal, Vol. 14, No. 2, pp. 227-234.

8. Tanney, J. W., "Fluidic Velocity Sensor," Instruments & Control Systems, June 1969, pp. 81-83.

9. Neradka, V. F., and Turek, R. F., "Fluidic Low Speed Wind Sensor Research Study," Final Report, Contract No. NAS 12-2038, Dec. 1969.

10. Tanney, J. W., "An Anemometer for Very Low Velocities," National Research Council of Canada, Aero Report, LR-472, February 1967.

11. Foreman, J. W., Jr., George, E. W., and Lewis, R. D., "Feasibility Study of a Laser Flowmeter for Local Velocity Measurements in Gas Flow Fields," Brown Engineering Company Inc., Technical Note R-149, May 1965.

12. Fridman, J. D., Huffaker, R. M., and Kinnard, R. F., "Laser Doppler System Measures Three-Dimensional Vector Velocity and Turbulence," Laser Focus, November 1968, p. 34.

13. Private Communication with Ratheon Company's Space and Information Systems Division (Sudbury, Mass.) and NASA's George C. Marshall Space Flight Center.

14. Kalmus, Henry P., "Electronic Flowmeter System," The Review of Scientific Instruments, Vol. 25, No. 3, March, 1954, pp. 201-206.

15. Brown, A. E., "Dual Path Ultrasonic Measurement of Fluid Flow," The Review of Scientific Instruments, Vol. 37, No. 9, September, 1966, pp. 1181-1186.

16. Werner, F. D., "An Investigation of the Possible Use of the Glow Discharge as a Means for Measuring Air Flow Characteristics," The Review of Scientific Instruments, Vol. 21, No. 1, January, 1950.

17. Durbin, D. J., and Born, G., "A New Mass Flow Measuring System Applicable to Aircraft Speed Measurement Including V/STOL," Instrumentation in the Aerospace Industry, Vol. 16, 1970.

18. Lilienfeld, Pedro, Solon, L. R., and DiGiovanni, H. J., "Ion Tracer Anemometer for the Measurement of Low Density Air Flow," The Review of Scientific Instruments, Vol. 38, No. 3, March 1967, pp. 405-409.

19 Mellen, Glenn L., "Gas-Flow Speedometer," Electronics, February 1950.

20. Loeb, L. B., "Basic Processes of Gaseous Electronics," Univ. of California Press, 1961, pp. 199-200.

21. Sivian, L. J., "High Frequency Absorption of Sound in Air and Gases," JASA, V. 19, p. 914, Sept. 1947.